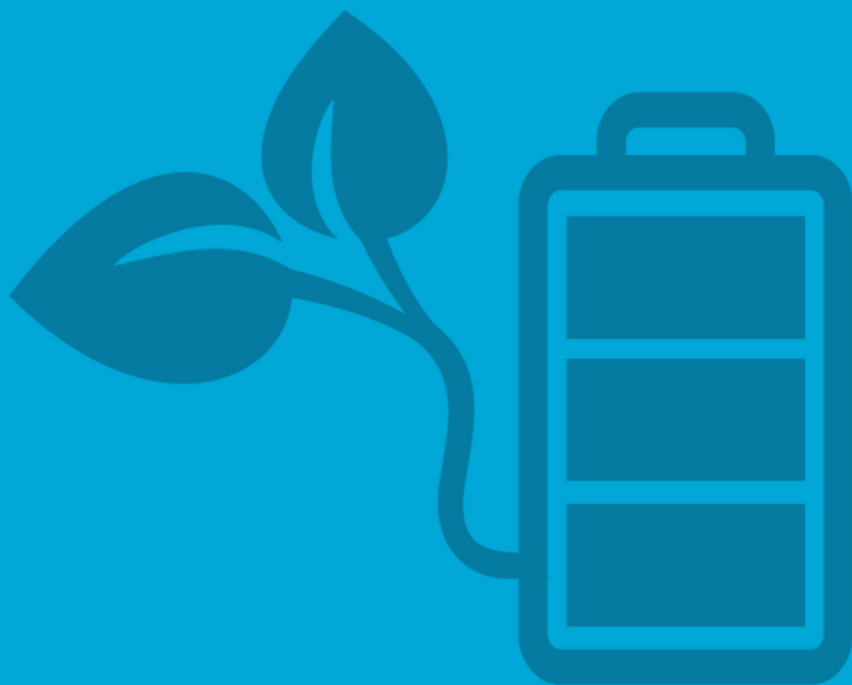


Si-air Battery

Alkaline cell modelling
in MATLAB (Simscape)

Nithin Jacob



Si-air Battery

Alkaline cell modelling in MATLAB (Simscape)

by

to obtain the degree of Master of Science
at the Delft University of Technology,
to be defended publicly on Monday October 19th, 2020 at 15:00.

Student number: 4841344
Project duration: January 2, 2020 – October 19, 2020
Thesis committee: Dr. Rene van Swaaij TU Delft, supervisor
Prof.dr.ir. Arno Smets, TU Delft
Dr. Erik Kelder, TU Delft
Dr.ir. Rudi Santbergen, TU Delft

This thesis is confidential and cannot be made public until October 19, 2020.

An electronic version of this thesis is available at <http://repository.tudelft.nl/>.

*Science is a wonderful thing
if one does not have to earn one's living at it.*

Albert Einstein

ABSTRACT

RENEWABLE energy sources (RES) such as Solar and Wind energy rely on the availability of natural resources like sunlight in the case of Solar and wind speed in the case of Wind energy generation which is variable in nature. There are periods where there is excess energy production than needed and periods of energy shortage where not enough energy is produced to meet the demand. To mitigate this mismatch, a short term solution is to use batteries in order to store energy at times where energy production is more than the energy demand. This stored energy would be later used at times where energy production is low and meet the energy demand. However, the current battery technology is still novel for this application making it uneconomical when compared to current energy infrastructure of using power plants. The current battery market is held by Li-ion batteries which uses lithium as a raw material which is a rare earth material. In 2009, a battery cell utilizing Si as its anode and air as its cathode was discovered. As this system relies on two of the most abundant elements in the earth's crust which is silicon and oxygen and has much higher theoretical energy density than Li-ion batteries, it has become a growing area of research and development.

Battery models are created to simulate battery operations based on empirical formulas and electrochemical reactions taking place in the battery. Development of these models are very critical as they provide results and optimum condition evaluations much faster than physical testing with minimal resources. A battery model for the alkaline Si-air battery which utilizes KOH as the cell electrolyte is developed in Simscape (MATLAB) as part of this thesis. The modelling parameters are also subjected various physical conditions such as varying electrolyte concentration and change in electrode materials and the variation is investigated for model validation to study whether changing physical conditions of the Si-air cell has an effect on the modelling cell parameters. It is supported with experimental results obtained from discharging a fabricated Si-air cell.

It was concluded that there are cell parameters which are dependent only on the state of charge (SOC) of the cell and one cell parameter that is a function of both the SOC as well as the discharge profile of the cell. The fabricated Si-air cell gives higher open-circuit potential (OCP) values than what was reported constant 1.4 V in literature which is speculated to be due to the usage of a 99% Aluminium and 1% Silicon (Al:Si) back contact layer. Average OCPs ranging from 1.5 V to 1.45 V which varies due to change in electrolyte (KOH) concentration is achieved. The MATLAB battery block is calibrated to be integrated with energy system models as a Si-air battery.

Keywords: Battery technology, Si-air battery, Silicon, Battery, Alkaline battery cell, Air cathode, Simscape, Simulink, MATLAB, Battery modelling, Battery Management System (BMS), Metal-air battery.

ACKNOWLEDGEMENTS

It feels like it was yesterday when I boarded my flight to Netherlands from Dubai and started my M.Sc chapter in TU Delft. It was a mixture of positive and negative emotions, moving into an unknown land, facing new cultures and new people. I always found myself questioning if this leap of faith was worth it. It was quite the journey filled with highs and lows and I am sure the experiences that TU Delft, my professors, my peers and my friends have imparted and shared with me, has certainly made me a better person today.

I would like to thank some people who pushed me to my limits and beyond. *My parents* who provided me with emotional strength and financial support needed for my studies. *My sister* who always supported me through my ups and downs and made an effort to understand what I was going through. My thesis supervisor *Dr. Rene van Swaij* who was always there for me even when I was at my lowest and made sure I was performing to the best of my abilities. *Dr.ir. Rudi Santbergen* who provided me with guidance in my simulation project, which was an area out of my expertise. The battery group of PVMD peers *Shihao Wang* and *Jasper Prins* who made it a positive work environment. My friends from various friend circles starting from my roommates of Zusterlaan 138 *Harsh Parasramka*, *Omkar Sane* and *Rishikesh Joshi* who were coincidentally studying M.Sc SET with me. *Food peeps of Zusterlaan* who were there to provide comfort food or just to listen to me. The lovely people of KSA who reminded me of my school days in Kerala. A special acknowledgment must be given to *Anand Iyer* who gave me a place to stay when I was homeless and provided a cup of chai whenever I needed it the most. Lastly, I am indebted to *ISA Delft* as it has given me so many memories with some of the most amazing people I will ever know. The impact that all these wonderful people have made on me as a person is inexplicable and I shall be forever grateful to them.

I dedicate this thesis to *my grandmothers* who always loved to me in their own special ways. *My paternal grandmother* who looked after me during my school days in Kerala and always made an effort to stay in touch with me. *My maternal grandmother* who instilled the fire of doing a M.Sc in me and always encouraged me to aspire for greater things in life.

Nithin Jacob
Delft, 2020

LIST OF FIGURES

1.1	Abundances of elements [1]. Si and O marked in red, Li is marked in yellow.	2
1.2	Different components of an energy system of the future.	3
1.3	Different types of metal-air batteries [2].	6
1.4	Experimental setup of the rechargeable Si-air cell using Ca stabilized ZrO_2 (CSZ) [3].	8
1.5	Si-air illustrative diagram showing flow of electrons and ions during discharge cycle.	9
1.6	Discharge profile of Si-air cells with 0.05 mA/cm^2 for various KOH concentrations [4].	10
1.7	Thesis outline	14
2.1	Air cathode rolls as given by manufacturer [5]	19
2.2	X ray of the full assembled system. The red block indicates the silicon anode and the blue block indicates the air cathode. A and B denotes the outer and inner cell component respectively	20
2.3	Isometric view of assembled Si-air cell	21
2.4	An example of the chrono potentiometry procedure in Nova software [6]	22
3.1	(a) OCP curve and (b) DP curve when the cell is n-Si anode with air cathode under normal condition for varying electrolyte concentrations. Blue, red and yellow indicates the potential curves when the electrolyte concentration is 10%, 30% and 60 % respectively.	26
3.2	(a) Open-circuit potential curve under n-type Si anode and normal air cathode condition and (b) Open-circuit potential curve when the cell is n-Si anode with air cathode under normal condition for varying electrolyte concentrations. Blue, red and yellow indicates the potential curves when the electrolyte concentration is 10%, 30% and 60 % respectively.	29
3.3	(a) DP curve under n-type Si anode and normal air cathode condition and (b) DP curve when the cell is n-type Si anode with air cathode under normal condition for varying electrolyte concentrations. Blue, red and yellow indicates the potential curves when the electrolyte concentration is 10%, 30% and 60 %, respectively.	29
3.4	(a) OCP curve and (b) DP curve when the cell is in KOH 60% electrolyte solution and pre-wetted air cathode condition. Blue trace indicates when a n-type Si anode is used and red line indicates a p-type Si anode is used.	31
4.1	Simple equivalent electrical circuit of the battery cell.	37
4.2	Circuit diagram of the battery (look-up table) block in Simscape.	39

4.3	Block parameters of the battery block under "Main".	39
4.4	Block parameters of the battery block under "Dynamics".	40
4.5	Complete Si-air simscape model 1.) Constant current source set at 150 μA 2.) Capacity calculator 3.) Simscape current source into battery 4.) Battery model (look-up table) 5.) SOC calculator 6.) Voltage sensor and 7.) Experi- mental voltage input and 8.) Simulated voltage output from model.	41
4.6	Flow chart of how the parameter estimation tool works.	42
4.7	Experimental and simulated voltages of Li-ion cell before parameter esti- mation. The blue indicates the experimental voltage and the red line indi- cates the simulated voltage.	43
4.8	Li-ion cell parameters changing with each iteration steps to fit the simu- lated data and experimental data. Where E_m is measured in Volts [V], R_0 and R_1 is measured in Ohms [Ω] and τ_{a1} is measured in seconds [s]. The multiple lines indicate the variation of the cell parameter for each state of charge (SOC).	44
4.9	Experimental and simulated voltages of Li-ion cell after parameter estima- tion. The blue indicates the experimental voltage and the red line indicates the simulated voltage.	44
5.1	Experimental (in blue) and simulated (in red) cell potential vs. Time using discharge current of 150 μA after parameter estimation is carried out for various concentrations under n-type Si anode and normal air cathode . . .	50
5.2	Cell parameter variation for KOH 10% before parameter estimation in blue and cell parameter variation after parameter estimation in red against the state of charge (SOC) of the Si-air cell. This trend is the same for KOH 30% and KOH 60% under n-type Si anode and normal air cathode	51
5.3	E_m variation with state of charge (SOC) of the cell against the initial guess (in blue).	52
5.4	Experimental (in blue) and simulated (in red) cell potential vs. Time using discharge current of 150 μA after parameter estimation is carried out for various concentrations under n-type Si anode and pre-wetted air cathode.	53
5.5	Cell parameter variation for KOH 10% before parameter estimation in blue and cell parameter variation after parameter estimation in red against the state of charge (SOC) of the Si-air cell. This trend is the same for KOH 30% and KOH 60% under n-type Si anode and pre-wetted air cathode	54
5.6	E_m variation with state of charge (SOC) of the n-type Si anode and pre- wetted air cathode Si-air cell against the initial guess (in blue).	55
5.7	Experimental (in blue) and simulated cell (in red) potential vs. Time using discharge current of 150 μA is with p-type Si anode, pre-wetted air cathode in KOH 60% electrolyte. (a) Before parameter estimation is done and (b) After parameter estimation is done.	56
5.8	E_m variation with state of charge (SOC) of p-type Si anode with pre-wetted air cathode in KOH 60% solution Si-air cell against the initial guess (in blue).	57
5.9	Cell parameter evaluation in a pulsed curve [7]	60
7.1	Broken Si sample.	65

7.2 Leaking Si-air cell.	65
A.1 Cell potential curve of Si-air cell with n type Si anode, KOH 10% and normal air cathode	69
A.2 Cell potential curve of Si-air cell with n type Si anode, KOH 10% and pre-wetted air cathode	70
A.3 Cell potential curve of Si-air cell with n type Si anode, KOH 30% and normal air cathode	70
A.4 Cell potential curve of Si-air cell with n type Si anode, KOH 30% and pre-wetted air cathode	71
A.5 Cell potential curve of Si-air cell with n type Si anode, KOH 60% and normal air cathode	71
A.6 Cell potential curve of Si-air cell with n type Si anode, KOH 60% and pre-wetted air cathode	72
A.7 Cell potential curve of Si-air cell with p type Si anode, KOH 60% and pre-wetted air cathode	72
A.8 Variation of open-circuit potential with pre-wetting of air cathode. The cell is n-type Si anode and in 10% KOH	73
A.9 Variation of discharge potential with pre-wetting of air cathode. The cell is n-Si anode and in 10% KOH	73
A.10 Variation of open-circuit potential with pre-wetting of air cathode. The cell is n-Si anode and in 30% KOH	74
A.11 Variation of discharge potential with pre-wetting of air cathode. The cell is n-Si anode and in 30% KOH	74
A.12 Variation of open-circuit potential with pre-wetting of air cathode. The cell is n-Si anode and in 60% KOH	75
A.13 Variation of discharge potential with pre-wetting of air cathode. The cell is n-Si anode and in 60% KOH	75
A.14 (a) OCP curve and (b) DP curve when the Si-air cell is placed under different conditions. n-Si indicates n-type Si is used as anode, 10% indicates KOH 10% solution is used as electrolyte and PW indicates that the cell is under pre-wetted air cathode condition.	76
B.1 Before parameter estimation	83
B.2 After parameter estimation	84
B.3 R_0 variation	84
B.4 R_1 variation	85
B.5 τ_1 variation	85
B.6 E_m variation	86
B.7 Cell capacity variation	86
B.8 Before parameter estimation	87
B.9 After parameter estimation	88
B.10 R_0 variation	88
B.11 R_1 variation	89
B.12 τ_1 variation	89
B.13 E_m variation	90

B.14 Cell capacity variation	90
B.15 Before parameter estimation	91
B.16 After parameter estimation	91
B.17 R_0 variation	92
B.18 R_1 variation	92
B.19 τ_1 variation	93
B.20 E_m variation	93
B.21 Cell capacity variation	94
B.22 Before parameter estimation	94
B.23 After parameter estimation	95
B.24 R_0 variation	95
B.25 R_1 variation	96
B.26 τ_1 variation	96
B.27 E_m variation	97
B.28 Cell capacity variation	97
B.29 Before parameter estimation	98
B.30 After parameter estimation	98
B.31 R_0 variation	99
B.32 R_1 variation	99
B.33 τ_1 variation	100
B.34 E_m variation	100
B.35 Cell capacity variation	101
B.36 Before parameter estimation	101
B.37 After parameter estimation	102
B.38 R_0 variation	102
B.39 R_1 variation	103
B.40 τ_1 variation	103
B.41 E_m variation	104
B.42 Cell capacity variation	104
B.43 Before parameter estimation	105
B.44 After parameter estimation	105
B.45 R_0 variation	106
B.46 R_1 variation	106
B.47 τ_1 variation	107
B.48 E_m variation	107
B.49 Cell capacity variation	108
D.1 SiO ₂ deposition in the air electrode a.) during high discharge current density b.) during low discharge current density [8]	125
D.2 Si-air cell illustration [9]	126
D.3 MnF ₂ formation on MnO ₂ particulates in air electrode [9]	126
D.4 ΔV cell, anode and cathode [10]	127
D.5 Impedences of the Si anode and the air cathode [10]	127
D.6 RTIL2 Chemical structure [11]	129
D.7 RTIL1 Chemical structure [11]	129

D.8	Chemical structure of EMI·(HF)2.3F RTIL (a) EMI cation, (b) H_3F_4 (30%) and H_2F_3 (70%) anions [8]	129
E.1	MECO Cu plating equipment	133
E.2	Fumehood used in MEMS lab	134
E.3	Weighing machine in MEMS lab	134
E.4	Metal sputtering equipment in EKL lab	135
E.5	Laser cutter in PV mini module manufacturing room	135

LIST OF TABLES

1	List of molecules mentioned in this thesis	xix
2	List of abbreviations mentioned in this thesis	xx
1.1	Different battery advantages and disadvantages [12] [13].	5
1.2	Batteries applied in Solar energy system [14].	6
1.3	Corrosion reactions that takes places in the alkaline Si-air [15]	9
1.4	Comparing the 3 Si-air cells covered in this literature.	12
1.5	Comparison between various battery models summarized from [16].	12
2.1	Different KOH concentrations used in the experiments	23
3.1	Average OCP and OCP voltage drop rate for each concentration.	27
3.2	Discharge voltage drop rate for each concentration.	28
3.3	Pre-wetting effect on Average OCP and voltage drop rates.	30
3.4	Pre-wetting effect on discharge voltage drop rates.	30
3.5	OCP analysis when different Si type is used as anode from Figure 3.4a.	31
3.6	DP analysis when different Si type is used as anode.	32
3.7	Comparison study of cell potential curves from this thesis and cell curves reported by Durmus et al. [4].	34
4.1	Variables used in the model.	38
4.2	Final values for the cell parameters for Li-ion battery model.	45
5.1	Cell capacity values for each concentration for n-type Si anode and normal air cathode.	52
5.2	Cell capacity variation with pre-wetting (PW)	56
5.3	Cell capacity value when under pre-wetted air cathode and KOH 60% conditions	58
B.1	R_0 values for each concentration for n-type Si anode and normal air cathode	77
B.2	R_1 values for each concentration for n-type Si anode and normal air cathode	78
B.3	τ_{1} values for each concentration for n-type Si anode and normal air cathode	78
B.4	E_m values for each concentration for n-type Si anode and normal air cathode	78
B.5	Cell capacity values for each concentration for n-type Si anode and normal air cathode	79
B.6	R_0 values under normal air cathode and pre-wetted (PW) conditions	79
B.7	R_1 values under normal air cathode and pre-wetted (PW) conditions	80
B.8	τ_{1} values under normal air cathode and pre-wetted (PW) conditions	80
B.9	E_m values under normal air cathode and pre-wetted (PW) conditions	80

B.10 Cell capacity variation with pre-wetting (PW)	81
B.11 R_0 value when under pre-wetted air cathode and KOH 60% conditions . .	81
B.12 R_1 value when under pre-wetted air cathode and KOH 60% conditions . .	82
B.13 τ_1 value when under pre-wetted air cathode and KOH 60% conditions .	82
B.14 E_m value when under pre-wetted air cathode and KOH 60% conditions . .	82
B.15 Cell capacity value when under pre-wetted air cathode and KOH 60% con- ditions	83
D.1 Different methods of electrodeposition of Si	128
D.2 Bond energies between different elements [17]	131
D.3 Comparing heat of formations	131

CONTENTS

Abstract	iii
Acknowledgements	v
List of Figures	vii
List of Tables	xiii
1 Introduction	1
1.1 Problem at hand	1
1.2 Mitigation.	2
1.3 Current battery technology	3
1.3.1 Role of batteries in the future	3
1.3.2 Metal-air batteries	6
1.4 Si-air battery	7
1.4.1 Primary non-aqueous Si-air cell	7
1.4.2 Rechargeable Si-air cell	7
1.4.3 Primary alkaline Si-air cell	8
1.5 Battery model.	12
1.6 Li-ion battery model	13
1.7 Research Objectives.	13
1.8 Thesis scope	14
1.9 Report outline and approach	14
2 Experimental Setup	17
2.1 Overview of experimental setup.	17
2.1.1 Criterion/Requirements	17
2.1.2 Sample electrode preparation	18
2.1.3 Cell preparation methodology	20
2.2 Voltage measurements	21
2.3 Experiment methodology.	22
2.3.1 Effect of varying electrolyte concentration.	23
2.3.2 Effect of pre-wetting air cathode	23
2.3.3 Effect of varying electrode materials	23
3 Experimental results	25
3.1 Variation with electrolyte concentration	25
3.2 Variation with pre-wetting air cathode	28
3.3 Variation with electrode materials	31
3.4 Discussion	33

4	Simscape Model	37
4.1	Battery model parameters	37
4.1.1	Simscape battery block	39
4.1.2	Complete model	41
4.1.3	Parameter estimation	42
4.2	Li-ion battery model	42
4.3	Si-air battery model	45
4.3.1	Assumptions	45
4.4	Conclusion	46
5	Modelling results	49
5.1	Variation with electrolyte concentration	50
5.2	Variation with pre-wetting air cathode	53
5.3	Variation with electrode materials	56
5.4	Discussion	58
6	Conclusions	61
6.1	Experimental conclusion	61
6.2	Modelling conclusion	62
7	Recommendations	65
7.1	Experimental side	65
7.2	Modelling side	66
A	Cell discharge curves	69
B	Model outputs	77
B.1	Variation with KOH concentration	77
B.2	Variation with air cathode pre-wetting	79
B.3	Variation with electrode materials	81
B.4	Model plots	83
C	MATLAB script	109
D	Si-air cell rechargeability using electrodeposition	123
D.1	Primary non-aqueous Si-air cell	123
D.2	Electrodeposition of Si in room temperature	125
D.3	Room temperature Ionic Liquids (RTILs)	129
D.4	Voltage measurement from AutoLAB	130
D.5	Conclusion	130
D.5.1	Previous thesis plan	130
D.5.2	Electrodeposited Si be used as anode for 2 nd discharge?	131
E	Equipment used	133
E.1	Meco CU plating equipment	133
E.2	Fumehood	134
E.3	Weighing machine	134
E.4	Trikon Sigma 204 Dealer	135
E.5	Laser cutter	135

[Bibliography](#) 137

NOMENCLATURE

Table 1: List of molecules mentioned in this thesis

Molecular structure	Meaning
CO ₂	Carbon dioxide
KOH	Potassium hydroxide
Li	Lithium
MnF ₂	Manganese(II) fluoride
MnO ₂	Manganese(IV) oxide
OH ⁻	Hydroxide ions
O ₂	Oxygen
RTIL1	1-butyl-1-methylpyrrolidiniumbis (trifluoromethanesulfonyl) imide
RTIL2	1-butyl-3-methylimidazoliumbis (trifluoromethylsulfonyl) imide
Si	Silicon
SiCl ₄	Silicon tetrachloride
SiF ₄	Silicon tetrafluoride
Si(OH) ₄	Silic acid
SiO ₂	Silicon dioxide
α – Si	Amorphous Si

Table 2: List of abbreviations mentioned in this thesis

Abbreviation	Meaning
ΔE_{cell}^0	Standard cell potential
ΔE_{cell}	Cell potential
ΔG	Gibb's free energy
AFM	Atomic force microscopy
BESS	Battery Energy Storage System
BMS	Battery management system
EDX	Energy-dispersive X-ray spectroscopy
EIS	Electrochemical impedance spectroscopy
E_m	No-load voltage parameter
EMI(HF)2.3	RTIL used by Eli and Cohn
EV	Electric vehicles
F	Faraday's constant
FTIR	Fourier-transform infrared spectroscopy
n	No of electrons exchanged
n-type Si	Silicon doped with Group 14 elements
OCP	Open circuit potential
OER	Oxygen evolution reaction
ORR	Oxygen reduction reaction
p-type Si	Silicon doped with Group 13 elements
Q	Reaction coefficient
R	Universal gas constant
R_0	Electrolyte resistance cell parameter
R_1	Polarization resistance cell parameter
RES	Renewable energy sources
RTIL	Room temperature ionic liquid
SEM	Scanning electron microscopy
SOC	State of charge
T	Temperature
τ_1	Polarization capacitance cell parameter
V	Voltage
V_{exp}	Experimental voltage
V_{sim}	Simulated voltage
XPS	X - ray spectroscopy
α - Si	Amorphous Si

1

INTRODUCTION

As there is a rise in demand for efficient and feasible battery systems with growing share in renewable energy production and electric vehicles. Si-air batteries is a battery system that could gain favor over Li-ion batteries due to abundance of its raw materials. However, it is still a niche topic and has not developed to compete with other battery systems in the current market. Further research and development can determine its feasibility. Although a working primary Si-air cell is present, it still has issues similar to the current metal-air battery technology. In order to determine its feasibility, various studies and experiments must be carried out.

1.1. PROBLEM AT HAND

It has come to the attention of most governmental bodies and the general public about the threat of global warming. It should also be noted that most countries recorded their highest ever temperature in 2019. For example, July 25th 2019 marked the hottest day ever since the first recorded temperature at 1901 in the Netherlands [18]. It was reported by Allen et al. in 2009 that the carbon dioxide emissions into the atmosphere is estimated to be over 3.67 trillion tonnes of carbon dioxide since beginning of industrialization, which would lead to a carbon dioxide caused warming of 2.2 °C above the pre-industrial temperatures by the year 2500 [19]. According to IPCC 2018 report, there is only one-in-two to two-in-three chance of warming remaining below or staying at 1.5 °C by around 2100 [20]. The promotion of renewable energy can aid in reducing these effects as it is reported by Gielen et al. that renewable energy could potentially supply two-thirds of the total energy demand and contribute to the bulk of the greenhouse emissions reductions that is needed between 2019 and 2050 to keep the surface temperature rise below 2 °C [21].

In the year 2004, the distribution of primary energy demand share among the various energy generation resources was 77.8% from fossil fuels such as oil, natural gas and coal. This has contributed significantly to green house emissions as we can see that for every tonne of energy in combustion of wood, coal, oil and natural gas we release 4.6, 4, 3.1

and 2.3 tonnes of carbon dioxide, respectively [22]. It is also worrisome to note that last century, 1100 gigatonnes of CO_2 was emitted to meet the energy needs. If this trend is left unchecked, it is predicted that another 2800 gigatonnes of CO_2 is emitted by the end of this century [22]. In order to address this emission, it is imminent to shift our primary energy demand to electricity [21]. This is mainly due to emission free production of electrical power using photovoltaic panels (solar) and wind turbines (wind) and the ease to convert electrical energy to heat energy when required. However, there are many issues that make power generation from renewable energy sources (RES) difficult.

1.2. MITIGATION

Even though it is possible to generate electrical power without any CO_2 emissions using solar and wind power, the availability of these resources are highly variable. They have seasonal and daily variations, which cause power fluctuations that might not meet the real-time energy demand. In order to address this issue of variability, we look into energy storage methods that are portable and economically feasible in the short term. One of the growing research is on battery energy storage systems (BESS), which is elaborated in Section 1.3.1. A growing interest in metal-air batteries is seen due to its higher theoretical energy density than the conventional Li-ion cell [2]. This makes it an ideal electrical storage unit for electrical vehicles and for power storage facilities. However, there are various issues that come with metal-air batteries.

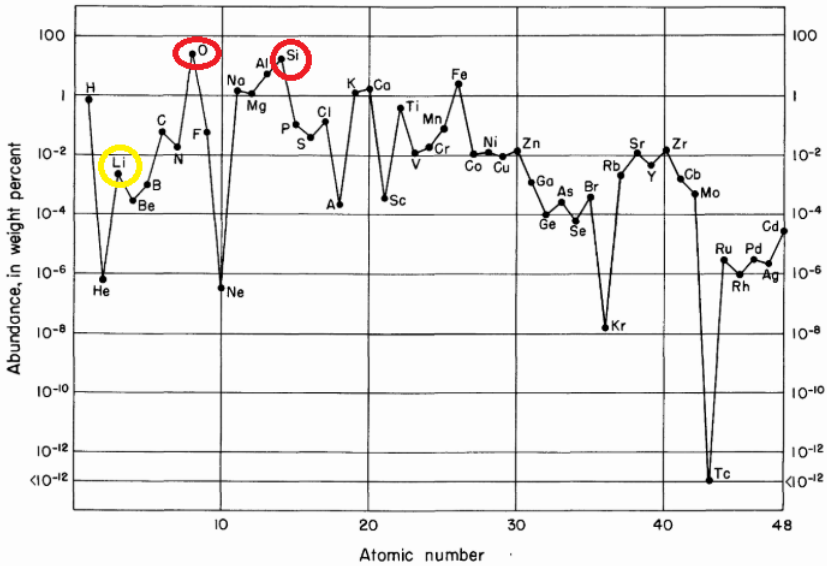


Figure 1.1: Abundances of elements [1]. Si and O marked in red, Li is marked in yellow.

Metal-air batteries have very high theoretical energy densities, their practical energy densities are much lower compared to the theoretical energy densities. For example,

Li-air batteries, which have the highest theoretical energy density among the metal-air batteries, in reality, have an energy density of about 0.26 times its theoretical values [23]. This is mainly due to the clogging of air cathodes with metal oxides [10]. It is also critical to note that Li is a rare earth metal, which has very low abundance in the earth's crust compared to other metals. Hence, we look into a battery system that utilizes the two most abundant materials in the earth's crust. These are oxygen and silicon which are about 46.6% and 27.72% in weight percent respectively [1]. This can be seen in Figure 1.1. This is further elaborated in Section 1.3.2.

The abundance of raw material makes Si-air batteries a viable candidate to replace Li-ion batteries for research and development. However, we see that further development must be made in these cells to make it competitive with the battery technologies in the market.

1.3. CURRENT BATTERY TECHNOLOGY

In this section, we shall cover why there is a need for a energy storage system in power systems of today and the future. We shall also explore the reasons why battery storage is the most preferred means of energy storage. Finally, we shall delve more into what makes metal-air batteries a growing area of interest for research.

1.3.1. ROLE OF BATTERIES IN THE FUTURE

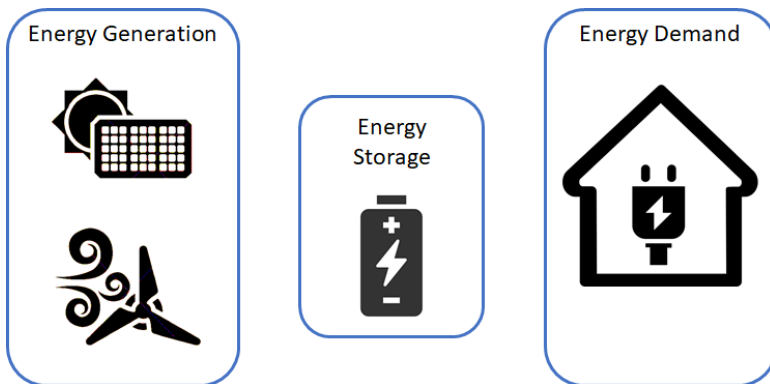


Figure 1.2: Different components of an energy system of the future.

We see that current electrical power generators that make use of fossil fuels like gas and coal or nuclear are able to meet the power demand in real-time. Hence, there was a lack of research into electrical storage technologies [12]. However, now that renewable electrical power generators such as solar power and wind power rely on the availability of natural resources (for solar power the availability of sunlight and the availability of wind for wind power), there are seasonal or even daily variations in power production. In the case of solar power, there will be no electrical power production at night but there is high demand. During the day, large amounts of electrical power can be produced but there

is relatively low electrical power demand. In Figure 1.2, we see the various components of this system. We see a mismatch occurring here which can be mathematically represented as:

$$\text{Mismatch} = \text{Generation} - \text{Consumption} \quad (1.1)$$

In Equation 1.1 we can see 3 cases occurring:

- *Case I - Power deficit:* When the mismatch is negative. It means that there is high electrical power demand but the electrical generator is not able to supply the electrical power demand completely. This can be due to lack of availability of natural resources or there is a very high electrical power demand. Hence, there is a power shortage and extra power must be supplied.
- *Case II - Power surplus:* When the mismatch is positive. It means that there is high electrical power generation due to large availability of natural resources such as nominal wind speeds or high irradiation and solar energy. Hence, there is excess power production and this power needs to be stored.
- *Case III - Power balance:* When the mismatch is zero. It means that the power generated and the power demand is equal. Electrical power grids at present work in this principle. Hence, the need for an energy storage system is not required.

An energy storage system is a solution to this conundrum in the short term such as for a mismatch that spans for days as it can store energy at the time of Case II - Power surplus. The stored energy can then be used as the extra energy needed when there is a Case III - Power deficit. However, if this mismatch seems to persist for more than a few days, other means of energy storage such as H₂ or NH₃ storage become more viable and economically feasible [24] [25] [26]. This gives battery energy storage technology a vital role for short term storage in the power grids of the future and energy storage in electric vehicles. It converts the electrical energy from PV panels or wind turbines to chemical energy in the battery during charging. The battery on discharging converts the stored chemical energy into electrical energy.

Some of the common BESS used in power system applications are reported by Divya et al. and Luo et al. and a brief description about them is given below:

1. *Lead acid:* Further divided into 2 types known as flooded types and valve regulated lead acid (VRLA) batteries - where the batteries are closed and the components are immobilized. The anode used is sponge lead. The cathode used is lead oxide. The cell electrolyte is aq. sulphuric acid [12] [13].
2. *Sodium sulphur (NaS):* Produces about voltages of about 2 V and is kept at around 300 °C. The anode used is molten sodium. The cathode used is molten sulphur. The cell electrolyte is solid beta alumina ceramic [12] [13].
3. *Lithium ion (Li-ion):* One of the most commonly used battery technology nowadays. Mostly used in electric vehicles now a days. The anode used is graphite. The cathode used is lithiated metal oxide. The cell electrolyte is lithium salts in organic carbonate [12].

4. *Metal-air*: Electrolyte can be in liquid or solid polymer membrane saturated with KOH. The anode used is aluminium or zinc metals. The cathode used is porous carbon or metal mesh with catalysts. The cell electrolyte is alkaline hydroxide solutions [12].
5. *Redox-polysulphide bromide (PSB)*: Produces voltages of about 1.5 V. The anodic solution used is sodium disulphide. The cathodic solution used is sodium tribromide. The cell membrane used is an ion exchange membrane [13].
6. *Vanadium re-dox (VRB)*: Produces about voltages of the range 1.4 V to 1.6 V. The anodic solution used contains V^{2+} & V^{3+} . The cathodic solution used is VO_2^+ & VO^{2+} . The cell membrane used is H^+ ion permeable polymer membrane [13].
7. *Zinc Bromine (ZnBr)*: Produces voltages of about 1.8 V. The anode used is zinc. The cathode used is Bromide. The cell membrane is micro-porous poly olefin membrane [12].

Table 1.1: Different battery advantages and disadvantages [12] [13].

Technology	Advantage	Disadvantage
Li-ion	Small size Low weight Highest energy density Storage efficiency close to 100%	High cost Deep discharging affects lifetime Low lifetime (about 5 years) Uses rare earth metal (Li) as raw material
NiCd & Lead Acid	Supply pulsed power	Very large Contains toxic materials Severe self-discharge
NaS	Smaller and lighter than NiCd	Operates at 300 degree C Continuous heat demand for electrolytes
Metal-air	Low cost High energy density	Very difficult to be recharged
Flow battery	Suitable for long durage storage	High capital High running costs A lot of machinery involved such as pumps and flow control.

Among all the battery technologies, the most commonly used battery energy storage system in the market today are Li-ion, NaS and NiCd. However, there are some major drawbacks among these technologies as listed in Table 1.1. The potential in which batteries and solar energy go hand in hand are studied even further by Li et. al [14]. Here, it was studied how solar energy charges a given battery technology and what is the active material in the battery energy storage system. It is summarized in the Table 1.2.

Table 1.2: Batteries applied in Solar energy system [14].

Battery technology	Active material	Effect
Li-ion	Cathode (Li) oxidized by photoexcited holes. Li is the active material.	Sluggish insertion/ extraction of ions in Li cathode
Li - O ₂	O ₂ is the active material.	Deposited Li ₂ O ₂ enables photoexcited holes to oxidise photoelectrode & High discharge capacity
Li - catholyte	Li is the anode in this case and Sulphur or Iodine is active electrode	Flowable design and high discharge capacity
Redox flow	Soluble redox species	Flowable design, no dendrite formation in the case of Li

1.3.2. METAL-AIR BATTERIES

In this section, we shall see the growing research and problems faced by metal-air batteries. This type of battery is known for its high theoretical energy density, which is about 3 to 30 times more than Li-ion batteries, and use of the air cathode that is a readily available resource [2]. In metal-air batteries, we see that the air cathode is always the limiting factor when it comes to determining the cell performance [2]. There are mainly 2 types of metal air batteries: aqueous and non - aqueous metal air batteries. Some of the main types of metal-air batteries and their theoretical densities are given in the Figure 1.3.

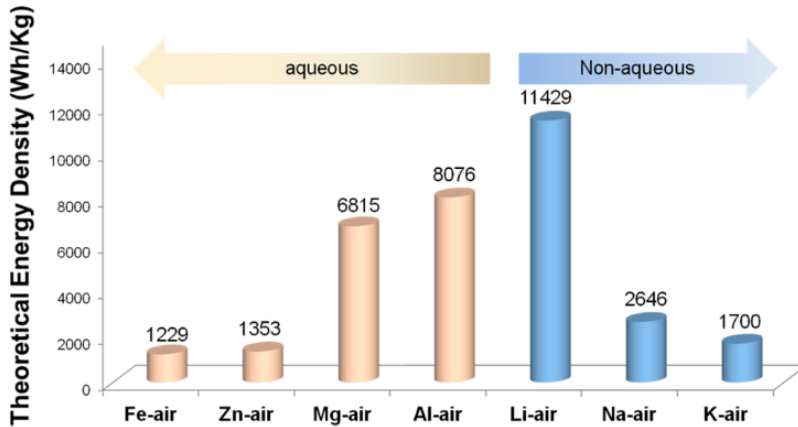


Figure 1.3: Different types of metal-air batteries [2].

In order to make a metal-air battery rechargeable, we need to make sure that there is an oxygen reduction reaction (ORR) at the cathode during the discharge process of the

battery and an oxygen evolution reaction (OER) during the charge process as well. This is done using a few approaches [2]:

1. with the help of bi-functional oxygen electrocatalysts at the air cathode.
2. flexibility of air-cathode design - optimize OER and ORR catalysts separately.

Common issue faced is the poor cycling stability of the air cathode [2]. One way to overcome this is to make it a bicathode configuration where there is one cathode for charging and another cathode for discharging [2]. Li et al. also gives more examples and studies on Li-air batteries and the specific issues they face as well [2].

1.4. SI-AIR BATTERY

Primary Si-air cells using alkaline [4] and non-aqueous room temperature ionic liquids (RTILs) [27] are discovered and a secondary Si-air cell using oxygen shuttle concept [3] is also developed that operates at a temperature of 1073 K, which is not desirable in practical applications [28]. However, in this thesis we shall focus on the alkaline Si-air battery and study its discharge characteristics in depth and more general information regarding the battery system can be found in Section 1.4.3. In this section we shall study literature on Si-air batteries. We shall discuss what are the main components, the various types and modelling so far and working principles.

1.4.1. PRIMARY NON-AQUEOUS SI-AIR CELL

Cohn et al. explored a potential electrochemical cell using Si-O₂ couple. The cell shows a potential specific energy of 8,470 W h/kg and an energy density of 21,090 W h/l, theoretically outperforming H₂/O₂ system and comparable to Al/O₂ couple which has a specific energy of 8,146 W h/kg and 21,994 W h/l [27]. More information regarding this cell can be found in Appendix D.1.

1.4.2. RECHARGEABLE SI-AIR CELL

Inoishi et al. reported that it is possible to recharge a Si-air cell using an solid oxide ion conducting electrolyte based on oxygen ion conducting electrolyte [3]. The cell employs Ca stabilized ZrO₂ (CSZ) and gave 20 stable charge-discharge cycles with a discharge capacity of 600 mAh g_{Si}⁻¹. However, it is critical to note that the temperature of this battery operation is at 1073 K making it very undesirable. In order to avoid cell degradation by oxidation of electrode and depletion of Si, space was given between Si and Pt electrodes in low partial pressure of oxygen (P_{O₂}) side so that reaction between Si powder and electrode is prevented [3]. It can also be observed that there is an increase in capacity which is associated to the increased porosity or decreased particle size of Si powder. It is critical to note that in this cell, the active ion is the oxygen ion and not Si as in the primary Si-air cell that is discussed in Appendix D.

The fuel electrode reaction for this Si-air cell is given as:



The air electrode reaction is given as:



The Si powder reacts chemically with atmospheric oxygen permeated from air cathode, this is done in order to create a low partial pressure in the anode chamber which creates a pressure difference in order to facilitate the flow of air through the cell:

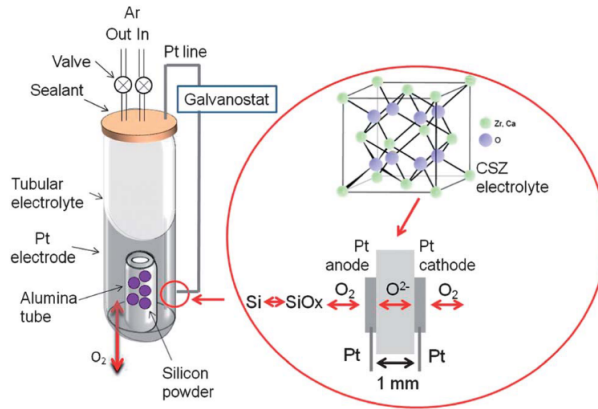


Figure 1.4: Experimental setup of the rechargeable Si-air cell using Ca stabilized ZrO_2 (CSZ) [3].

It is found that although SiO is the major discharge product, there is SiO_2 being formed after discharge. The experimental set-up of this cell is shown in Figure 1.4. Although it is confirmed that Si-air cells can be rechargeable using a solid state battery system and operating it at high temperature conditions. The cost of this system really expensive with the use of Zr and Pt electrodes. Hence, looking into replenishing the Si anode during charging is another way we can try to obtain recharge-ability in the primary Si-air cell as these systems will be at room temperature and much cheaper compared to the above system.

1.4.3. PRIMARY ALKALINE SI-AIR CELL

The Figure 1.5 is a simple illustration of the alkali Si-air cell is shown and how the components interact with each other. Extensive studies on As-doped crystalline Si of thickness 0.6 to 3.0 mm in KOH solution was carried out by Durmus et al. [29]. The battery cell was discharged in a 5 M KOH electrolyte. The discharge times varied from 260 hrs to 1100 hrs at a current density of 0.05 mA/cm^2 . It was reported that, when a discharge current density of more than a passivation threshold current density of 0.05 mA/cm^2 , passivation of the Si anode layer occurs [29] which will be elaborated in this section. It was found that

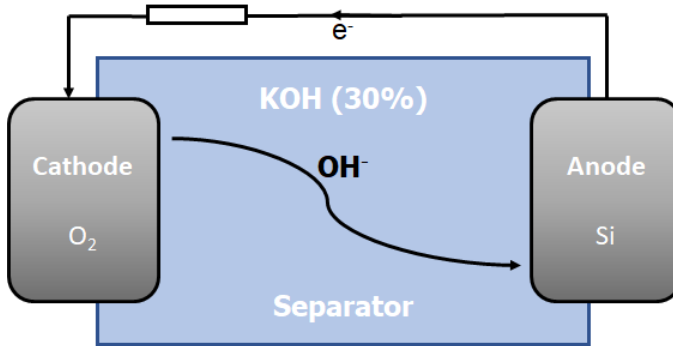


Figure 1.5: Si-air illustrative diagram showing flow of electrons and ions during discharge cycle.

the cell performed to specific energy of 140 Wh/ kg. However, due to the contact of aqueous electrolyte, which is in this case KOH solution, some of the Si is corroded or etched away into the solution. The electrochemical reactions during discharge that takes place in the Si anode and air cathode can be seen in detail as reported by Weinrich et al. where the cell discharges to form silicic acid ($\text{Si}(\text{OH})_4$) [15] [4] [30]:

The anodic electrochemical reaction:



The cathodic electrochemical reaction:



The overall electrochemical reaction:



Table 1.3: Corrosion reactions that takes places in the alkaline Si-air [15]

Reaction site	Reaction
Anodic	$\text{Si} + 4\text{OH}^- \rightleftharpoons \text{Si}(\text{OH})_4 + 4e^-$
Formation of Silicate:	$\text{Si}(\text{OH})_4 + 2\text{OH}^- \rightleftharpoons \text{SiO}_2(\text{OH})_2^{2-} + 2\text{H}_2\text{O}$
Cathodic:	$\text{O}_2 + 2\text{H}_2\text{O} + 4e^- \rightleftharpoons 4\text{OH}^-$
Corrosion:	$\text{Si} + 2\text{OH}^- + 2\text{H}_2\text{O} \rightleftharpoons \text{SiO}_2(\text{OH})_2^{2-} + 2\text{H}_2$

From the above equations and from Figure 1.5 during discharge, the electrons from the external circuit react with the oxygen in the air cathode to form OH^- ions that moves

through the electrolyte to the positive Si anode. At the anode the OH^- reacts with Si to form silicate. At current densities higher than the passivation threshold of 0.05 mA/cm^2 , these silicates form SiO_2 which creates a passivation layer on the Si anode reducing the performance of the cell as reported by Durmus et al. [4].

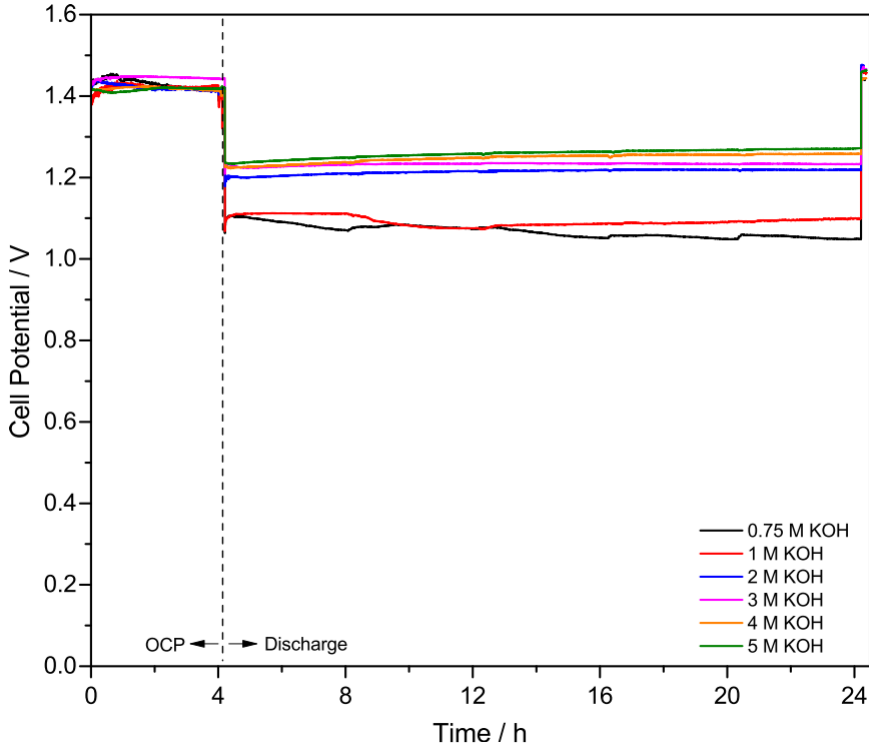


Figure 1.6: Discharge profile of Si-air cells with 0.05 mA/cm^2 for various KOH concentrations [4].

It was also reported by Durmus et al. [4] about the influence of KOH concentration on the cell potential profile which is crucial to this thesis. Si-air cell experiments were conducted at 25°C with 0.05 mA/cm^2 which is plotted in Figure 1.6. Some key takeaways from this plot are:

1. Open-circuit potentials (OCPs) were around 1.4 V and KOH concentration had no major influence on the OCP profile.
2. Discharge potentials (DP) tend to increase with discharging time. It is attributed to the surface reaction kinetics of the Si anode.
3. Passivation of Si anode surface occurs for currents more than 0.05 mA/cm^2 .

It is known that the open-circuit potential (OCP) is mainly the chemical thermodynamics of the electrochemical reaction.

The cell potential of a battery cell is calculated using the Nernst equation as shown in Equation 1.9 [31]:

$$\Delta E_{cell} = \Delta E_{cell}^0 - \frac{RT}{nF} \times \ln Q \quad (1.9)$$

$$\Delta G = -nFE_{cell} \quad (1.10)$$

where,

ΔE_{cell}	: Cell potential at temperature T	Voltage [V]
T	: Temperature	Kelvin [K]
Q	: Reaction Quotient	[-]
n	: Electrons transferred in reaction	[-]
F	: Faraday's Constant = 96500	Coulomb per mol [C/mol]
ΔE_{cell}^0	: Cell potential at standard conditions	Voltage [V]
ΔG	: Gibbs's Free Energy	Joules [J]

The reaction quotient (Q) for a reversible chemical reaction $aA + bB \rightleftharpoons cC + dD$ is:

$$Q = \frac{[C]^c [D]^d}{[A]^a [B]^b} \quad (1.11)$$

where,

a	: Stoichiometric coefficient of reactant A	[-]
b	: Stoichiometric coefficient of reactant B	[-]
c	: Stoichiometric coefficient of product C	[-]
d	: Stoichiometric coefficient of product D	[-]

In the Equation 1.9, the reaction quotient is the natural logarithm of the ions participating in the electrochemical cell which is further elaborated in Equation 1.11. The reaction quotient is the ratio of the rate of product formation reaction and the rate of reactant consumption reaction. The concentration of an electrolyte plays a role in the cell's open-circuit potential (OCP) contrary to what was reported earlier by Durmus et al. of a steady 1.4 V OCP for KOH concentrations ranging from 0.75 M to 5 M.

In order for a reaction to be spontaneous we know that the Gibbs's free energy (ΔG) of the reaction should be negative. This means that the cell potential (ΔE) of the given cell must be positive for it to be a spontaneous reaction [31]. The observation of discharge potentials increasing with constant current discharge is noteworthy as it would mean the cell potential increases as the battery gets used up or as the state of charge (SOC) of the cell drops.

To summarize on Si-air batteries and their components. We can see the Table 1.4 below where some interesting points that can be made between the 3 Si-air cells are:

Table 1.4: Comparing the 3 Si-air cells covered in this literature.

	Cohn et al. [27]	Inoishi et al. [3]	Durmus et al. [4]
Rechargeability	Primary	Secondary	Primary
Anode	heavily doped Si	Si powder	heavily doped Si
Electrolyte	RTIL	Oxide ion conductor	KOH
Cathode	Porus carbon	Porus carbon	Porus carbon
Temperature	Room temperature	1073 K	Room temperature
Active element	Si	O ₂	OH ⁻

In this thesis, a Simscape model of the battery operation of the alkaline Si-air cell is developed using the Li-ion battery model as reference in MATLAB. Experiments were carried out in the MEMS lab using a fabricated Si-air cell in order to support the Simscape model with the necessary input data.

1.5. BATTERY MODEL

Experimenting with batteries is a time consuming and tasking procedure. Computer simulations of the battery operation are made in order to predict battery performance under various conditions and several types of battery models are available. These battery models are mainly used to calculate the ohmic loses in batteries, hysteresis and polarization time constants. The battery models are mainly classified as [16]:

Table 1.5: Comparison between various battery models summarized from [16].

	Electrochemical	Behavioural	Equivalent circuit-based
Working	Partial differential equations	Empirical functions	RC circuit elements
Accuracy	High	Not as high as electrochemical models	Most simplified model of the three
Computational intensity	High	Moderate	Least
Battery management system modelling	Not suitable	Weak candidate	Best candidate

- *Behavioural models*: use empirical functions to model battery dynamics. Examples of a zero-state hysteresis model, one-state hysteresis model and a self-correcting model were given in [16].
- *Electrochemical models*: use partial differential equations to simulate the mass transfer and reaction rates of the electrochemical cell [16].

- *Equivalent circuit-based models:* use simple (resistance capacitive) RC circuit elements to model the battery dynamics. The battery is modeled using the Thevenin based model [32].

As seen in Table 1.5, although electrochemical models provide a physical insight into the battery operation, it is computationally intensive that makes it very time consuming [16]. Hence, it is not an ideal candidate for a real-time battery management system (BMS) simulation.

The Photovoltaic Materials and Devices (PVMD) research group of TU Delft has developed a toolbox that is used for monitoring Photovoltaic (PV) system and to predict the energy yield for different PV system configurations such as bifacial floating PV systems and Photovoltaic thermal hybrid (PVT) systems [33]. In order to integrate with the existing PVMD toolbox that can operate with solar panel simulations, an equivalent circuit-based model makes the computation much simpler and has the appropriate level of accuracy [16].

1.6. LI-ION BATTERY MODEL

Simscape is a subset tool of MATLAB Simulink environment that helps in creating models of established physical systems such as DC motors, wind turbines, actuators and many other such systems [34]. Battery models are physical component blocks that are available in Simscape which use the equivalent circuit model to simulate the battery dynamics. A battery model example is made by MATLAB for a Li-ion cell (LiFePO_4) [7]. This example is used as a reference and as guide for making the Si-air battery model and further details can be found in the Section 4.

1.7. RESEARCH OBJECTIVES

The primary objective of this thesis is to **develop a battery model of the alkaline Si-air battery**. In order to reach this objective, this thesis aims to answer the effect of cell parameters used in the model on:

- *Constant current discharge.*
- *Electrolyte concentration variation.*
- *Pre-wetting of air cathode.*
- *Si anode variation.*

By answering the above questions, the battery model can be validated and analyzed for its operation in different physical conditions that the Si-air cell can be subjected to. It can also answer whether we can simulate Si-air battery performance at different conditions by changing the cell parameters.

1.8. THESIS SCOPE

Si-air batteries is a very novel research topic and it can be very exploratory. It is imperative that the scope of the thesis must be defined before hand. Hence, the below statements have been made:

- The mathematical model being developed will be in Simscape which utilizes the inbuilt physical block for battery operation modeling in MATLAB developed by MathWorks.
- The literature study consists of three Si-air cells but the battery model has been validated only for alkaline Si-air cell which utilized KOH as its electrolyte due to the easy access to the raw materials required for the experiments.
- There are several physical conditions that can be changed in the Si-air cell but the effect of variation in electrolyte concentration and electrode materials is only explored in this thesis.
- Temperature is a significant factor that influences a battery operation. In this model however, temperature effect is not accounted for as the experiments were conducted in the MEMS lab where large temperature variations is not possible.

1.9. REPORT OUTLINE AND APPROACH

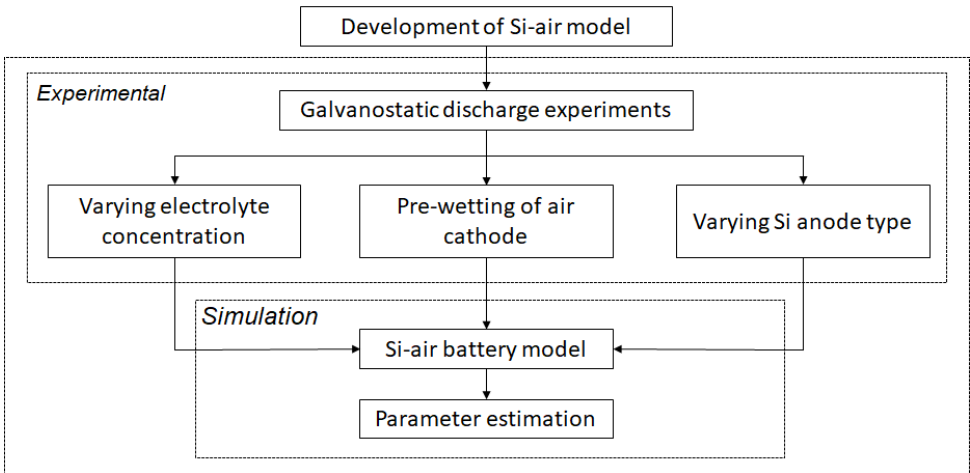


Figure 1.7: Thesis outline

Figure 1.7 shows the general thesis outline. The report begins with Chapter 1 where the topic of batteries is introduced in Section 1.3. The different kinds of batteries are explored and their limitations are discussed here as well. A general background into battery modelling is given in Section 1.5. Chapter 2 reports the experimental setup and details of the fabrication of Si-air cell used to conduct the galvanostatic discharge measurements is given here. A brief description about the experiment methodology is also

given in the section. The experimental results are given in Chapter 3 where the experimental results are reported and discussed. The Simscape model and its parameters are further elaborated in Chapter 4 and the modelling results are illustrated and discussed in Chapter 5. The thesis concludes with Chapter 6 with the thesis conclusions and some recommendations on the experimental and modelling side of this thesis in Chapter 7.

The appendix of this thesis consists of cell discharge curves in Appendix A which contains the galvanostatic voltage measurements of the samples. Appendix B contains the model outputs that calculates the variation in cell parameters and the model matching the simulated voltage and experimental voltage. The MATLAB script used for running the model is given in Appendix C. Appendix D contains data and some research on the investigation of Si-air cell rechargeability using electrodeposition of Si using room temperature ionic liquids (RTILs) which was changed due to the closure of EKL labs as an effect of the COVID19 outbreak. The thesis is closed with Appendix E which contains the list of experimental equipment used.

2

EXPERIMENTAL SETUP

THE goal of this thesis is to simulate the working dynamics of a battery operation during discharge using Simscape modelling in MATLAB. In order to validate this model, input from experimental battery discharge operation is taken and compared. The various cell parameters of the battery model is studied and having experimental data to support the model is critical to this thesis. This chapter presents an overview of the experimental setups in Section 2.1 , the requirements of the experiments in Section 2.1.1, the experimental methodology and about the sample preparation in Section 2.3 and Section 2.1.2 respectively. More details on the equipment used is available in Appendix E.

2.1. OVERVIEW OF EXPERIMENTAL SETUP

In order to study the Si-air battery using experiments, first we must note the criteria and requirements of the experiments based on the research objectives of the thesis to create a Simscape model and understand the working of the Si-air cell and find the significant cell parameters of the model.

2.1.1. CRITERION/REQUIREMENTS

According to previous studies and literature, it is understood what are the necessary materials required for the experiments and how to set it up in-order to study the variation between various components in the Si-air cell such as the electrolyte, the anode and the cathode and its effect on the battery discharge curves. The following criteria needs to be considered for the experimental setup:

- *Discharge curves* - in order to study the discharge curves of a battery an experimental equipment is required where the discharge current can be controlled and maintained. The equipment must also facilitate the ability to read potential readings of the cell throughout the discharge period.
- *Fumehoods* - in order to fabricate the Si-air cell and prepare the electrode and electrolyte for the cell in a safe working environment with no spillage.

- *Personnel protective equipment (PPE)* - in order to promote safe working practise. It is essential that lab coats and eye wear is used while working in the MEMS lab.

It is noted what all are the output parameters of the experiments. In this section, the preparation of each cell component for the experiment before discharge potential evaluation is elaborated below. The cell design and its motivation is detailed and mentioned later.

2.1.2. SAMPLE ELECTRODE PREPARATION

In this section, we shall cover how to prepare the electrodes of the Si-air cell. The electrodes used are the silicon anode and the air cathode.

SI ANODE

Before the Si anode is fixed into the battery system, it must be prepared properly by cutting it to the sample size and adding a back contact surface. In order to study the effects of the electrode materials on the discharge curves of the battery system, both n-type and p-type Si wafers are used. These wafers are four inches in diameter and purchased from Topsil Semiconductor Materials A/S. The Si wafer undergoes the following preparation steps:

- *Back contact:* In order to improve the performance of the Si-air battery cell, a 375 nm thick layer of aluminium containing 1% silicon (Al:Si) which would function as a current collector. The Al:Si layer is deposited on the Si-anode using the Trikon Sigma 204 sputtering coating machine in the EKL CR10,000. This is done as it is reported by Krawczak et al. that the solar cell resistances decreased considerably when aluminium contacts were used in CIGS cells [35]. This was also seen when heterojunction solar cells and silicon solar cells [36] [37]. This could aid in obtaining a Si-air cell with higher performance. Further details regarding the equipment can be found in the Appendix E.
- *Laser cutter:* After back contact Al:Si layer deposition, the wafers need to be cut into small square pieces of 2 cm x 2 cm. The laser cutter available in the PV mini-module assembly workshop can be used to scribe deep lines and the wafers can be broken in to small pieces by hand. The laser cuts the Al:Si deposited side in order to keep the front Si side defect free.

AIR CATHODE

The air cathode used in the Si-air battery cell system in the experiments are provided by the E-4 air cathode manufactured by Electric Fuel [5]. The air cathode is obtained from the manufacturer as a roll shown in the Figure 2.1. The air cathode is manganese based catalysed carbon and supported onto a nickel mesh. This air cathode is mostly used in metal-air batteries. For the experiments presented in this thesis the air electrode is prepared and used in two different ways:

- *Normal (non-wetted):* From the air cathode roll as shown in Figure 2.1 above a piece of approximately 2 cm x 2 cm is cut. The activated charcoal side is protected

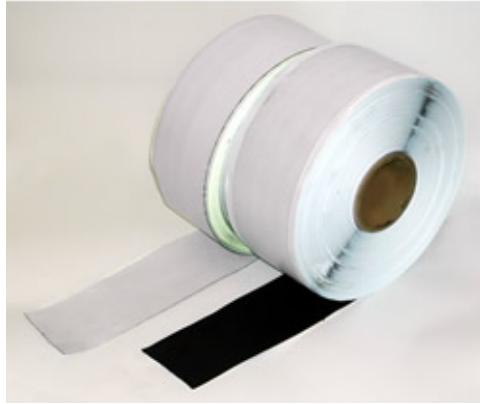


Figure 2.1: Air cathode rolls as given by manufacturer [5]

using an adhesive covering, which is removed right before the air cathode is fixed into the battery system so that there is minimal external environment exposure on the air cathode surface.

- *Pre-wetted*: Similar to non-wetted air cathode operation condition, the air cathode sample is cut. However, in this condition the air cathode is soaked in the electrolyte solution which is in this case the KOH solution overnight. This is done in order to study the discharge curves when the air is under pre-wetted conditions as it was found that pre-wetting the battery had significant effects on the battery performance [30].

KOH ELECTROLYTE

The KOH electrolyte solution is prepared using KOH pellets purchased from Sigma Aldrich. As per the manufacturer, the pellets are $\geq 95\%$ pure. The purity is assumed to be at 95% for approximation. The following steps are carried out in order to prepare the KOH solution with 'x' g KOH in 100 ml water:

1. A mass of 'x' g of KOH pellets is measured using a weighing balance in the MEMS lab in EKL using a spatula. The KOH pellets are used as the solute of the solution.
2. A beaker is filled with 100 ml of water to act as the solvent of the solution.
3. The measured KOH pellets is slowly added into water with slow stirring.
4. Once the KOH pellets are completely dissolved into the solution, the solution is ready for experimentation.

The prepared KOH solution is poured into the inner cell compartment of the assembled Si-air cell. The Si-air cell is placed on a glass dish in order to observe any leakage from the system. The KOH solution is also used to soak the air cathode for the pre-wetted air cathode condition.

2.1.3. CELL PREPARATION METHODOLOGY

In order to hold the electrodes, electrolyte solution, and the connecting wires together, a custom battery cell was designed and manufactured. It is designed in such a way that the electrodes must stay in place throughout the operation and the electrolyte can be poured into the system once the electrodes were fixed. Provisions for outlets for air intake and for connecting wires to come out the battery cell system is incorporated in the design stage. The fabrication of the Si-air cell is detailed further below.

FABRICATION OF SI-AIR CELL

The Si-air cell components are manufactured out of polytetrafluoroethylene (PTFE), commonly known under the brand name Teflon. The components were then outsourced by DEMO for manufacturing.

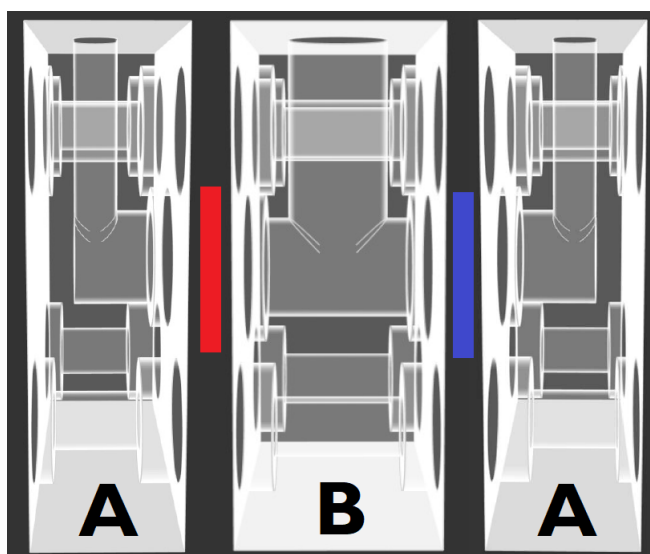


Figure 2.2: X ray of the full assembled system. The red block indicates the silicon anode and the blue block indicates the air cathode. A and B denotes the outer and inner cell component respectively

The Si-air cell comprises of three parts in total - 2 outer cell components and 1 thicker inner cell component. The outer cell components is attached to the inner cell component, which fixed the electrode sample between them in place as seen in Figure 2.2. The electrodes - Si anode (indicated in red) and the air cathode (indicated in blue), are fixed in the system. The three Si-air cell parts are 50 mm x 50 mm in size. The inner cell components is thicker than the other 2 components with a width of 20 mm which means the distance between the electrode distance is 20 mm. The active area of the electrodes that are exposed to the electrolyte reservoir in the middle is exactly 1 cm². This is done so that it can be easily compared to the results from other publications and calculation simplicity.

ASSEMBLY OF SI-AIR CELL

After the Si-air cell components were fabricated. The electrodes are fixed into the cell using tweezers as shown in Figure 2.2 between the outer and inner cell components. They are pressed tightly to the contact surface using springs and soldered to copper wires which come out the top of the outer cell components. The electrolyte solution is poured from the top of the inner cell component. The cell components are tightened together using nylon screw threads and bolts. PTFE O-rings were used in order to make the Si-air cell seal tight in the electrode and electrolyte interfaces. It is to be noted that there was minor leakage during the running of the experiments which will be elaborated in chapter recommendations. In the Figure 2.3 the final assembled Si-air cell is shown.



Figure 2.3: Isometric view of assembled Si-air cell

2.2. VOLTAGE MEASUREMENTS

Once the KOH solution which is the electrolyte is poured into the Si-air cell and the cell is placed onto the glass dish, the Si-air cell is placed into the MECO Copper plating equipment where galvanostatic discharge experiments are carried out. During these experiments, the connecting wires of the Si-air cell are connected into the positive and negative wires of the equipment. The galvanostat used in the copper plating equipment gives the cell potential output on a computer system using the Metrohm NOVA software by Autolab B.V. The potential of the battery cell is evaluated with a time step of 1 second. The discharge current is kept constant during these experiments and the potential curves are evaluated but with different conditions which is elaborated below:

- *Open-circuit potential (OCP)*: The discharge current is set to 0 A for the initial 30

minutes (1800 seconds) in order to evaluate the open-circuit potential.

- *Discharge potential (DP)*: The discharge current is set $150\ \mu\text{A}$ for the rest of the run in order to evaluate the discharge. It was covered that the active area of the electrode is $1\ \text{cm}^2$ which means the current density in the battery cell used is $150\ \mu\text{A}/\text{cm}^2$

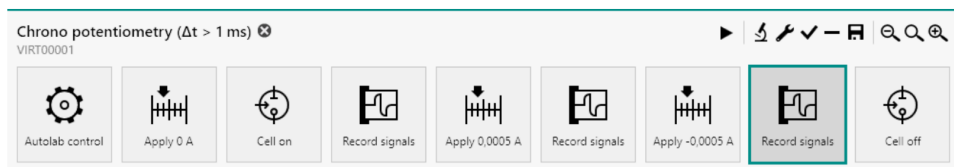


Figure 2.4: An example of the chrono potentiometry procedure in Nova software [6]

In Figure 2.4, we see an example of the sequence of steps in the chrono-potentiometry procedure in Nova software which is what we use for our experiment as well. For the experiments that are conducted for this thesis, the following steps are carried out:

1. *Apply 0 A*: to set the discharge current at 0 A to evaluate the open-circuit potential (OCP) of the cell.
2. *Cell on*: the device is turned on and connected to the Si-air cell.
3. *Record signals*: the software starts to record the circuit potential using an inbuilt galvanostat. The amount of time to record the signal is also given as input in this step. The open-circuit potential is measured for 1800 seconds or 30 minutes.
4. *Apply -150 μA current*: to set the discharge current at $150\ \mu\text{A}$ to evaluate the discharge potential (DP) of the cell. The negative sign is given as the current is withdrawn from the system and not supplied by the system.
5. *Record signals*: the circuit potential is recorded for 3600 s or 1 hour.
6. *Cell off*: to turn off the cell and revert back to its initial stage.

In order to study the Si-air cell in different physical conditions and to study its effects on the Simscape model's cell parameters. The galvanostatic experiments are conducted in varying conditions which is elaborated in the next section.

2.3. EXPERIMENT METHODOLOGY

The cell voltage of the Si-air cell is measured for varying physical conditions such as varying electrolyte conditions, air cathode pre-wetting and Si anode type. This data is later used as input for the Si-air Simscape model in order to evaluate the cell parameters and their variation with these different physical conditions at a constant current discharge of value $150\ \mu\text{A}$.

2.3.1. EFFECT OF VARYING ELECTROLYTE CONCENTRATION.

In Section 1.4.3, it is reported that the active ion in the alkali Si-air battery is OH^- ions of the KOH electrolyte solution. However, according to Durmus et al. the voltage reaches a maximum at 6 M KOH and then starts dropping [4]. It would be interesting to see these effects on the Si-air cell parameters and see their variation with varying electrolyte concentrations. The electrolyte concentration used in these investigations are given in Table 2.1:

Table 2.1: Different KOH concentrations used in the experiments

Sl no.	KOH mass per 100 ml	Molarity
	g/ml	M
1	10	1.78
2	30	5.34
3	60	10.69

Since we know from Equation 1.9 that the " $\ln Q$ " component depends on the concentration of ions in the solution, it is imperative that concentration of a solution has a significant effect on the cell potential. We now investigate the discharge curves due to these concentration changes and study the change in cell parameter change as well.

2.3.2. EFFECT OF PRE-WETTING AIR CATHODE

It was observed while evaluating the potential curves of the Si-air battery the performance of the battery is significantly improved when the air cathode is soaked in the electrolyte solution. It would be interesting to see how this pre-wetting affects the battery cell parameters of the Si-air battery since this would be affecting the electrode material (air cathode to be specific). It is predicted to affect the polarization RC circuit elements which is R_1 and τ_{a1} .

2.3.3. EFFECT OF VARYING ELECTRODE MATERIALS

According to literature, Cohn et al. states that n-type Si anode and p-type Si anode have different effects on the potential curves of the battery [38]. It would be interesting to study the cell parameters variation with discharge for the different type of anode type. Observing the best option among the two option in terms of ohmic losses is the aim of this study.

The experimental data obtained from the voltage measurements are later used as input into the Simscape Si-air battery. The experimental results are further discussed in Section 3. More information on the equipment used in the experiments can be in Appendix E.

3

EXPERIMENTAL RESULTS

TO study how the modelling cell parameters change when the Si-air cell is subjected to different physical conditions such as varying electrolyte concentrations and varying electrode conditions under constant current discharge conditions, galvanostatic discharge potential curves under a constant discharge current of 150 μA are studied. The experimental data from the galvanostatic discharge tests on the Si-air cell are shown and discussed in this section. The cell is worked under varying electrolyte concentrations, pre-wetted air cathode and different Si anode material. The open-circuit potential (OCP) plots and discharge potential (DP) plots given here and for individual plots refer Appendix A.

In order to study the different OCPs and DPs we use two parameters, the average OCP and the voltage drop rate. This allows us to compare the different potential curves of each case. The average OCP ($V_{average}$) values are calculated using the mean function in MATLAB:

$$V_{average} = \frac{\int_0^t V(t) dt}{\int_0^t dt} \quad (3.1)$$

The voltage drop rates ($\frac{dV}{dt}$) are calculated using the polyfit function available in MATLAB which gives the slope of the simple linear regression curve of the voltage curve:

$$\frac{dV}{dt} = \lim_{\Delta t \rightarrow 0} \frac{\Delta V}{\Delta t} \quad (3.2)$$

3.1. VARIATION WITH ELECTROLYTE CONCENTRATION

The electrolyte (KOH) solution concentration is varied for values of 1.78 M, 5.34 M and 10.67 M, which is denoted as 10%, 30% and 60% weight/volume concentrations, respectively. The Si-air cell consists of n-type Si anode and air cathode. In this thesis we refer to "normal condition air cathode" when this air cathode is not wetted in the alkaline electrolyte prior to incorporation in the Si-air cell. The results of the open-circuit potentials

(OCP) and discharge potentials (DP) of the cell are shown in the Figure 3.1a and Figure 3.1b respectively.

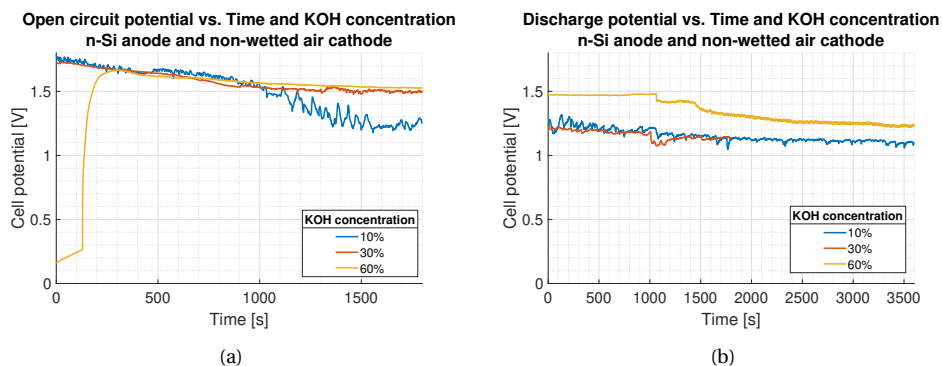


Figure 3.1: (a) OCP curve and (b) DP curve when the cell is n-Si anode with air cathode under normal condition for varying electrolyte concentrations. Blue, red and yellow indicates the potential curves when the electrolyte concentration is 10%, 30% and 60 % respectively.

In Figure 3.1a, the following observations can be made on inspection:

1. It can be seen that all the OCPs have a gradual decline to a lower value as time goes. This decline is most prominent where KOH 10% is used as the electrolyte and least prominent where KOH 60%.
2. It is known from the Nernst equation in Equation 1.9 that the concentration of the active ions which is in this case OH^- ions have a direct effect on the cell voltage potential [31]. In Section 1.4.3, corrosion reactions takes place between then Si anode and KOH electrolyte as per equations in Table 1.3 which use up the OH^- ions to form silicates, thereby reducing the OH^- ion concentration in the electrolyte solution which affects the OCP curves of the Si-air cell [4] [15].
3. The variation in the OCP curves with electrolyte concentration can be explained due to the corrosion rate increases with KOH concentration which reaches a maximum rate at 6 M KOH and reduces slightly with further increase in concentration [29] [4] [15].
4. The curves becomes less noisy as the concentration of the KOH solution increases. This means using a higher concentration of KOH solution will show much lesser variation in the OCP readings. It can speculated that this is because the amount of active OH^- is higher at higher concentration and the corrosion rates decrease with increase in concentration past 6 M KOH concentration [15].
5. The OCP curve for KOH 60% starts at a very low value of 0.2 V and rises to a steady voltage of around 1.6 V. However, this observation is very case specific and could be due to the change in temperature that could affect the cell potential according

to Nernst equation in Equation 1.9. It is reported that battery lifetimes are reduced at working in elevated temperatures [?]. It could also be speculated that the purity of the electrodes could have been compromised which affects the electrode-electrolyte interface that affects the cell voltage as there was not large temperature variations in the MEMS lab.

Table 3.1: Average OCP and OCP voltage drop rate for each concentration.

KOH conc.	Average OCP	Voltage drop rate (dV/dt)
%	V	V/s
10	1.509	-3.34×10^{-4}
30	1.516	-7.54×10^{-5}
60	1.482	$+4.15 \times 10^{-5}$

Table 3.1 shows that KOH 10% has the highest voltage drop rate in Si-air cell potential and KOH 60% has the least. In the case of average OCP in Table 3.1, we see the cell potential reach a maximum of 1.516 V at KOH 30% or 5.34 M KOH, which is closest to 6 M KOH where the corrosion rate is the maximum as per Weinrich et al. [15]. Hence, it is concluded that the corrosion rate and cell potential have a direct correlation where as the corrosion rate increases, the cell potential also increases.

On studying the discharge potential curves in Figure 3.1b, the following observations are made:

1. It can be seen that all the curves here have a downward trend which is contrary to the reported increasing trend by Durmus et al. [4]. This is due to the consumption of OH^- ions due to the electrochemical reactions as shown in Equation 1.7 and Equation 1.6. As time goes, the amount of available OH^- ions reduces due to the corrosion reaction and passivation reaction which inhibits cell performance in Table 1.3. During discharge, more silicon from the anode is consumed to form silicates using OH^- ions produced from O_2 in the air cathode. Assuming there is not much temperature variation in the system, it can be concluded that the rate of OH^- consumption is higher than the rate of its production. The literature states that corrosion rates of Si increases with KOH concentration to a maximum of 1.56 $\mu\text{m}/\text{h}$ and only reduces slightly at higher concentrations [29]. This means that the corrosion reaction rates also increase with KOH concentration so OH^- ions are being consumed at a faster rate to produce silicates than the production rate at the air cathode end. It is reported by Zhong et al. who discharges the Si-air cell at 0.1 mA/cm^2 which is twice the passivation threshold current density of 0.05 mA/cm^2 , that the rate of dissolution of $\text{Si}(\text{OH})_4$ is slower than its production rate which leads its build up on the Si anode surface [39]. The increase in discharge potential which was reported by Durmus et al. could be due to higher production rate of OH^- ions than the consumption rate at the air cathode who does not observe passivation since the applied current density is right passivation threshold at 0.05 mA/cm^2 .

2. It is to be noted that on using KOH 60%, the discharge voltage measurement of the Si-air cell is less noisy than for the other two potential curves for the other two concentrations used in the experiment.
3. Although we observed that KOH 60% had the highest OCP in Figure 3.1a, it drops to a lower discharge potential after approximately 600 s of discharge than KOH 30%. It could be that the purity of the electrode was compromised due to usage of defective sample, which affects the electrode-electrolyte interface in turn affect the cell potential.
4. For KOH 10%, the discharge potential curve is consistently the lowest and the most noisy compared to the that of other concentration used in this study.

Table 3.2: Discharge voltage drop rate for each concentration.

KOH conc	Discharge drop rate (dV/dt)
%	V/s
10	-4.18×10^{-5}
30	-5.34×10^{-5}
60	-8.78×10^{-5}

Table 3.2 shows that KOH 10% has the least voltage drop rate in Si-air DP compared to other KOH concentrations used in this study. It can be said for certain that the concentration of the electrolyte has an important role in the cell potential and the rate at which the voltage increases for each 20% increase in KOH concentration.

3.2. VARIATION WITH PRE-WETTING AIR CATHODE

It was observed that the Si-air cell performed much better when the air cathode is soaked in the KOH solution for about 8 hours [30]. The galvanostatic discharge tests were conducted using this soaked air cathode with n-type Si anode and with varying concentration solution. Their effects on the discharge curves are studied and compared to that of a Si-air cell with non-wetted or normal air cathode condition below. The average OCPs and the voltage drop rates are calculated and tabulated in the end of this section. For more case wise analysis, refer Appendix A.

Figure 3.2 draws a comparison between the OCP of Si-air cells studied in the previous section which have n-type Si anode and normal or non-wetted air cathode condition under various electrolyte concentrations and Si-air cells with n-type Si anode and pre-wetted air cathode under the same concentrations. The following observations can be made on comparing the two graphs for OCPs in Figure 3.2a:

1. All the OCPs show a general downward trend which was explained in the previous section was due to corrosion reaction taking place inside the cell.
2. It is noted that the OCP of the Si-air cell drops on pre-wetting. The OCP drop is most dominant in the case of KOH concentration 60%.

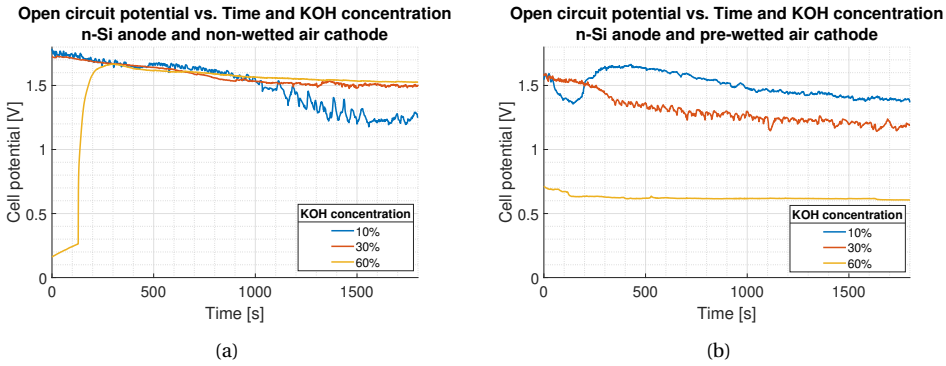


Figure 3.2: (a) Open-circuit potential curve under n-type Si anode and normal air cathode condition and (b) Open-circuit potential curve when the cell is n-Si anode with air cathode under normal condition for varying electrolyte concentrations. Blue, red and yellow indicates the potential curves when the electrolyte concentration is 10%, 30% and 60 % respectively.

3. The OCP curve for KOH 10% is less noisy in the pre-wetted air cathode condition than the non-wetted air cathode condition.

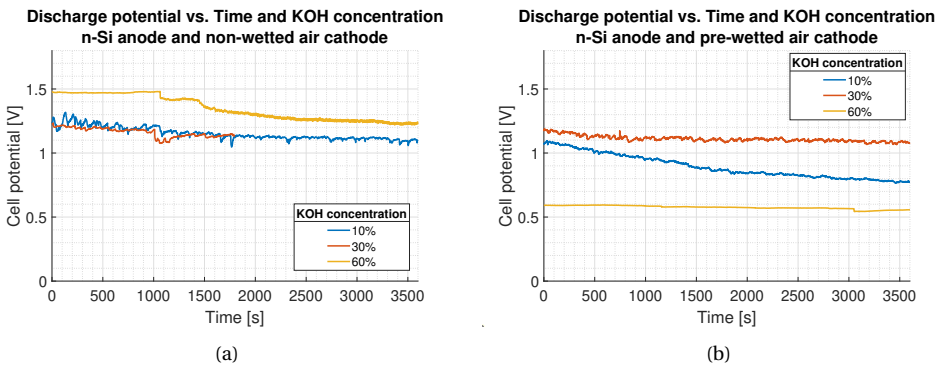


Figure 3.3: (a) DP curve under n-type Si anode and normal air cathode condition and (b) DP curve when the cell is n-type Si anode with air cathode under normal condition for varying electrolyte concentrations. Blue, red and yellow indicates the potential curves when the electrolyte concentration is 10%, 30% and 60 %, respectively.

Figure 3.3 compares the DP curve for a Si-air cell with non-wetted or normal air cathode in Figure 3.3a and that with pre-wetted air cathode condition. The following observations can be made from the graphs:

1. There is a downward trend for all the curves which confirms the effect of discharging in the cell as energy is being extracted from the Si-air cell during discharging.
2. Similar to what was seen in the case of OCPs, we see that DPs also are lowered

when pre-wetting of air cathode is done compared to its non-wetted or normal air cathode counterpart.

3. Pre-wetting makes the DP curves less noisy when compared to the normal or non-wetted air cathode Si-air cell.

Now that we have seen the performance of a Si-air cell under normal air cathode condition and that under pre-wetted air cathode condition case by case. On tabulating all the average open-circuit potentials (OCP) and the calculated voltage drop rates in Table 3.3 and all the calculated discharge potential (DP) drop rates for all the KOH concentrations in Table 3.4.

Table 3.3: Pre-wetting effect on Average OCP and voltage drop rates.

KOH conc.	Air cathode condition	Average OCP	Voltage drop rate (dV/dt)
%	[-]	V	V/s
10	Normal	1.509	-3.34×10^{-4}
10	Pre-wetted	1.3767	-1.37×10^{-4}
30	Normal	1.516	-7.54×10^{-5}
30	Pre-wetted	1.3042	-2.00×10^{-4}
60	Normal	1.482	4.15×10^{-5}
60	Pre-wetted	0.6101	-1.48×10^{-5}

Table 3.4: Pre-wetting effect on discharge voltage drop rates.

KOH conc.	Air cathode condition	Discharge drop rate (dV/dt)
%	[-]	V/s
10	Normal	-4.18×10^{-5}
10	Pre-wetted	-8.69×10^{-5}
30	Normal	-5.34×10^{-5}
30	Pre-wetted	-1.80×10^{-5}
60	Normal	-8.78×10^{-5}
60	Pre-wetted	-2.96×10^{-6}

On seeing the above tables, we can conclude the following about the study carried to compare the potential curves when we use a Si-air which has n-type Si anode and normal air cathode and one that uses a pre-wetted air cathode:

1. In the case of open-circuit potentials, it can be seen that pre-wetting the air cathode seems to lower the average OCP of the Si-air cell for the same electrolyte concentration.
2. It can be seen that the voltage drop rate is lower when a pre-wetted air cathode compared to the when a normal air cathode is used in the Si-air cell for the same electrolyte concentration.

3. In the case of discharge potentials, we observe that same trend as well with the only exception being when the Si-air cell electrolyte concentration is KOH 10%. However, this could be a case specific observation.
4. The discharge voltage drop rate is lower than in the case of a Si-air batter that uses pre-wetted air cathode rather than a normal air cathode.

It can be seen that in general pre-wetting the air cathode results in lower cell potentials in both open-circuit and discharge conditions. However we can also conclude that pre-wetting the air cathode makes the cell potential curves also more stable and has much less noise compared to its normal air cathode conditions as seen in the above figures and tables.

3.3. VARIATION WITH ELECTRODE MATERIALS

It is stated in literature that using n-type Si and p-type Si has its own effects on the Si-air cell and that p-type Si is the best due to its lower corrosion rate than n-type Si [8]. It is to be noted that this statement was made for a non-aqueous Si-air battery using room temperature ionic liquids (RTILs) as the electrolyte. In this section, the discharge curves for Si-air cell with a n-type Si anode and a p-type Si anode under electrolyte KOH concentration of 60% and with pre-wetted air cathode as this showed the least noise in voltage measurement of the Si-air cell.

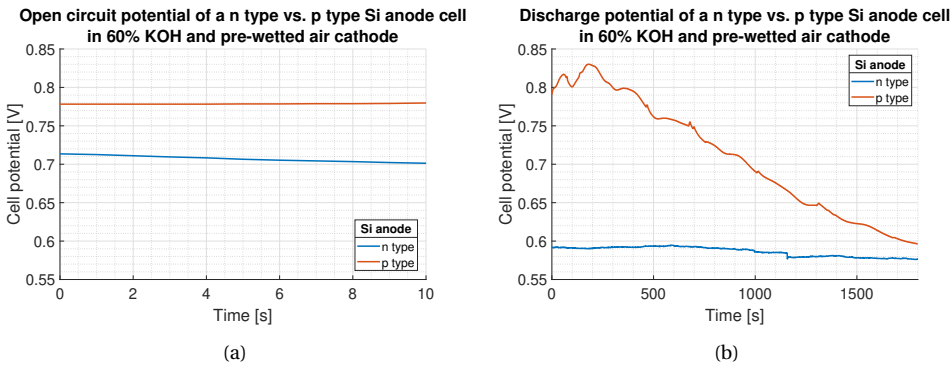


Figure 3.4: (a) OCP curve and (b) DP curve when the cell is in KOH 60% electrolyte solution and pre-wetted air cathode condition. Blue trace indicates when a n-type Si anode is used and red line indicates a p-type Si anode is used.

Table 3.5: OCP analysis when different Si type is used as anode from Figure 3.4a.

KOH conc	Air cathode condition	Si type	Average OCP	Voltage drop rate (dV/dt)
%	[-]	[-]	V	V/s
60	Pre-wet	n-type	0.6101	-1.48×10^{-5}
60	Pre-wet	p-type	0.7822	$+2.40 \times 10^{-4}$

The OCP of the Si-air cells is plotted and the corresponding curves in Figure 3.4a are analysed and the findings are tabulated in Table 3.5. On observing the above figure and table, the following conclusions and observations can be made about the OCP comparison when using a p-type Si as anode instead of the n-type Si as the Si anode in 60% KOH and air cathode is pre-wetted:

1. The curves are very stable and have little to no noise in them.
2. It can be seen that there is a slight increase in the OCP when the Si anode used is p-type compared to the steady decline seen in the case of a n-type Si anode. It is reported by Cohn et al. that the corrosion rate for p-type is lower than that of n-type in the case of non-aqueous Si-air cell [8]. However, it is reported by Gao et al. that p-type Si substrates has better etching property than n-type Si substrate under molten KOH [40]. This can be speculated why p-type Si anode is a better candidate than n-type Si.
3. The voltage difference between the OCP curves is about 0.05 V during the initial time of analysis to 0.08 V at the final time of analysis. The OCP of the p-type Si anode case is higher with an average OCP of 0.7822 V consistently and more stable, this makes it much better candidate for a Si anode in this case than the n-type Si anode which has an average OCP of 0.6101 V.

The discharge potential (OCP) of the Si-air cells is plotted and the corresponding curves in Figure 3.4b are analysis and the findings are tabulated in Table 3.6.

Table 3.6: DP analysis when different Si type is used as anode.

KOH conc	Air cathode condition	Si type	Voltage drop rate (dV/dt)
%	[-]	[-]	V/s
60	Pre-wet	n-type	-2.96×10^{-6}
60	Pre-wet	p-type	-1.41×10^{-4}

On observing the above figure and table, the following conclusions and observations can be made about the discharge potential comparison when using a p-type Si as anode instead of the n-type Si as the Si anode in 60% KOH and air cathode is pre-wetted:

1. The curves are quite stable and have little to no noise in them.
2. It can be seen that there is a slight decline in the DPs. However, in the case the Si anode used is p-type compared to the steady decline seen in the case of a n-type Si anode the drop in voltage is more prominent.
3. The voltage difference between the discharge curves is about 0.2 V during the initial time of analysis to 0.02 V at the final time of analysis. The DP of the p-type Si anode case is higher consistently and more stable.
4. However, the discharge voltage drop rate is higher when p-type Si is used as anode in the Si-air cell. This could be very case specific as well as the voltage drop for n-type Si case is only 0.01 V after 1 hour of discharge at constant 150 μ A.

It can be concluded that on using p-type Si, the cell gives higher potentials consistently in open-circuit conditions and while discharging as well. This can be said for certain the case where the KOH concentration the cell electrolyte is 60% and the air cathode is under pre-wetted conditions. The individual potential curves for the various samples are plotted in Appendix A.

3.4. DISCUSSION

Galvanostatic discharge experiments were conducted in order to support the Simscape model. The results in Chapter 3 and this section shall conclude this experimental data based on the above findings. The study is also compared to what was reported by Durmus et al., where the influence of concentration on potential curves on an Si-air battery is studied [4].

It can be concluded that the Si-air cell OCPs range from 1.2 to 1.6 V with the exception of when an n-type Si and p-type Si under pre-wetted air cathode condition in 60% KOH concentration electrolyte. The relation of cell voltage and concentration can also be seen in the Figure 3.1 as we see the OCPs climbing on increasing the concentration of the electrolyte in accordance with the Nernst equation relationship. KOH 60% and normal cathode condition shows the highest OCP at the end of the analysis followed by KOH 30% in normal air cathode and the n-Si 10% PW. It can also be seen that as the concentration of the Si-air electrolyte increases, there is much less noise in the OCP curve and the voltage drop rate is lowered as well.

It can be observed that pre-wetting the air cathode has lowered the OCPs of the Si-air cell when in the same concentration except in the case of KOH 10%. It can be seen that the difference between the OCPs under normal air cathode condition and pre-wetted air cathode condition at the same concentration increases as concentration is increased at the end of analysis period. For example, in the case of KOH 10%, the Δ OCP is about 0.04 V. In the case of KOH 30%, the Δ OCP which is the difference between the OCP of the cell at non-wetted air cathode and the OCP of the cell with a pre-wetted air cathode (Δ OCP = $OCP_{\text{non-wetted}} - OCP_{\text{pre-wetted}}$) is about 0.2 V and finally in the case of KOH 60%, Δ OCP is about 1 V. On using a p-type Si anode under 60% KOH concentration and pre-wetted air cathode condition, higher OCP is achieved that that of when a n-type Si anode is used under the same conditions.

In Figure 3.1 the DP curves of the Si-air cell is plotted under all conditions used in this thesis. These potentials are used as the input for the Simscape battery model for cell model parameters to be calibrated with. Unlike what was observed in the OCP, it can be seen that KOH 30% has the highest discharge potential. This could be case specific as there is an upward spike in cell potential at 550 seconds of increase in cell potential of approximately 10%. The effect of temperature on the Si-air cell is speculated to be a reason for this spike as it is known that temperature (T) is a factor that affects cell operation according to Nernst equation in Equation 1.9. This is confirmed as Johnson et. al reports that temperature and cell potential have a strong positive correlation by reporting the maximum cell potential increase of 1.95% when temperature is increased

from 24 °C to 69 °C. However, this was for Galvanic cells and can be concluded that the effect of temperature on Si-air cell performance must be studied elaborately [41].

Quite similar to what was observed in the OCPs, DPs have a direct relation with the cell concentration. Pre-wetting the air cathode lowers the Si-air cell potential and the ΔDP which is the difference between the DP of the cell at non-wetted air cathode and the DP of the cell with a pre-wetted air cathode ($\Delta DP = DP_{\text{non-wetted}} - DP_{\text{pre-wetted}}$) increases with increase in concentration. The highest discharge voltage potential drop rate is observed in the case when p-type Si anode, KOH 60% and pre-wetted air cathode is used in the Si-air cell. The voltage drop is 0.2 V in 1800 seconds whereas the n-type Si anode counterpart under the same conditions shows little to no variation. This means that the Si-air cell with n-type Si anode, 60% KOH and pre-wetted air cathode has the lowest discharge rate among all the studied cases in this thesis. The individual cell potential curves are plotted in Appendix A.

To conclude this study, the results obtained from this analysis in Figure 3.1 for OCPs and DPs is compared to the results obtained by Durmus et al. where alkaline Si-air cell have been studied with different KOH concentrations [4]. This study is briefly discussed in Section 1.4.3 and plotted in Figure 1.6 and in Table 3.7.

Table 3.7: Comparison study of cell potential curves from this thesis and cell curves reported by Durmus et al. [4].

	Current density	KOH conc. studied	Open-circuit	Discharge
	$\frac{\mu\text{A}}{\text{cm}^2}$	M	[-]	[-]
Durmus results	50	0.75	No variation with concentration. Stays at 1.4 V.	Increases with discharging time
		1		
		2		
		3		
		4		
Study results	150	1.78	Concentration showed to have a significant effect and average OCP range 1.509 V to 1.482 V	Decreases with discharging time
		5.34		
		10.69		

Table 3.7 illustrates the comparisons between the values reported by Durmus et al. and the values reported in my work. It can be seen that there are contrary observations made in the case of OCP and DP which is mainly due to the passivation reaction and corrosion reaction that occurs during the experiments conducted in my work [15] [4]. It is reported that the silicates formed during discharge as discharge products get converted to SiO_2 when the applied current density crosses a passivation threshold of $50 \mu\text{A}/\text{cm}^2$ [15] [4]. Since in my work the applied current density is $150 \mu\text{A}/\text{cm}^2$ and is more than the thresh-

old value, there is passivation occurring and it is affecting the cell curves that is reported in my work.

It is noteworthy to see that contrary to what was reported by Durmus et al. about the discharge potential increasing with discharge time [4], we observed in Figure 3.1 that the discharge potential decreases with discharge time. This effect can be explained due to:

1. *Higher discharge current density used:* Durmus et al. studies the effects of discharge using a current density of $50 \mu\text{A}/\text{cm}^2$ in order to avoid passivation of the Si anode. In this study, a current density of $150 \mu\text{A}/\text{cm}^2$ is used. This would discharge the battery at a faster rate compared to the Si-air cell used by Durmus et al. [4].
2. *Inactivation of Si anode due to passivation:* As explained earlier about the current density being more than the passivation threshold current density of $50 \mu\text{A}/\text{cm}^2$. This would mean that there is formation of SiO_2 that blocks the Si from participating in the electrochemical reaction in the cell thereby reducing the cell potential.

It is critical to note that in this thesis, high OCPs of more than 1.4 V have been observed in Table 3.1. This is contrary to the reported constant 1.4 V that does not change with KOH concentration by Durmus et al. [4]. The usage of Al:Si layer as the back contact on the Si anode is to be noted in the Si-air cell used in this thesis compared to that described by Durmus. It is reported that having aluminium contacts reduces sheet resistance in solar cells [35] [37]. Hence, we think that the observed higher OCPs compared to the reported 1.4 V in literature are due the sputtering of Al:Si layer that improves the electron collection at the Si anode.

4

SIMSCAPE MODEL

TO simulate the battery dynamics and replicate the discharge curves through computer simulations for a real-time battery management system (BMS), a model based on the MathWorks example on Li-ion battery cell is modified to make it suitable for Si-air battery in Simscape [7]. A brief description of the various battery parameters in the model is given in Section 4.1 and the Si-air battery model is explained even further in Section 4.3 and the working of the model is explained in Section 4.2 where an example using Li-ion battery is shown. The main objective of this model is to calculate the various cell parameters of the battery and to predict battery behavior for different conditions. This is done using the experimental data obtained from experimental results obtained in Section 2.3

4.1. BATTERY MODEL PARAMETERS

The equivalent circuit battery model as conveyed earlier uses resistance-capacitance (RC) circuit elements such as resistors and capacitors to model the battery dynamics. For the sake of simplicity, we consider only one RC block. A simple illustration of the equivalent circuit used to evaluate the Simscape battery model is shown in Figure 4.1.

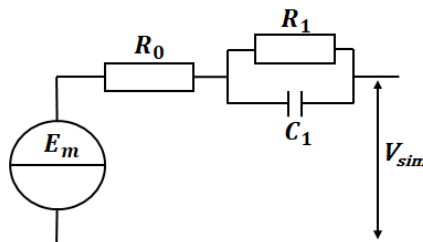


Figure 4.1: Simple equivalent electrical circuit of the battery cell.

It can be seen in Figure 4.1 that there are various components in the circuit. According to Madani et al., the various cell parameters and their physical significance are summarized below [42]:

1. R_0 : it is the internal DC resistance which is mainly responsible for the sudden voltage decrease when a discharge current is applied. This is mainly attributed to the electrolyte properties. This parameter is a function of SOC and temperature. It is measured in Ohm (Ω). It can be speculated that any change in the concentration of KOH can affect the R_0 parameter as the number of conduction ions which is OH^- ions in this case is changing which will affect the conductivity of the cell [43].
2. R_1 : it is resistance component of the first time constant of battery cell feedback that can model the charge transfer and diffusion procedures in the battery cell model. This is mainly attributed to the electrode material. This parameter is a function of SOC and temperature. It is measured in Ohms (Ω). It is the transient response of the simulated voltage and is modelling the charge transfer procedures [42]. It can be speculated that on changing the electrode material or the electrode conditions, we can observe changes in the R_1 parameter.
3. τ_1 : it is the first time constant of the RC block in the equivalent circuit of battery cell which models the charge transfer and diffusion procedures in the battery cell model and this is attributed to the electrode material and interaction with the electrolyte. This parameter is a function of SOC and temperature. In the model we use this cell parameter in the under the variable name τ_{au_1} . The value of τ_{au_1} is calculated as $\tau_{au_1} = R_1 C_1$ where C_1 is the capacitance of the capacitor in the RC block. τ_1 is measured in seconds (s). Similar to R_1 , it is the transient response of the simulated voltage and is modelling the double layer capacitance [42]. It can be speculated that on changing the electrode material or the electrode conditions, we can observe changes in the τ_{au_1} parameter.
4. E_m : it is the predicted open-circuit voltage or no load voltage of the battery cell from simulation for the corresponding state of charge (SOC) of the battery. This parameter is a function of SOC and temperature. It is measured in Volts (V).
5. V_{sim} : it is the output cell potential of the Simscape model which is the simulated voltage. Which is dependent on all the other cell parameters in the system. It is measured in Volts (V).

Table 4.1: Variables used in the model.

Physical entity	Model variable name	Unit
R_0	R_0	Ω
R_1	R_1	Ω
τ_1	τ_{au_1}	s
E_m	E_m	V

Now that the cell parameters are defined, let's take a look into the Simscape battery block and see how we input the cell parameters into the model. Since these cell parameters are a function of the state of charge (SOC) of the cell, we plot the cell parameters for ten SOC points ranging from 0.1 to 1.0. The input parameters are input as an array of 10 elements which have . For example in the case of R_0 , the array variable will be $R_0 = [R_0(0.1); R_0(0.2) \dots R_0(1.0)]$ where the element $R_0(0.9)$ is the R_0 value and SOC point 0.9. This the case for all the other cell parameters as well.

4.1.1. SIMSCAPE BATTERY BLOCK



Figure 4.2: Circuit diagram of the battery (look-up table) block in Simscape.

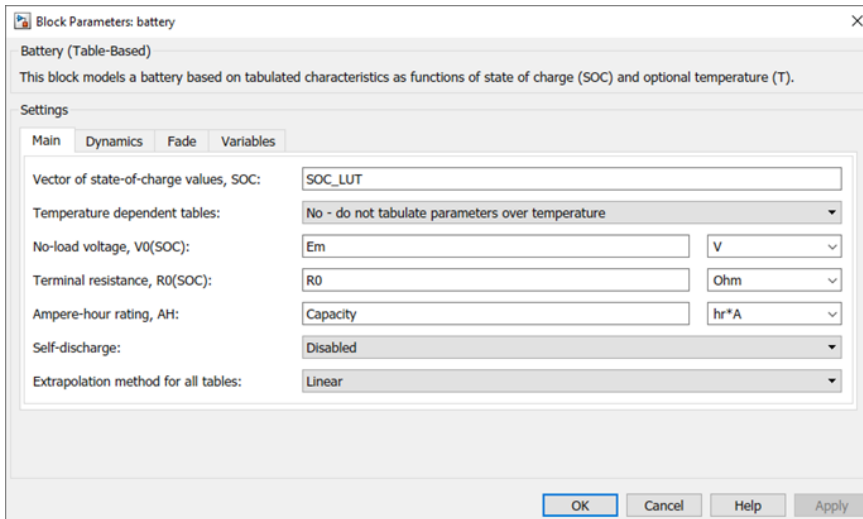


Figure 4.3: Block parameters of the battery block under "Main".

In Figure 4.2 we see the Simscape block for the battery (look-up table) which is used in the model. On right-clicking the block, we enter the block parameters which are elaborated in the Figure 4.3 under the "Main" settings where you enter the variable E_m consists of a no-load voltage and the terminal resistance R_0 .

In Figure 4.4 we see the dynamic block parameters that we used for the model. It is to be noted that we only used one time-constant dynamics in the model for the sake of sim-

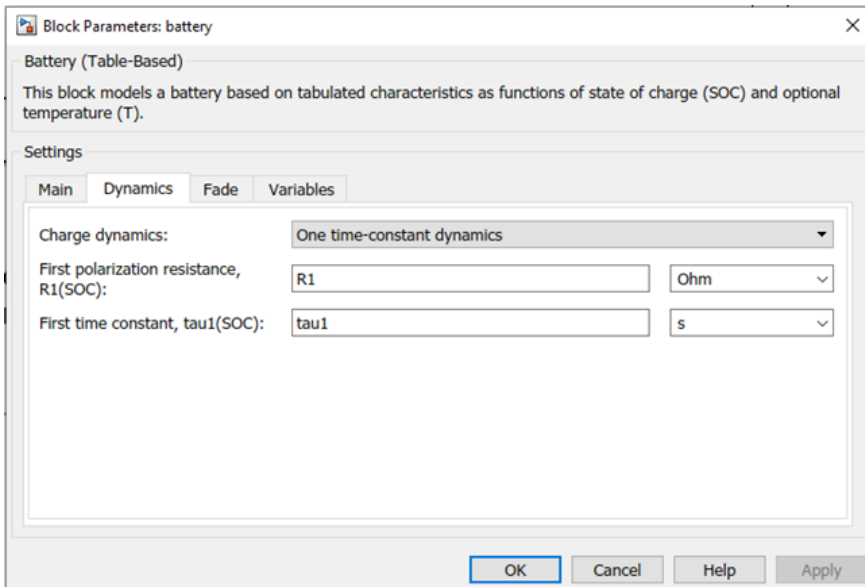


Figure 4.4: Block parameters of the battery block under "Dynamics".

plicity. In the "Dynamics" settings, we initialize the first polarization resistance which is R_1 and first time constant which is τ_{a1} . These cell parameters have been described in the earlier Section in Section 4.1.

Note: The MATLAB battery block, allows even temperature dependency in the model as we can see in Figure 4.3. However, since this is just a simple model and the experiments were not conducted in a temperature controlled environment. The cell potential voltages are not evaluated across temperature. Similarly, we set the charge dynamics in one time-constant dynamics for simplicity.

4.1.2. COMPLETE MODEL

In this section, we shall cover the various elements in the Simscape model of the Si-air battery and elaborate on the different components and its role in the model using the illustration in Figure 4.5.

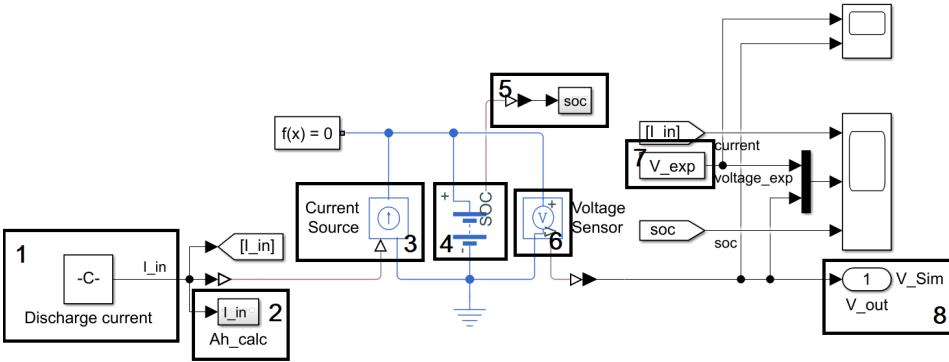


Figure 4.5: Complete Si-air simscape model 1.) Constant current source set at $150\ \mu\text{A}$ 2.) Capacity calculator 3.) Simscape current source into battery 4.) Battery model (look-up table) 5.) SOC calculator 6.) Voltage sensor and 7.) Experimental voltage input and 8.) Simulated voltage output from model.

1. *Constant current source set at $150\ \mu\text{A}$* : A constant current magnitude of $1.5\text{E-}4$ is set into the Simscape model that acts as the model input. This is used as the discharge current of $150\ \mu\text{A}$ in the model.
2. *Capacity calculator*: It is a sub-system that uses the integral function in Simulink to calculate charge extracted from the battery. This is later used in the state of charge calculation (SOC) of the battery.
3. *Simscape current source into battery*: This block converts the simscape signal to $150\ \mu\text{A}$ into the model.
4. *Battery model (look-up table)*: This is the battery block which is further elaborated in the previous Section 4.1.1.
5. *SOC calculator*: In this sub-system the SOC of the battery is calculated by comparing the SOC value of the previous iteration and reduces as charge is extracted from the battery cell.
6. *Voltage sensor*: This block evaluates the voltage drop across the cell electrodes and outputs it into voltage simscape signal. This is the output simulated voltage of the model.
7. *Experimental voltage input*: This block is the experimental voltage that we input into the model to compare the experimental value and the simulated value of the cell potential in the model.

8. *Simulated voltage output from model:* This is the simulated voltage of the battery and gives the output signal as simulated voltage of the simscape model.

The Simscape model up and running and the experimental voltage and simulated voltage is evaluated. The model must be calibrated so the simulated voltage and the experimental voltage is identical and this is done by adjusting the cell parameters in the battery (look-up table) block. This is done using a design optimization tool available in the Simulink environment which is elaborated in the coming section below.

4.1.3. PARAMETER ESTIMATION

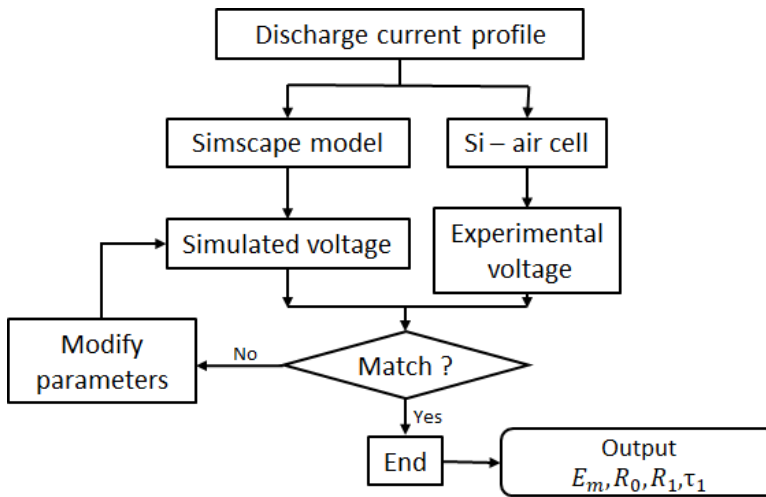


Figure 4.6: Flow chart of how the parameter estimation tool works.

In the Simscape environment there is a model tool named as the "Parameter estimator" which allows the user to estimate the values of the parameters used in the model. The basic working of the Si-air battery model's parameter estimation is shown as a flow chart in Figure 4.6. It is used mainly to evaluate coefficients of the model, entries in space-time matrices and most importantly regression coefficients based on the input real data [34].

It is to be noted that in the reference Li-ion model, this parameter estimator tool is used to estimate the values of different cell parameters in the model so that it fits the experimental data accurately. An example case of the working of the parameter estimator is shown below for the Li-ion cell.

4.2. LI-ION BATTERY MODEL

To understand the model better and to explain it working, a test case using the data and methodology from MathWorks fileexchange for Li-ion cell (LiFePO₄ to be specific) is shown here to study how the different model parameters change with discharge or state

of charge (SOC) of the battery is done in this section [44]. The variation of SOC points 0.1, 0.2, 0.5, 0.8 and 1.0 is only shown as this is only an example case.

1. First, the battery cell parameters of the model is initialized using initial guesses close to the actual values to aid in the computation of the model. It must be noted that data required for the Li-ion model is available in MathWorks and is saved in workspace [45]. The initial guesses used for the Li-ion battery model are for each SOC point since the voltage of cell is depending on the state of charge (SOC) of the cell are:

- (a) R_0 value of 10 m Ω .
- (b) R_1 value of 50 $\mu\Omega$.
- (c) τ_{u1} value of 10 s.
- (d) E_m value of 3.8 V.

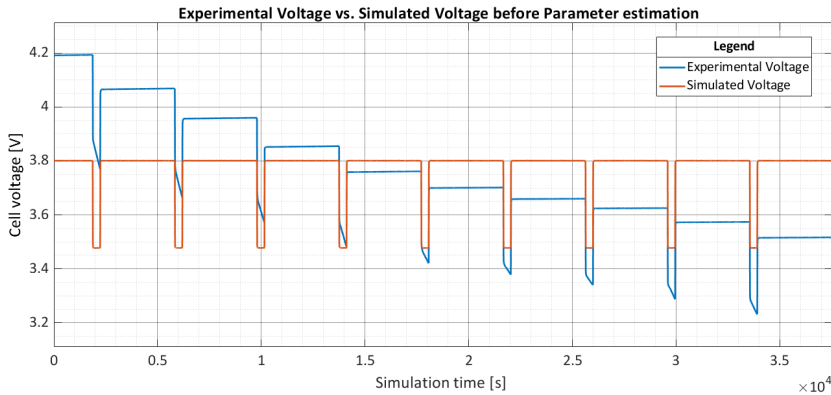


Figure 4.7: Experimental and simulated voltages of Li-ion cell before parameter estimation. The blue indicates the experimental voltage and the red line indicates the simulated voltage.

2. The pulsed voltage is simulated for a pulsating discharging current of 30 A. This simulated voltage is plotted next to the experimental voltage that was already saved in the file from MathWorks in Figure 4.7 [45].
3. The parameter estimator tool which is available in as Design Optimisation tool in Simulink (MATLAB) is run in order to estimate the new cell parameter values by matching the simulated voltage curve with the experimental voltage curve and flows the flowchart indicated in Figure 4.6. This is done by changing the cell parameters at each SOC values till the error function is minimal after each iterations.
4. It can be seen in Figure 4.8 how the cell parameters change with each iteration step in order to evaluate the best fit of the simulated voltage curve and the experimental voltage curve. It can be seen that there are multiple lines for one cell parameter,

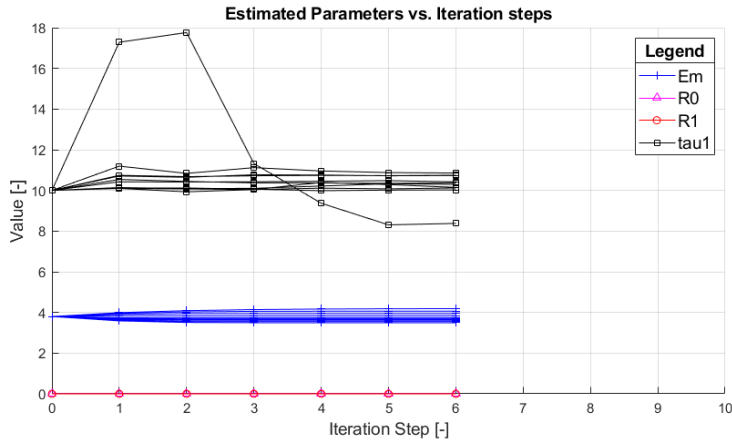


Figure 4.8: Li-ion cell parameters changing with each iteration steps to fit the simulated data and experimental data. Where E_m is measured in Volts [V], R_0 and R_1 is measured in Ohms [Ω] and τ_{u1} is measured in seconds [s]. The multiple lines indicate the variation of the cell parameter for each state of charge (SOC).

this is because the cell parameter is an array variable that contains ten elements for the different cell parameters at each state of charge (SOC). Hence, there are ten multiple lines showing the variation of each cell parameter at each SOC. It is concluded that the model is varying the cell parameters in order to fit the simulated voltage into the experimental voltage.

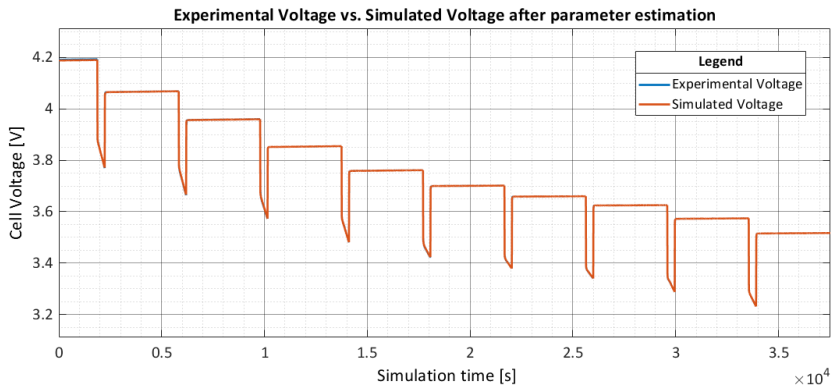


Figure 4.9: Experimental and simulated voltages of Li-ion cell after parameter estimation. The blue indicates the experimental voltage and the red line indicates the simulated voltage.

5. Once the parameter estimator finishes evaluating the cell parameters at different state of charge (SOC) points by fitting the simulated voltage signal from the battery block in Simscape model to the experimental data. The experimental voltage

and simulated voltage is plotted in Figure 4.9. This shows that the simulation is a success and the model has been validated.

- Now in order to see how the cell parameters have changed from their initial guess values. They are tabulated in Table 4.2 for each SOC point. It is reported that all cell parameter values changed from their respective initial guesses given in the previous point. It is observed that the R_0 , τ_{1} and E_m parameter has a decreasing trend whereas the R_1 parameter has a increased trend as the battery is discharged.

Table 4.2: Final values for the cell parameters for Li-ion battery model.

SOC	R_0	R_1	τ_{1}	E_m
	m Ω	$\mu\Omega$	s	V
0.1	8.1	1200	8.38	3.4938
0.2	8.7	588	10.15	3.5526
0.5	8.6	487	10.08	3.6886
0.8	9.0	508	10.12	3.9482
1.0	9.7	477	10.74	4.1872

Using this model, a battery block that can simulate the behaviour of a Li-ion cell at different state of charge points of the cell is designed. This procedure is used for making alkaline Si-air battery model which is discussed further in the next section.

4.3. SI-AIR BATTERY MODEL

The battery cell component in Simscape can be entered using look-up tables which means for given particular value of state of charge (SOC) there is a table that MATLAB looks-up and give the corresponding output with the extrapolated data for the various modelling cell parameters which is R_0 , R_1 , τ_{1} and E_m which has been described in Section 4.1. The initial values of the battery are given as initial guesses and very close to the actual value to aid the simulation. Once, the battery component is ready for simulation and run for the initial values. The inbuilt parameter estimation is used in MATLAB in-order to evaluate the cell parameters values from the input experimental values that was evaluated from discharge experiments in the MEMS lab. This procedure is further elaborated in the coming sections. There are some assumptions that has been made in order to fit the experimental data that was observed in the Section 3 into the model which is elaborated in the Section below.

4.3.1. ASSUMPTIONS

It was necessary to make certain assumptions about the data and the model so that the experimental data from preliminary experimental investigation can be used in the model. This is because of the difference in cells, working principle of the cell, lab equipment available and various other reasons that will be reasoned as well below:

- The workings of the reference Li-ion cell and the Si-air cell is similar. This is what makes using the model working possible. According to Jackey, a battery can be

modelled in this method [7]. It is important to assume that the Si-air cell is no exception to this.

2. In the Li-ion battery model, pulsed discharge current is used in order to evaluate the pulsed discharge curves for cell potential. This is because it gives a very accurate evaluation of the cell parameters and can model the polarization parameters R_1 and τ_{11} values accurately [7]. It is assumed that having constant current discharge curves would still give feasible results and the evaluated cell parameters can simulate the battery operation.
3. In this Si-air battery model, only one time-constant charge dynamics is used. This means only one RC block is used to simulate the battery operation. However, it is to be noted that using more RC blocks increases the system complexity and makes the model very accurate as well. Since, constant discharge curves are used in this model. It can be said not much significant difference can be observed on using more RC blocks in the equivalent circuit.
4. The capacity of the Si-air cell is assumed to be 100 μAh since the galvanostatic measurements are done under 150 μA constant current for 1 hour. The cell capacity is treated as a parameter so that the model can estimate its value to best fit with the experimental value.
5. Similar to the initial guesses made for the Li-ion battery model, the Si-air battery model cell parameters are given the following values for each state of charge (SOC) based on experimental data and on the Li-ion battery model:
 - (a) R_0 value of 10 $\text{m}\Omega$.
 - (b) R_1 value of 50 $\mu\Omega$.
 - (c) τ_{11} value of 10 s.
 - (d) E_m value of 1.1 V.

4.4. CONCLUSION

A Si-air battery model that evaluates the cell parameters and simulates the cell voltage under current discharge using experimental data is made using the working principle of the Li-ion battery model. However, in the Li-ion battery model case, it can be seen that all the cell parameters change in order to fit the experimental potential curve and that it is a function of the state of charge (SOC) of the cell and the input experimental curve.

It is seen in this thesis that putting the Si-air cell in different physical conditions such as varying concentrations and varying electrode material conditions yields different results. It is noteworthy to see if the modelling cell parameters change with the Si-air cell potential curves at different conditions thereby obtaining the research objectives posed in Section 1.7.

It is evaluated from experimental data where the Si-air battery is operated in different physical conditions such as different electrolyte concentrations, with air cathode pre-wetting and with different anode materials which is elaborated in Chapter 3. The results of the Simscape model is presented in Chapter 5. The MATLAB script used to run the model and plot the results are given in Appendix C and the output model plots are given in Appendix B.

5

MODELLING RESULTS

SIMSCAPE model simulates the operation of an alkaline Si-air cell which uses potassium hydroxide (KOH) solution in MATLAB is developed. The simulation is made with reference to the Li-ion battery model that is available in MathWorks repository. The model utilizes experimental data as its input to calibrate the cell parameters. The analysis graphs are clearly shown in the Appendix B. The results of the study evaluates how the cell parameters change with varying conditions as described below.

The modelling methodology follows the same methodology followed by the Li-ion battery model discussed in Section 4.2. The results shall be shown in the following manner:

1. *Experimental and simulated voltages before parameter estimation:* The simulated voltage is run using the initial guesses of the cell parameters given in Section 4. This is to show that the model hasn't been calibrated to the new physical conditions that the Si-air cell was experimentally subjected to. Since, all the simulated voltages before calibration outputs a constant voltage of 1.1 V. It is not plotted in this Chapter however, they are plotted in Appendix B.
2. *Experimental and simulated voltages after parameter estimation:* The simulated voltage is run with using the estimated parameters after parameter estimation. This is to illustrate that the model has been calibrated to the new experimental data. The experimental voltage from discharge experiments and simulated voltages after calibration is plotted in this Chapter.
3. *Variation of cell parameters with state of charge (SOC):* The calibrated cell parameters R_0 , R_1 , τ_{a1} and E_m are plotted against their initial guesses to evaluate their role in the model. It is found that parameters R_0 , R_1 and τ_{a1} showed no variation with the change in physical condition or change in input potential profile and kept repeating for different cases. However, E_m has showed change with respect to both the state of charge (SOC) and the input experimental potential curve and this is plotted separately.

4. *Predicted capacity*: The cell capacity is given as a variable in the model and input into the parameter estimator. The model predicts what is the best fit value for the cell capacity by fitting the simulated voltage with experimental voltage data, thereby predicting what the cell capacity. This tabulated in this Chapter.

5.1. VARIATION WITH ELECTROLYTE CONCENTRATION

The alkaline Si-air cell is placed in different electrolyte (KOH) concentrations ranging from 1.78 M, 5.34 M to 10.69 M which is denoted as 10%, 30% and 60% weight/volume concentration. In Section 4, we speculated that parameters R_0 will have variations as it responsible for electrolyte resistance which is a dependent on the electrolyte concentration [42]. The Si anode used for all the discharge experiments was n-type Si and the air cathode is placed in non-wetted conditions. The cell was discharged under a constant discharge current of $150 \mu\text{A}$. The model plots the simulated voltages based on the initial guesses which was tabulated in Section 4.

5

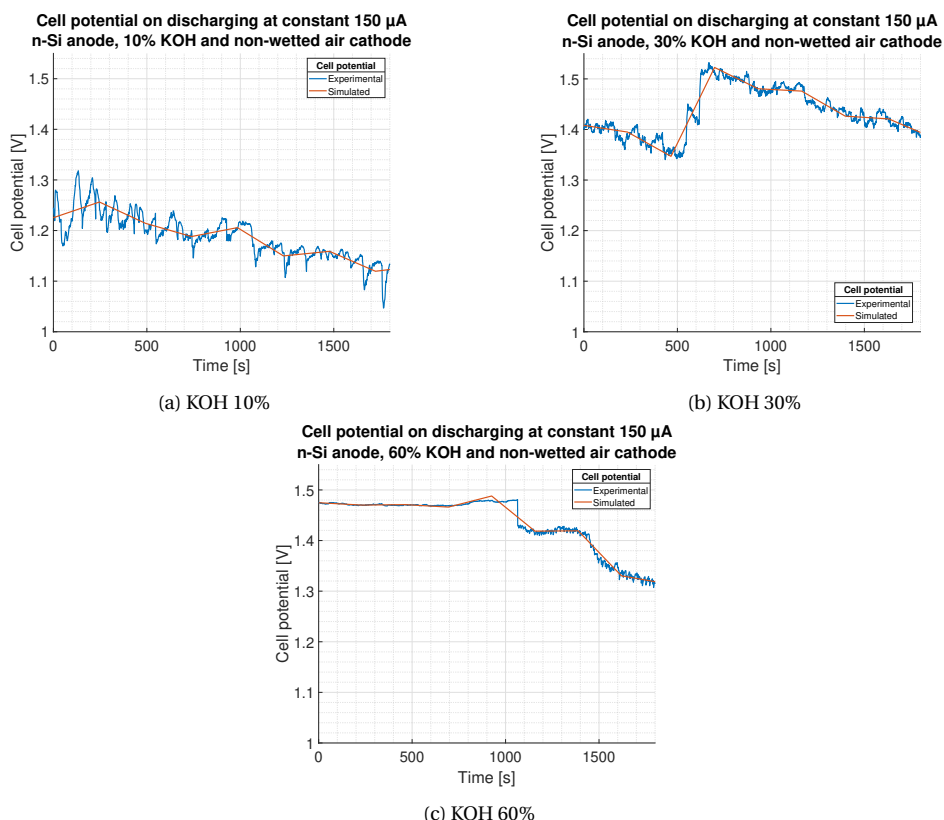


Figure 5.1: Experimental (in blue) and simulated (in red) cell potential vs. Time using discharge current of $150 \mu\text{A}$ after parameter estimation is carried out for various concentrations under n-type Si anode and normal air cathode

Using the parameter estimator tool in Simulink design optimization environment. The Si-air battery model cell parameters are calibrated. The simulated voltage curve is made to fit the experimental voltage by varying the cell parameters. The simulated voltage (plotted in red) after calibration with the experimental voltage is plotted with Figure 5.1.

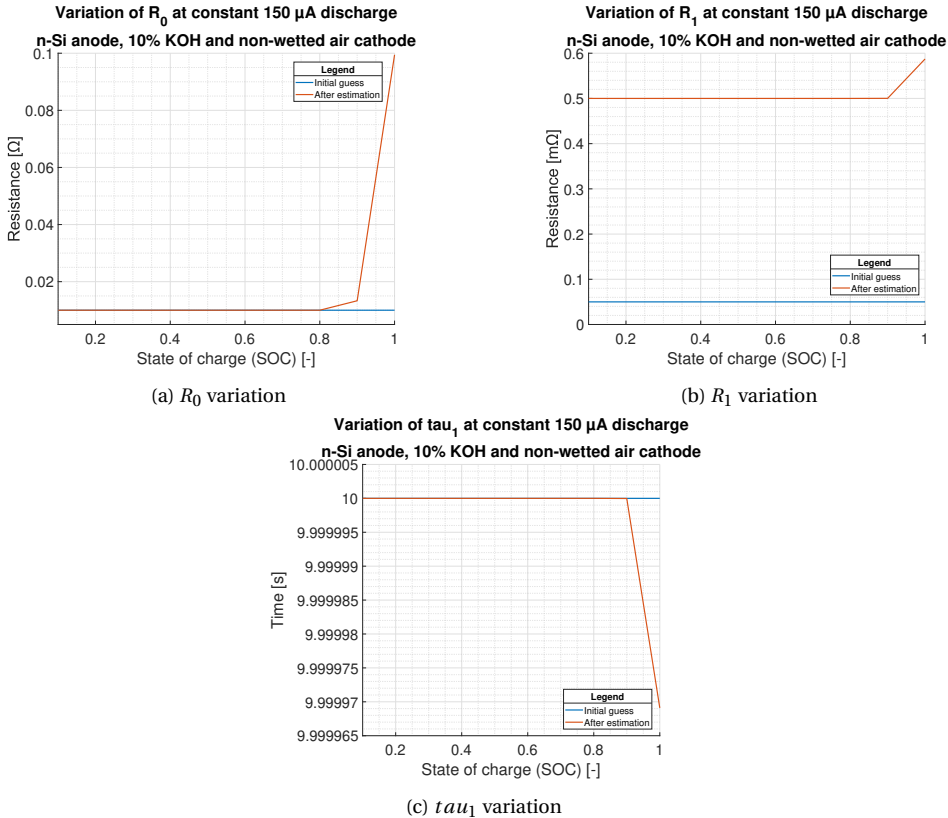


Figure 5.2: Cell parameter variation for KOH 10% before parameter estimation in blue and cell parameter variation after parameter estimation in red against the state of charge (SOC) of the Si-air cell. This trend is the same for KOH 30% and KOH 60% under n-type Si anode and normal air cathode

Note: During modelling it is seen that the cell parameters R_0 , R_1 and τ_{a1} showed no dependency with concentration and the plots and data was similar across all the KOH concentration used in the analysis. In Figure 5.2 the variation of cell parameters in a Si-air cell with KOH 10% is plotted which is the same when KOH 30% and KOH 60% is used as the Si-air cell. The individual plots of the following individual cases can be found in the Appendix B. From this Figure 5.2, we can conclude that the cell parameters R_0 , R_1 and τ_{a1} are:

- Only a function of the state of charge (SOC) of the cell.

- Not a function of the KOH concentration.
- Only deviates from the initial guess at SOC points of 0.9 and 1.0.
- There is no variation R_0 modelling parameter due to change in concentration as predicted in Section 4.

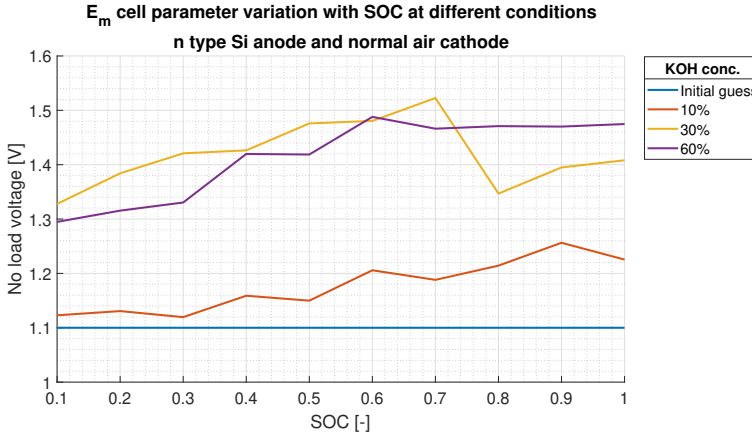


Figure 5.3: E_m variation with state of charge (SOC) of the cell against the initial guess (in blue).

Figure 5.3 plots the variation of the E_m cell parameter across various state of charge (SOC) points of the cell. It is the only parameter that shows deviation from the initial guess of 1.1 V for all SOC points. From this we can conclude that the cell parameter E_m is:

- A function of the state of charge (SOC) of the cell.
- Deviates from the initial guess at all SOC points.
- A function of the input discharge profile. The effect of concentration change cannot be predicted from this cell parameter variation.

Table 5.1: Cell capacity values for each concentration for n-type Si anode and normal air cathode.

KOH concentration	Initial guess	Cell capacity
%	μAh	μAh
10	100	102.56
30	100	97.06
60	100	96.34

In Section 4.3.1, it is assumed that the cell capacity is 100 μAh . The capacity of the cell was kept as a parameter of the model and was allowed to change by the parameter estimator to best fit value till it fits the experimental voltage obtained from the discharge

measurements. The Table B.5 illustrates the values of the best fit capacity values for the Si-air cells according to the Simscape model which reports that the predicted cell capacity is the highest in the case of a Si-air battery with n-type Si and normal air cathode conditions with an electrolyte concentration of KOH 10%.

It is concluded that R_0 , R_1 and τ_{11} parameters shows no variation with electrolyte concentration under constant current discharge. This disproves the speculation made in Section 4.1 about the R_0 parameter being affected with the increase in concentration as the conductivity of the cell increases cannot be predicted by the Simscape model that is developed. Hence, the E_m cell parameter is affected when the concentration of the cell is changed.

5.2. VARIATION WITH PRE-WETTING AIR CATHODE

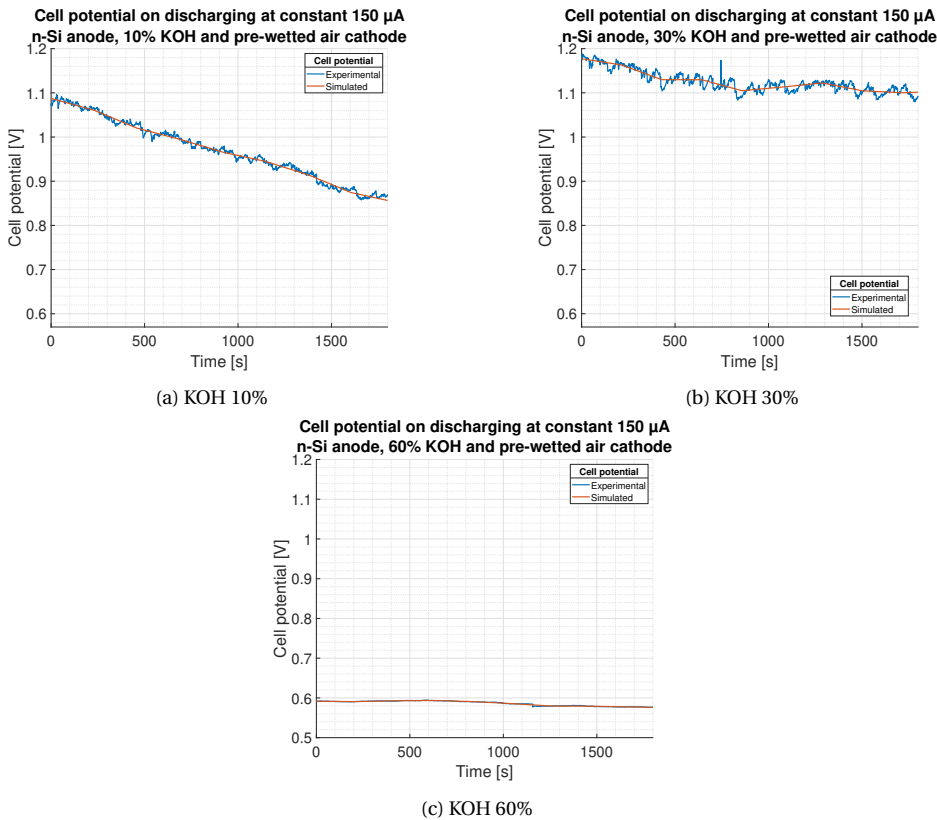


Figure 5.4: Experimental (in blue) and simulated (in red) cell potential vs. Time using discharge current of $150 \mu\text{A}$ after parameter estimation is carried out for various concentrations under n-type Si anode and pre-wetted air cathode.

Pre-wetting the air cathode improves the Si-air cell performance [30]. In Section 4, we

speculated that parameters R_1 and τ_{a1} will vary as it is electrode-electrolyte interaction dependent [42]. The model parameters are compared using a n-type Si anode under normal air cathode conditions for varying KOH conditions as shown in the previous section.

Once the cell parameters have been calibrated according to the input discharge profile curves. We see that the simulated voltages in red and the experimental voltage in blue coincide with each other in Figure 5.4. This proves that the battery block as been calibrated to the experimental cell and the cell parameters have changed accordingly.

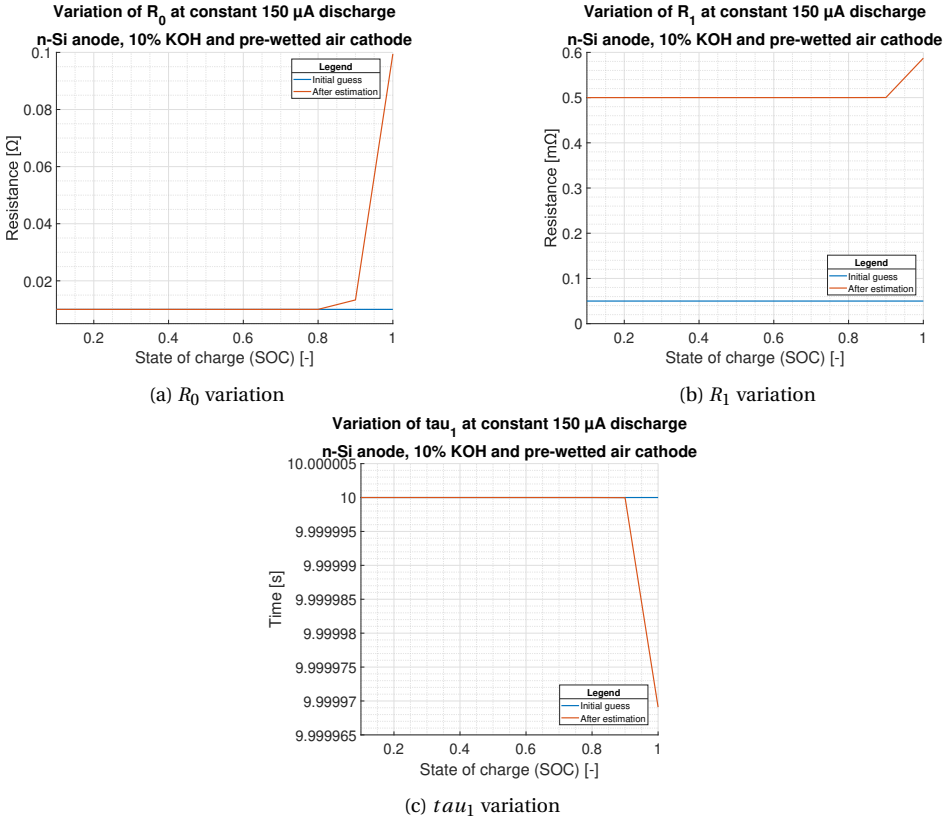


Figure 5.5: Cell parameter variation for KOH 10% before parameter estimation in blue and cell parameter variation after parameter estimation in red against the state of charge (SOC) of the Si-air cell. This trend is the same for KOH 30% and KOH 60% under n-type Si anode and pre-wetted air cathode

Note: Similar to what is seen in the case of variation in concentration. The cell parameters R_0 , R_1 and τ_{a1} are not affected with pre-wetting of air cathode and show the same value as in the case of variation in concentration. Hence, in the Figure 5.5 shows only the variation of cell parameters in a Si-air cell with n-type Si and pre-wetted air cathode with

an electrolyte of KOH 10%. The individual plots can be found for KOH 30% KOH 60% in Appendix B. The following observations can be made from Figure 5.5 about R_0 , R_1 and τ_{a1} :

- Similar to what was seen in variation in concentration, the cell parameters show the same values as in the varying electrolyte concentration. The parameters are again proved to be a function of the cell state of charge (SOC) only.
- Pre-wetting the air cathode has no effect on the cell parameters.
- Only the cell parameter values at the SOC points 0.9 and 1.0 are affected.
- No variation in R_1 and τ_{a1} parameter due to pre-wetting contrary to what was speculated in Section 4.

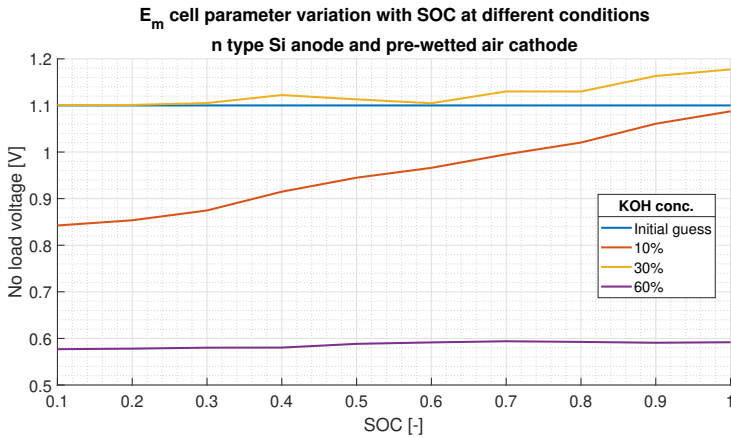


Figure 5.6: E_m variation with state of charge (SOC) of the n-type Si anode and pre-wetted air cathode Si-air cell against the initial guess (in blue).

Similar to what is reported for the case of varying electrolyte concentrations. The Figure 5.6 illustrated the variation of E_m parameter of a Si-air cell with n-type Si anode, pre-wetted air cathode and with varying electrolyte concentration from the initial guess value of 1.1 V. The following observations can be made about E_m parameter variation with SOC under pre-wetted air cathode condition:

- It is also a function of state of charge (SOC) of the cell.
- Deviates from the initial guess value at all points similar to what was seen in varying concentrations case.
- The effect of pre-wetting of air cathode can not be predicted from this cell parameter as it is a function of both SOC and the input discharge profile.

Table 5.2: Cell capacity variation with pre-wetting (PW)

KOH concentration	Initial guess	Cell capacity
%	μAh	μAh
10% PW	100	95.38
10%	100	102.56
30% PW	100	88.81
30%	100	97.06
60% PW	100	81.49
60%	100	96.34

It can be said that pre-wetting the air cathode has an effect on the cell capacity according to the Simscape model as it shows in Table 5.2 that pre-wetting reduces the cell capacity. However, the Simscape model can not simulate the physical significance of cell capacity unlike an electrochemical COMSOL model. It does not take into account for the various inner mechanisms occurring in the Si-air battery that will have a significant effect on the battery. It only tries to fit the different variable values according to the best fit.

It can be concluded that pre-wetting the air cathode has no effect on the cell parameters R_0 , R_1 and τ_{a1} parameters under constant current discharge. This also debunks the speculation made that the model can predicted the variation in R_1 and τ_{a1} as these cell parameters are directly linked to the electrode material characteristics. Although it is reported that there is a variation in the E_m parameter, the variation cannot explain whether the air cathode is pre-wetted or not.

5.3. VARIATION WITH ELECTRODE MATERIALS

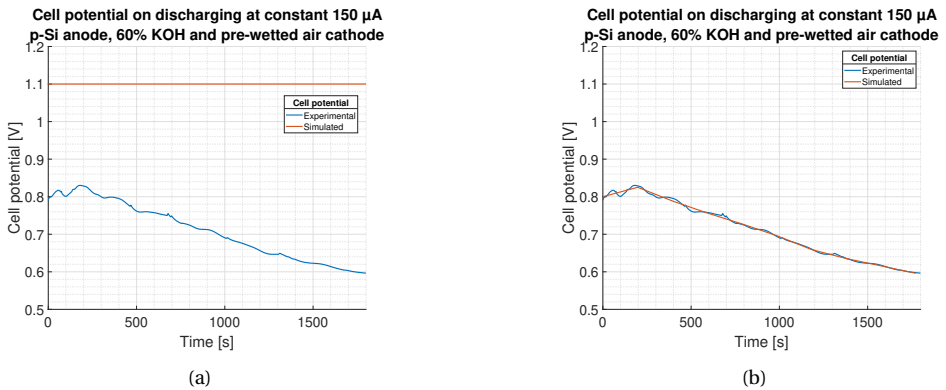


Figure 5.7: Experimental (in blue) and simulated cell (in red) potential vs. Time using discharge current of 150 μA is with p-type Si anode, pre-wetted air cathode in KOH 60% electrolyte. (a) Before parameter estimation is done and (b) After parameter estimation is done.

The cell parameters are compared to when the Si-air cell is in pre-wetted air cathode

condition in 60% KOH concentration and has n-type Si anode and a Si-air cell under the same conditions but with a p-type Si anode since it is reported to have lower corrosion rate than n-type Si [27].

The Figure 5.7a shows the simulated voltage in and the experimental voltage of the Si-air cell for a p-type Si anode, pre-wetted air cathode condition and with an electrolyte concentration of KOH 60% before the model has been calibrated. The simulated voltage is calculated based on the initial guess values for the cell parameters given in Section 4.

Once the Si-air battery model is calibrated to the experimental cell potential curve, the Figure 5.7b is plotted where it can be concluded that the Si-air cell has been calibrated to the Si-air cell behaviour with a p-type Si, pre-wetted air cathode in KOH 60% solution. The cell parameters have also been changed in order for the simulated voltage to fit the experimental voltage curve.

Similar to what was seen in the previous sections, R_0 , R_1 and τ_{a1} parameters showed the same variation as shown previously and only varied with respect to the state of charge (SOC) of the cell. The cell parameter values for R_0 and R_1 only vary from the initial guess for SOC points 0.9 and 1.0 and they were speculated to change in Section 4 however, this was not observed here. The parameters also showed same values as the previous case thereby confirming that by changing the Si anode of the Si-air cell, there is no effect on the modelling cell parameters R_1 and τ_{a1} which was speculated to be affected when electrode materials are changed.

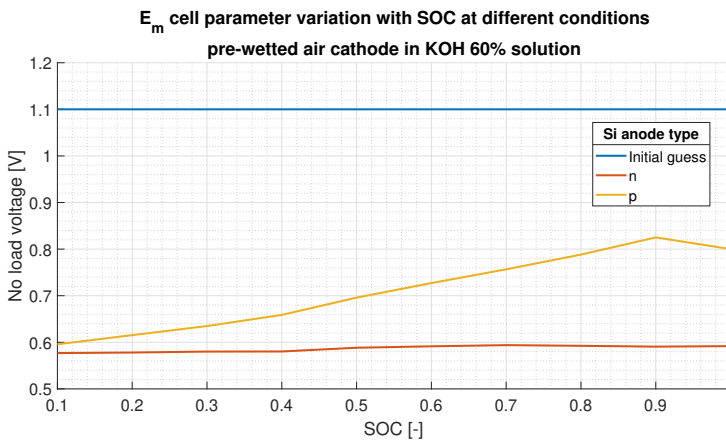


Figure 5.8: E_m variation with state of charge (SOC) of p-type Si anode with pre-wetted air cathode in KOH 60% solution Si-air cell against the initial guess (in blue).

The only cell parameter that changes consistently on all the cases is E_m cell parameter or the no load voltage parameter. This is because out of all the four cell parameters, E_m cell parameter is the only parameter that depends on both the state of charge (SOC) of

the cell as well as the input experimental cell potential profile. However, on studying the variation E_m cell parameter, one cannot predict the Si anode condition that the Si-air cell uses. This is plotted in Figure 5.8.

Table 5.3: Cell capacity value when under pre-wetted air cathode and KOH 60% conditions

Si type	Initial guess	Cell capacity
[-]	μAh	μAh
n	100	81.49
p	100	93.54

The following statements is made about the predicted cell capacity from Table B.15:

1. The values of cell capacity changes from initial guess as indicated in bold text.
2. As per the Simscape model, on using a p-type Si as the Si anode. It will yield higher cell capacity. It can be seen that when we use n-type Si for pre-wetted air cathode under 60% KOH the cell capacity is 81.49 μAh . It increases to 93.54 μAh when we use p-type Si as the anode.

As stated in the previous sections, the Simscape model stating that the Si-air cell capacity is less than 150 μAh is incorrect as galvanostatic measurement are done at constant 150 μA for more than 1 hour. However, the Simscape model stating that one can get higher capacity if you use a p-type Si than an n-type Si is something that needs to be experimentally proven. It can be concluded that the cell parameters R_0 , R_1 and τ_{11} showed the same variation as in the previous cases and proved that they are only dependent on the state of charge (SOC) of the cell. It was speculated that the values R_1 and τ_{11} would change in Section 4 but this was not observed and can be concluded that the model cannot predict the type of Si anode used in the Si-air cell using the input voltage discharge curve. There is variation observed in E_m parameter however this can not state about the Si anode condition as well.

5.4. DISCUSSION

This section concludes the findings from running the model using the experimental data which was elaborated in Chapter 5. The change in the model cell parameters was observed as the Si-air cell is discharged under constant current under varying conditions. The following conclusions can be made from the modelling results in the previous section:

1. The cell parameters R_0 , R_1 and τ_{11} are the mostly the same value given any physical condition change. It is observed that all the R_0 , R_1 and τ_{11} columns are mostly identical when the variation of cell parameters with electrolyte concentration is studied in Section 5.1, variation of cell parameters with pre-wetting of air cathode is studied in Section 5.2 and variation of cell parameters with Si anode type in Section 5.3.

2. It must be also noted that for the R_0 and R_1 cell parameters, the only values that changed from the initial guess are at SOC points 0.9 and 1.0. τ_1 displayed minimal to no variation among these SOC points. From this observation, one can conclude that the cell parameters R_0 , R_1 and τ_1 are solely a function of the state of charge (SOC) of the cell and not on dependent on the experimental voltage input of the cell in case of galvanostatic discharge.
3. The cell parameter E_m which is the simulated no load voltage of the cell is the only cell parameter that varies with both state of charge of the cell (SOC) as well as the different conditions the Si-air cell was subjected to. This means that the E_m cell parameter is a function of both the SOC as well as the input experimental potential profile for the various conditions. The experimental battery cell potential (V_{cell}) can be written as:

$$V_{cell} = E_m - IR$$

$$E_m = V_{cell} + IR$$

where, I is the discharge current which is a constant current of $150 \mu\text{A}$ and R is the internal resistance of the Si-air cell which is a function of SOC as established in the previous point.

4. The capacity parameter of the model was used to calculate the predicted capacity of the Si-air cell. In all the various cases except for when the KOH concentration is 10% with n-type Si as anode in normal air cathode condition, the capacity of the cell was predicted to be less than $100 \mu\text{Ah}$. This could not be the case as stated in the previous section, galvanostatic measurements were conducted at $150 \mu\text{A}$ for more than 1 hour thereby proving that the cell capacity is much more than $100 \mu\text{Ah}$. According to the model and Table 5.2 and Table 5.3, the cell capacity decreases when:
 - (a) The concentration of electrolyte is increased.
 - (b) The air cathode is pre-wetted.
 - (c) The Si anode is n-type.

In order to predict the cell parameters across all the state of charges of the battery accurately, pulsed discharge measurements must be used as the input potential profile [7]. It can be observed from the previous Section 5 that the cell parameters from SOC points 0.1 to 0.8 did not deviate from the initial guess at all in the case R_0 , R_1 and τ_1 although the battery could simulate the experimental voltage for constant current discharge conditions.

This is mainly because of the method of evaluation of the model which is illustrated in Figure 5.9 where it can be seen that a pulsed discharge current is required in order to evaluate the RC transients which is R_1 and τ_1 accurately. Therefore, the initial assumption that was made that having constant current discharge curves can yield the

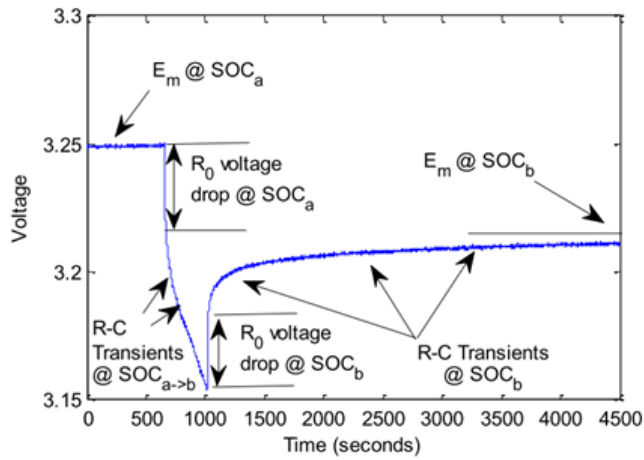


Figure 3: One pulse from the discharge test.

Figure 5.9: Cell parameter evaluation in a pulsed curve [7]

same results as the pulsed discharge curves was incorrect. The individual plots of the parameter variation is in Appendix B and the MATLAB script used to run the model is in Appendix C. Some recommendations for the experimental side and modelling side of thesis is given in the next Section for making this model more realistic and accurate.

6

CONCLUSIONS

IN this thesis, an alkaline Si-air cell was fabricated using KOH electrolyte. This cell is then run through different physical conditions and discharged at a constant discharge current of 150 μA . The discharge curves for different KOH concentration, different electrode materials and effects of air cathode pre-wetting are observed. The results of these experimental data is discussed in Section 3. Furthermore, a Si-air battery model is made in Simscape model using a Li-ion battery model as reference in order to evaluate the cell parameters of the cell. The experimental data obtained from lab work under different conditions is used as input data for this model and the cell parameters of the Si-air cell is calculated for the particular conditions. There results are shown and discussed in Section 5. This is done in order to evaluate if the model can simulate Si-air cells with different physical conditions by inputting the cell parameters.

6.1. EXPERIMENTAL CONCLUSION

Galvanostatic discharge tests were conducted on the fabricated Si-air cell to evaluate the potential curves under varying physical conditions to feed as input to the Simscape model and the experimental data are compared to the data reported by Durmus et al. and Prins [4] [30]. The following conclusions are drawn:

- *Higher average open-circuit potentials (OCPs)*: It is reported by Durmus et al., that open-circuit potential (OCP) of the alkaline Si-air cell has no influence on the cell's OCP and showed a steady value of 1.4 V for various electrolyte (KOH) concentrations [4]. In the study reported in this M.Sc thesis, we get average OCPs ranging from 1.509 V and 1.482 V and reduces with KOH concentration. It is speculated that, this is attributed to the usage of a 99% Aluminium 1% Si (Al:Si) layer that has proven to reduce sheet resistance in (Copper indium gallium selenide solar cells) CIGS solar cells and silicon solar cells [36] [35]. The Si anode reported by Durmus et al. does not have a back contact as is used in this study. This speculation is further supported with Prins's findings of using the same Al:Si back contact used in this study and has reported higher OCPs for Si-air cell n-type Si, pre-wetted air

cathode and KOH 30% electrolyte concentration [30].

- *Reducing open-circuit potentials (OCPs):* In Section 3.4 Table A.14a we see that the OCP decreases as a function of time. This is in agreement with the Nernst equation which is explained in Equation 1.9 and contrary to the reported steady 1.4 V by Durmus et al. [4]. This is because of the change in concentration of OH^- due to corrosion (formation of silicates). As the KOH concentration increases, the corrosion rates also increase till a maximum of 6 M KOH [15].
- *Reducing discharge potentials (DPs):* It is observed that the discharge potential increases as a function of discharging time in the readings by Durmus et al. [4]. This is not what was observed in this thesis, it is reported that there is decreasing DP as a function of discharging time from Figure A.14b. This would be because using a current density of $150 \mu\text{A}/\text{cm}^2$ is more than the threshold value of $50 \mu\text{A}/\text{cm}^2$ required for passivation making the Si anode less inactive due to the formation of a SiO_2 layer [15][4]. This is also because of using a much higher current density which three times more than what was used in Durmus et al. which is $50 \mu\text{A}/\text{cm}^2$ [4]. This would mean that the Si-air battery discharges at faster rate than the one reported by Durmus et al.
- *Effect of pre-wetting air cathode:* It was reported by Prins that pre-wetting the air cathode for 8 hours, one can discharge the Si-air cell for upto 110.75 hours [30]. In this study, it is reported that pre-wetting the air cathode lowers the OCP and DP when comparing it with non-wetted air cathode condition for all cases, which is confirmed with Prins's readings for Si-air cell with KOH 30% concentration [30].
- *Effect of Si anode:* It was reported by Cohn et al. that using p-type Si would lead to lower corrosion rate [27]. This is confirmed in the OCP curve in Figure 3.4a where higher OCP is achieved when using p-type Si anode rather than n-type Si anode for a Si-air cell that has pre-wetted air cathode and KOH concentration of 60%.

The experimental data done in this thesis is used to support the alkaline Si-air battery model and to simulate its effect in a constant current discharge condition.

6.2. MODELLING CONCLUSION

The alkaline Si-air battery model is fed with experimental data by varying different physical conditions in order to evaluate and test the cell parameter variation under constant current discharge conditions. This is done to verify whether the model parameters change according to the different physical conditions that the Si-air cell was subjected to.

In Chapter 4, the physical significance of each modelling cell parameter used in the alkaline Si-air cell model developed for this thesis is reported. It was speculated that these cell parameters would change and vary when the physical conditions that the Si-air cell is subjected varies. It was speculated the Si-air cell's electrolyte resistance (R_0) would alter with the change in concentration of the electrolyte in the cell [43]. It was speculated

that the cell parameters R_1 and τ_{11} would change with electrode condition changes as they model the electrode-electrolyte interface mechanisms [42].

In Chapter 5, it is reported for constant current discharge of $150 \mu\text{A}/\text{cm}^2$, it was observed that the Si-air cell modelling parameters R_0 and R_1 had changed only at the state of charge (SOC) points 0.9 and 1.0. τ_{11} cell modelling parameter showed little to no variation with SOC of the cell irrespective of the different physical conditions the cell was subjected. However, since the E_m or open-circuit voltage parameter is directly related to the discharge potential curve since it is evaluated as $E_m = V_{exp} + IR$ where V_{exp} is the input experimental voltage, I is the discharge current and R is the internal resistance of the battery. Hence, it is concluded that E_m cell parameter is directly correlated to the input experimental voltage or V_{exp} for all cases.

The alkaline Si-air battery model are made in Simscape (MATLAB) can simulate the battery behaviour based on the experimental data that the Si-air cell would be physically subjected to. It is not possible to simulate the battery operation under different physical conditions by changing the cell model parameters compared to other battery models such as behavioural battery model and electrochemical battery model from Simscape. However, the calibrated battery block can be used as part of a larger system and to simulate real-time battery managements systems (BMS) with lower computational intensity [46].

7

RECOMMENDATIONS

THE first Si-air cell was discovered and reported in 2009 by Cohn et al. [27]. Hence, there is very limited information regarding Si-air battery cell. The goal was to make a simple and functional model using experimental data that support the model. However, there are a few shortcomings to this thesis that can be addressed in the future and some future applications of this model shall be elaborated below.

7.1. EXPERIMENTAL SIDE

Galvanostatic measurements were conducted on a fabricated alkaline Si-air cell using KOH as the electrolyte. There are were a few limitations to the conducted experiments which will be pointed out here:

1. *Better cell design:* The Si-air cell that was used in these experiments took quite a lot of time for assembly and had a lot of parts in its assembly. It had to be made sure that all the nuts were tight enough to not leak any of the KOH in the cell but not so tight that it breaks the sample. This required a lot of patience and practise to get a feeling on the right tightness of the Si-air cell. However, there were still times were the Si-air cell leaked or the Si sample broke as seen in the Figure 7.1.



Figure 7.1: Broken Si sample.

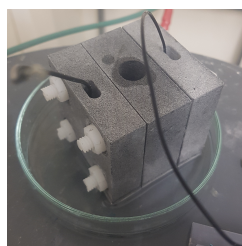


Figure 7.2: Leaking Si-air cell.

A Si-air cell design that allows the user to only change the Si anode and air cathode and can easily change the electrolyte would be the ideal case. It should require the least amount of human interaction.

2. *Pulsed discharge tests:* It is stated in literature for the Li-ion model to predict the correct cell parameter, pulsed discharge measurements must be carried out [7]. This was a big limitation on using the MECO Cu plating equipment since such an option wasn't available.
3. *Temperature controlled testing:* It is known that temperature has a direct effect on the cell potential as seen in Nernst equation in Equation 1.9. However this wasn't possible in the MEMS lab and due to the usage of the incorrect equipment.
4. *Effect of doping concentration:* It is seen that using n-type Si and p-type Si as the Si anode yields different results in Section 5.3. A study of the effect varying the doping concentration on the alkaline Si-air cell would be noteworthy. A study on the effect of doping concentration has been reported for the primary non-aqueous Si-air cell by Cohn et al. [27] and can be compared to this study.
5. *Proving Al:Si layer effectiveness:* It has been speculated in this thesis that using an Al:Si back contact layer in the Si anode yields higher OCPs. Experiments must be carried out where a normal n-type or p-type Si with no back contact layer is compared with one that has back contact layer. This will confirm the speculation made in this thesis.

7.2. MODELLING SIDE

Now there are something recommendations that can be made for the simulation side of the thesis:

1. *Pulsed discharge inputs:* As explained in Section 5.4, it can be seen how the Li-ion battery model evaluates the cell parameter using a pulsed voltage curve. For the model to evaluate the Si-air cell parameters at all SOC, the discharge voltage profile must be pulsed. In Figure 2.4, we can see that we can set the current to go to different values, one can reduce the time step of signal recording here and simulate a pulse in the discharge current.
2. *Increasing the number of time constants:* In the model in this thesis, only one time constant dynamics is used. However, it is known that using more time constants can make the model much more accurate although it becomes more computationally intensive.
3. *Calculation of heat generation:* The intended use of the Li-ion model is to calculate the amount of heat dissipation of the Li-ion battery due to charging/discharging and formulate the amount of cooling packs required for the battery for optimum performance as temperature has a direct effect on the cell state of charge (SOC).
4. *Modelling for self-discharge and Temperature:* MATLAB allows the incorporation of self discharge dynamics and temperature effect on the battery block. This is

also something that can be explored in the future to make the Si-air battery model more realistic.

Using the above recommendations, the alkaline Si-air battery model can more realistic and more accurate. It can be also further integrated with other electrical components in Simscape to create circuit modelling that requires a battery source.

A

CELL DISCHARGE CURVES

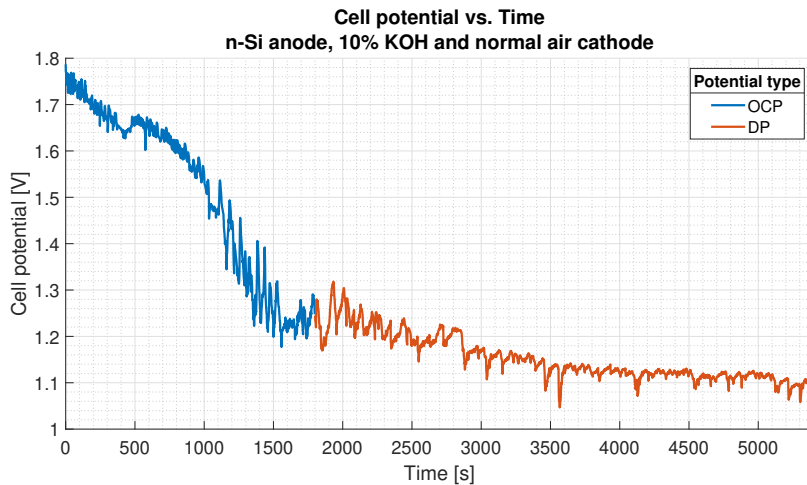


Figure A.1: Cell potential curve of Si-air cell with n type Si anode, KOH 10% and normal air cathode

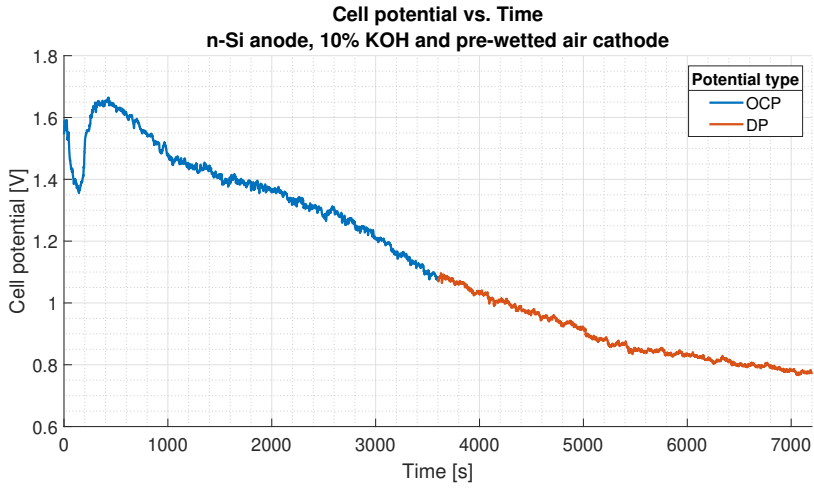


Figure A.2: Cell potential curve of Si-air cell with n type Si anode, KOH 10% and pre-wetted air cathode

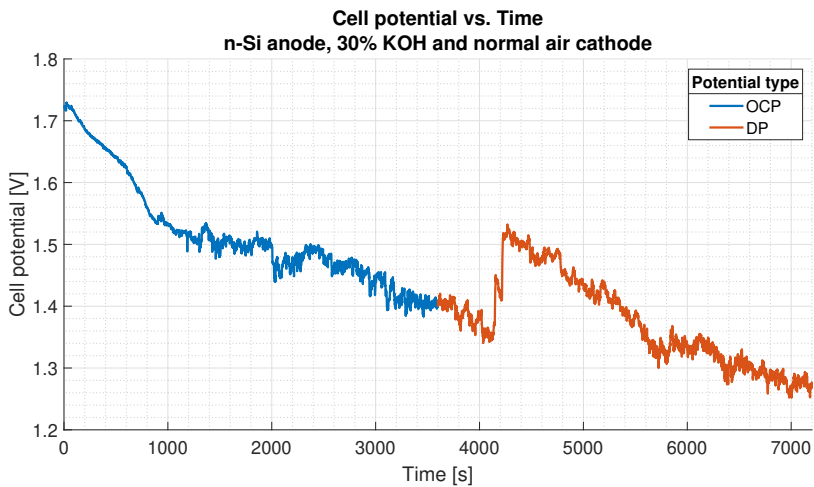


Figure A.3: Cell potential curve of Si-air cell with n type Si anode, KOH 30% and normal air cathode

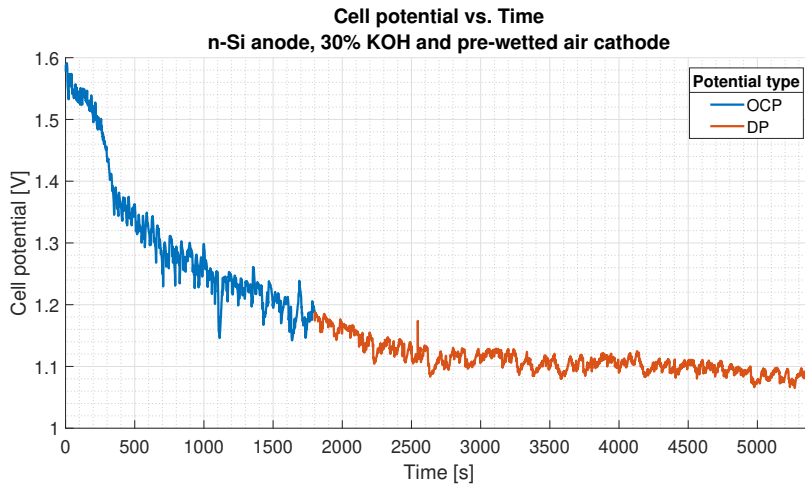


Figure A.4: Cell potential curve of Si-air cell with n type Si anode, KOH 30% and pre-wetted air cathode

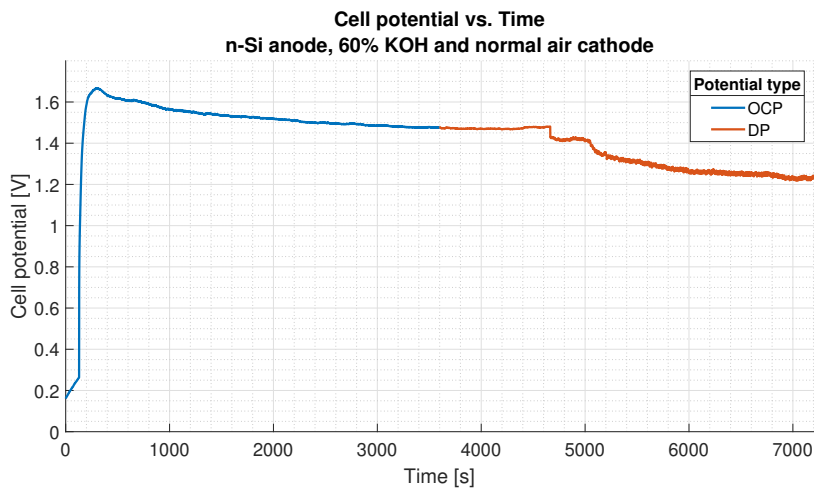


Figure A.5: Cell potential curve of Si-air cell with n type Si anode, KOH 60% and normal air cathode

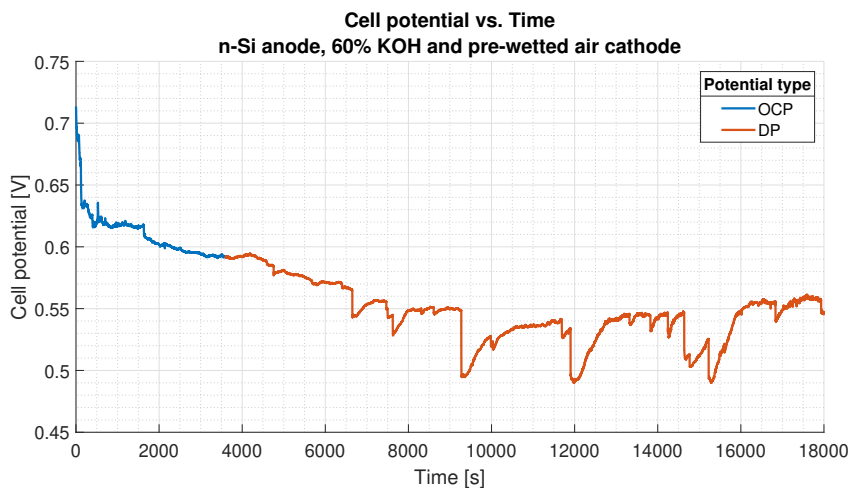


Figure A.6: Cell potential curve of Si-air cell with n type Si anode, KOH 60% and pre-wetted air cathode

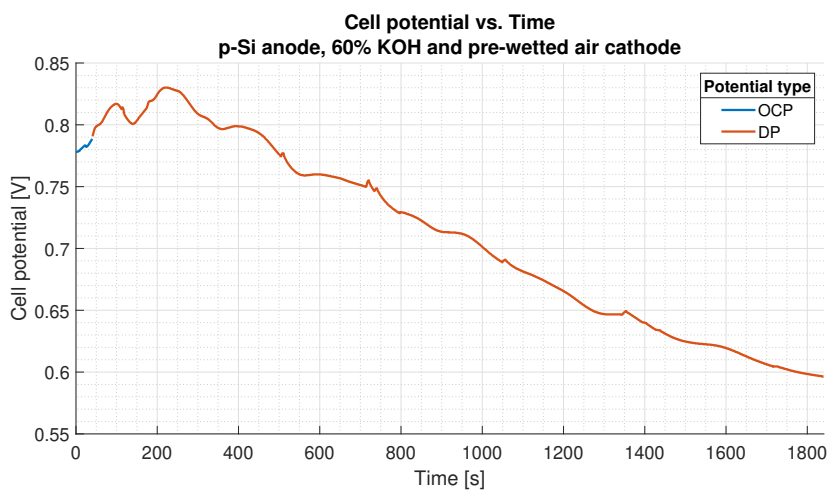


Figure A.7: Cell potential curve of Si-air cell with p type Si anode, KOH 60% and pre-wetted air cathode

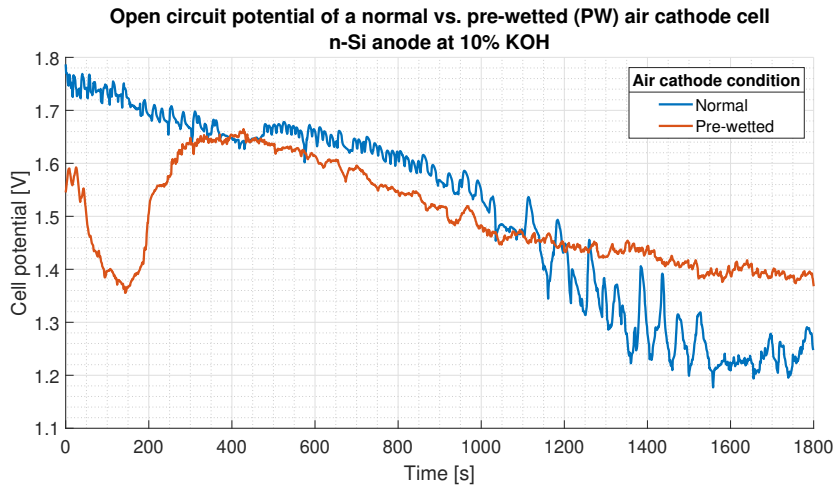


Figure A.8: Variation of open-circuit potential with pre-wetting of air cathode. The cell is n-type Si anode and in 10% KOH

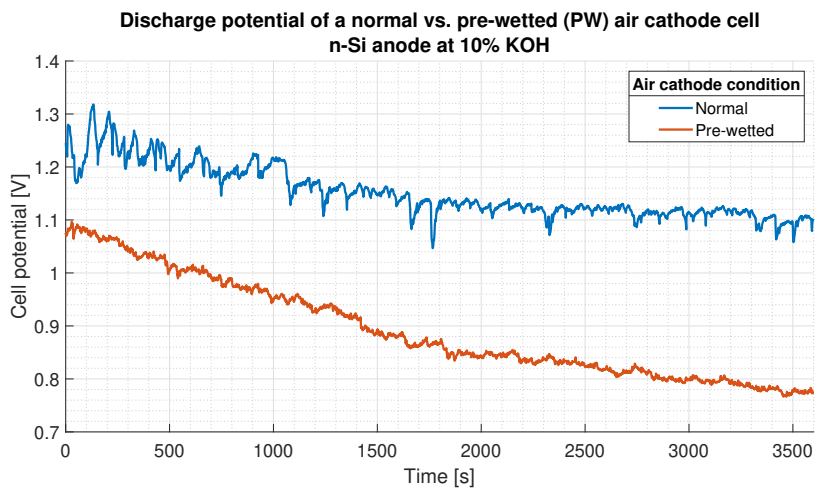


Figure A.9: Variation of discharge potential with pre-wetting of air cathode. The cell is n-Si anode and in 10% KOH

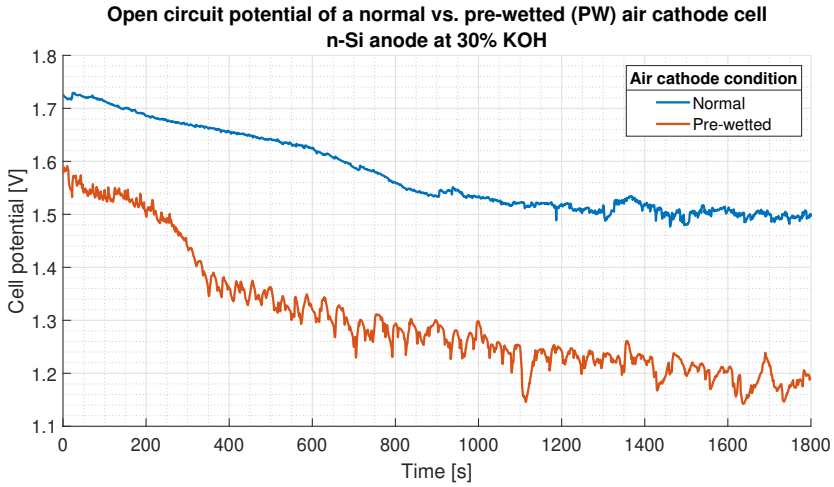


Figure A.10: Variation of open-circuit potential with pre-wetting of air cathode. The cell is n-Si anode and in 30% KOH

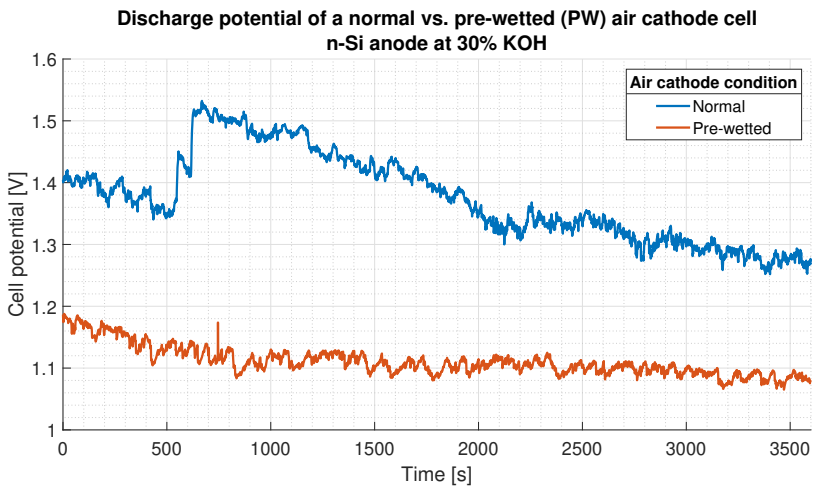


Figure A.11: Variation of discharge potential with pre-wetting of air cathode. The cell is n-Si anode and in 30% KOH

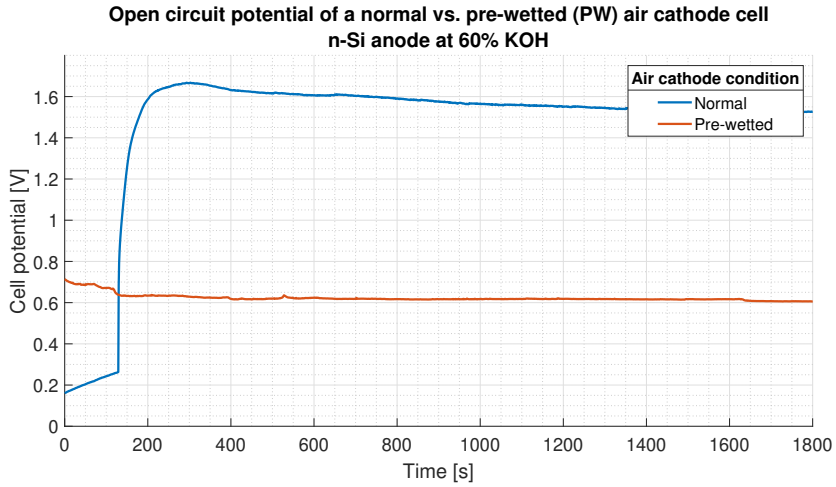


Figure A.12: Variation of open-circuit potential with pre-wetting of air cathode. The cell is n-Si anode and in 60% KOH

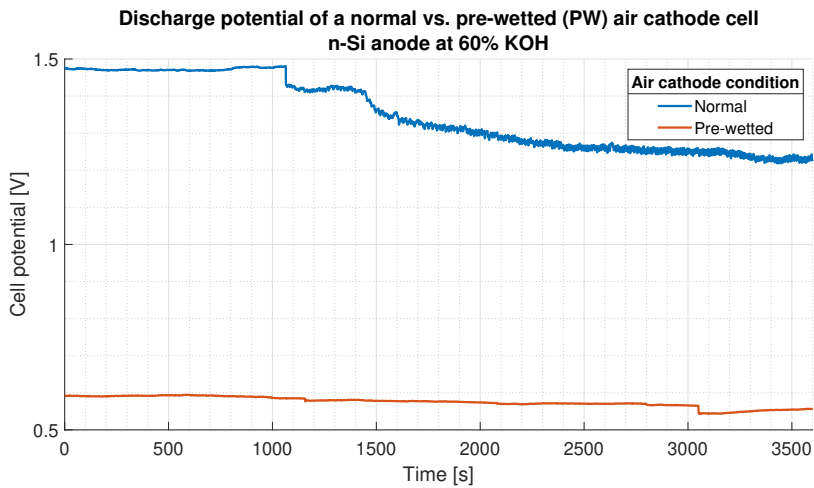


Figure A.13: Variation of discharge potential with pre-wetting of air cathode. The cell is n-Si anode and in 60% KOH

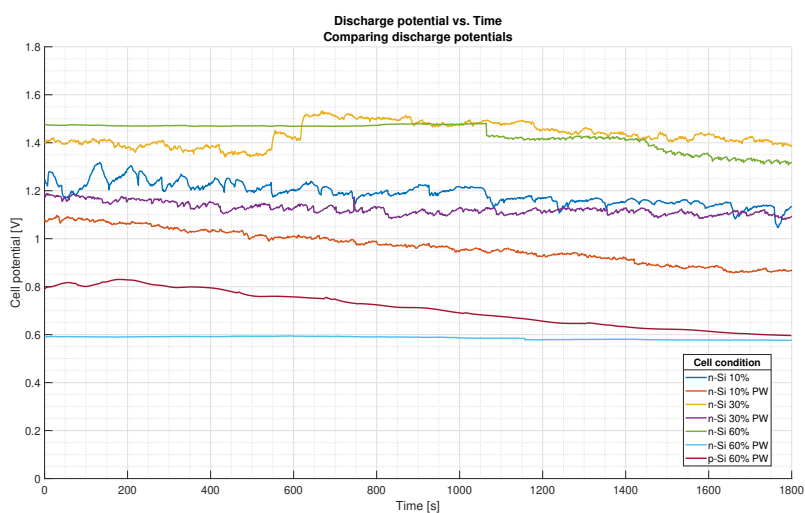
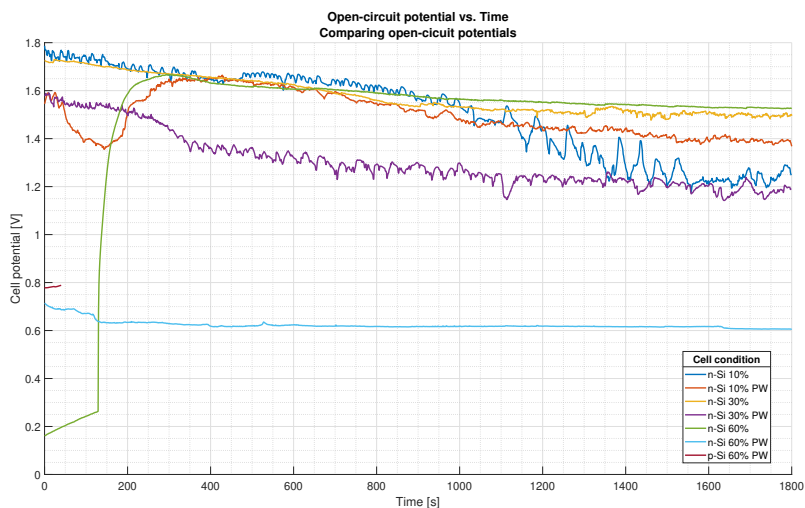


Figure A.14: (a) OCP curve and (b) DP curve when the Si-air cell is placed under different conditions. n-Si indicates n-type Si is used as anode, 10% indicates KOH 10% solution is used as electrolyte and PW indicates that the cell is under pre-wetted air cathode condition.

B

MODEL OUTPUTS

B.1. VARIATION WITH KOH CONCENTRATION

Table B.1: R_0 values for each concentration for n-type Si anode and normal air cathode

SOC	Initial guess	KOH 10%	KOH 30%	KOH 60%
[-]	$\mu\Omega$	$\mu\Omega$	$\mu\Omega$	$\mu\Omega$
0.1	10.00	10.00	10.00	10.00
0.2	10.00	10.00	10.00	10.00
0.3	10.00	10.00	10.00	10.00
0.4	10.00	10.00	10.00	10.00
0.5	10.00	10.00	10.00	10.00
0.6	10.00	10.00	10.00	10.00
0.7	10.00	10.00	10.00	10.00
0.8	10.00	10.00	10.00	10.00
0.9	10.00	13.31	13.31	13.31
1	10.00	99.43	99.43	99.43

Table B.2: R_1 values for each concentration for n-type Si anode and normal air cathode

SOC	Initial guess	KOH 10%	KOH 30%	KOH 60%
[-]	$\mu\Omega$	$\mu\Omega$	$\mu\Omega$	$\mu\Omega$
0.1	500	500.00	500.00	500.00
0.2	500	500.00	500.00	500.00
0.3	500	500.00	500.00	500.00
0.4	500	500.00	500.00	500.00
0.5	500	500.00	500.00	500.00
0.6	500	500.00	500.00	500.00
0.7	500	500.00	500.00	500.00
0.8	500	500.00	500.00	500.00
0.9	500	500.20	500.20	500.20
1	500	587.22	587.22	587.22

Table B.3: τ_{a1} values for each concentration for n-type Si anode and normal air cathode

SOC	Initial guess	KOH 10%	KOH 30%	KOH 60%
[-]	s	s	s	s
0.1	10.00000	10.00000	10.00000	10.00000
0.2	10.00000	10.00000	10.00000	10.00000
0.3	10.00000	10.00000	10.00000	10.00000
0.4	10.00000	10.00000	10.00000	10.00000
0.5	10.00000	10.00000	10.00000	10.00000
0.6	10.00000	10.00000	10.00000	10.00000
0.7	10.00000	10.00000	10.00000	10.00000
0.8	10.00000	10.00000	10.00000	10.00000
0.9	10.00000	10.00000	10.00000	10.00000
1	10.00000	9.99997	9.99997	9.99997

Table B.4: E_m values for each concentration for n-type Si anode and normal air cathode

SOC	Initial guess	KOH 10%	KOH 30%	KOH 60%
[-]	V	V	V	V
0.1	1.1	1.123	1.328	1.295
0.2	1.1	1.131	1.384	1.315
0.3	1.1	1.120	1.421	1.330
0.4	1.1	1.159	1.426	1.420
0.5	1.1	1.150	1.476	1.419
0.6	1.1	1.206	1.480	1.488
0.7	1.1	1.188	1.523	1.466
0.8	1.1	1.214	1.347	1.471
0.9	1.1	1.256	1.395	1.470
1	1.1	1.225	1.408	1.475

Table B.7: R_1 values under normal air cathode and pre-wetted (PW) conditions

SOC	10% PW	10%	30% PW	30%	60% PW	60%
[-]	$\mu\Omega$	$\mu\Omega$	$\mu\Omega$	$\mu\Omega$	$\mu\Omega$	$\mu\Omega$
0.1	500.00	500.00	500.00	500.00	500.00	500.00
0.2	500.00	500.00	500.00	500.00	500.00	500.00
0.3	500.00	500.00	500.00	500.00	500.00	500.00
0.4	500.00	500.00	500.00	500.00	500.00	500.00
0.5	500.00	500.00	500.00	500.00	500.00	500.00
0.6	500.00	500.00	500.00	500.00	500.00	500.00
0.7	500.00	500.00	500.00	500.00	500.00	500.00
0.8	500.00	500.00	500.00	500.00	500.00	500.00
0.9	500.20	500.20	500.20	500.20	500.20	500.20
1	587.22	587.22	587.22	587.22	587.22	587.22

Table B.8: τ_{u1} values under normal air cathode and pre-wetted (PW) conditions

SOC	10% PW	10%	30% PW	30%	60% PW	60%
[-]	s	s	s	s	s	s
0.1	10.00	10.00	10.00	10.00	10.00	10.00
0.2	10.00	10.00	9.99	10.00	9.99	10.00
0.3	10.00	10.00	10.00	10.00	10.00	10.00
0.4	10.00	10.00	9.99	10.00	9.99	10.00
0.5	10.00	10.00	10.00	10.00	9.99	10.00
0.6	10.00	10.00	10.00	10.00	10.00	10.00
0.7	10.00	10.00	10.00	10.00	10.00	10.00
0.8	10.00	10.00	9.99	10.00	9.99	10.00
0.9	9.99	10.00	10.00	10.00	10.00	10.00
1	9.99	10.00	9.99	10.00	9.99	10.00

Table B.9: E_m values under normal air cathode and pre-wetted (PW) conditions

SOC	10% PW	10%	30% PW	30%	60% PW	60%
[-]	V	V	V	V	V	V
0.1	0.84	1.12	1.10	1.33	0.57	1.29
0.2	0.85	1.13	1.10	1.38	0.57	1.32
0.3	0.87	1.12	1.10	1.42	0.58	1.33
0.4	0.91	1.16	1.12	1.43	0.58	1.42
0.5	0.94	1.15	1.11	1.48	0.59	1.42
0.6	0.97	1.21	1.10	1.48	0.59	1.49
0.7	1.00	1.19	1.13	1.52	0.59	1.47
0.8	1.02	1.21	1.13	1.35	0.59	1.47
0.9	1.06	1.26	1.16	1.39	0.59	1.47
1	1.09	1.23	1.17	1.41	0.59	1.47

Table B.10: Cell capacity variation with pre-wetting (PW)

KOH concentration	Initial guess	Cell capacity
%	μAh	μAh
10% PW	100	95.38
10%	100	102.56
30% PW	100	88.81
30%	100	97.06
60% PW	100	81.49
60%	100	96.34

B.3. VARIATION WITH ELECTRODE MATERIALS

Table B.11: R_0 value when under pre-wetted air cathode and KOH 60% conditions

SOC	Initial guess	n type Si	p type Si
[-]	$\text{m}\Omega$	$\text{m}\Omega$	$\text{m}\Omega$
0.1	10.00	10.00	10.00
0.2	10.00	10.00	10.00
0.3	10.00	10.00	10.00
0.4	10.00	10.00	10.00
0.5	10.00	10.00	10.00
0.6	10.00	10.00	10.00
0.7	10.00	10.00	10.00
0.8	10.00	10.00	10.00
0.9	10.00	13.31	13.31
1	10.00	99.43	99.43

Table B.12: R_1 value when under pre-wetted air cathode and KOH 60% conditions

SOC	Initial guess	n type Si	p type Si
[-]	$\mu\Omega$	$\mu\Omega$	$\mu\Omega$
0.10	500.00	500.00	500.00
0.20	500.00	500.00	500.00
0.30	500.00	500.00	500.00
0.40	500.00	500.00	500.00
0.50	500.00	500.00	500.00
0.60	500.00	500.00	500.00
0.70	500.00	500.00	500.00
0.80	500.00	500.00	500.00
0.90	500.00	500.20	500.20
1.00	500.00	587.22	587.22

Table B.13: τ_{a1} value when under pre-wetted air cathode and KOH 60% conditions

SOC	Initial guess	n type Si	p type Si
[-]	s	s	s
0.10	10.00	10.00	10.00
0.20	10.00	9.99	10.00
0.30	10.00	10.00	10.00
0.40	10.00	9.99	10.00
0.50	10.00	9.99	10.00
0.60	10.00	10.00	10.00
0.70	10.00	10.00	10.00
0.80	10.00	9.99	10.00
0.90	10.00	10.00	10.00
1.00	10.00	9.99	10.00

Table B.14: E_m value when under pre-wetted air cathode and KOH 60% conditions

SOC	Initial guess	n type Si	p type Si
[-]	V	V	V
0.10	1.10	0.58	0.85
0.20	1.10	0.58	0.59
0.30	1.10	0.58	0.61
0.40	1.10	0.58	0.64
0.50	1.10	0.59	0.67
0.60	1.10	0.59	0.71
0.70	1.10	0.60	0.74
0.80	1.10	0.59	0.78
0.90	1.10	0.59	0.82
1.00	1.10	0.59	0.80

Table B.15: Cell capacity value when under pre-wetted air cathode and KOH 60% conditions

Si type	Initial guess	Cell capacity
[-]	μAh	μAh
n	100	81.49
p	100	93.54

B

B.4. MODEL PLOTS

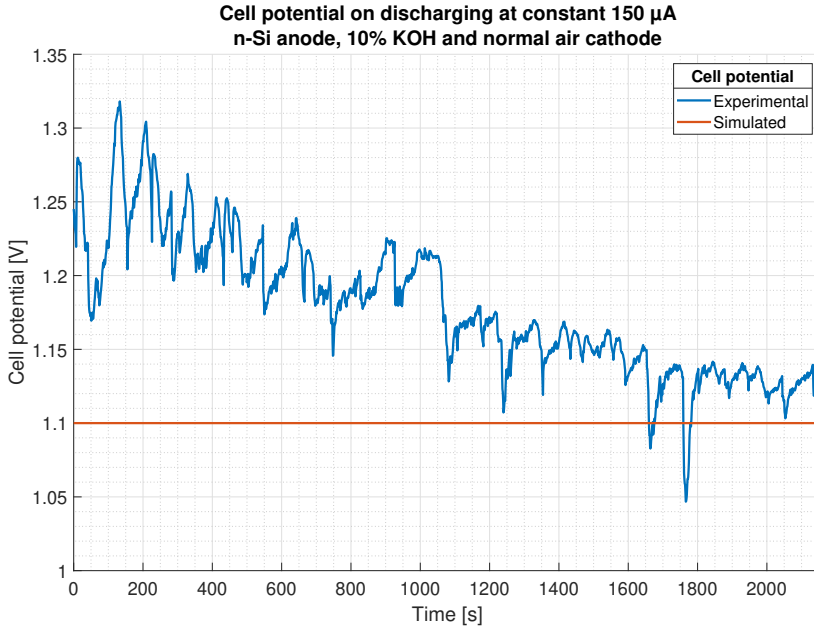


Figure B.1: Before parameter estimation

B

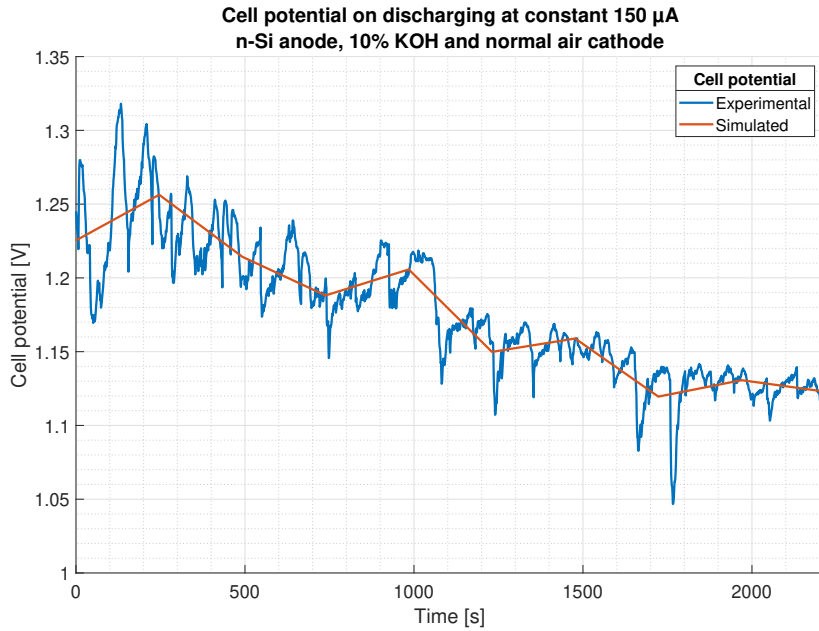
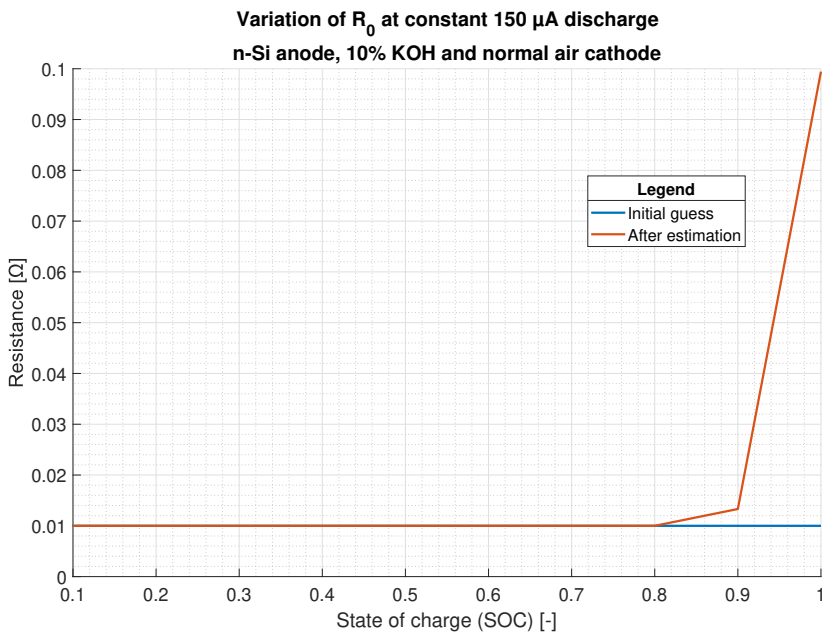


Figure B.2: After parameter estimation

Figure B.3: R_0 variation

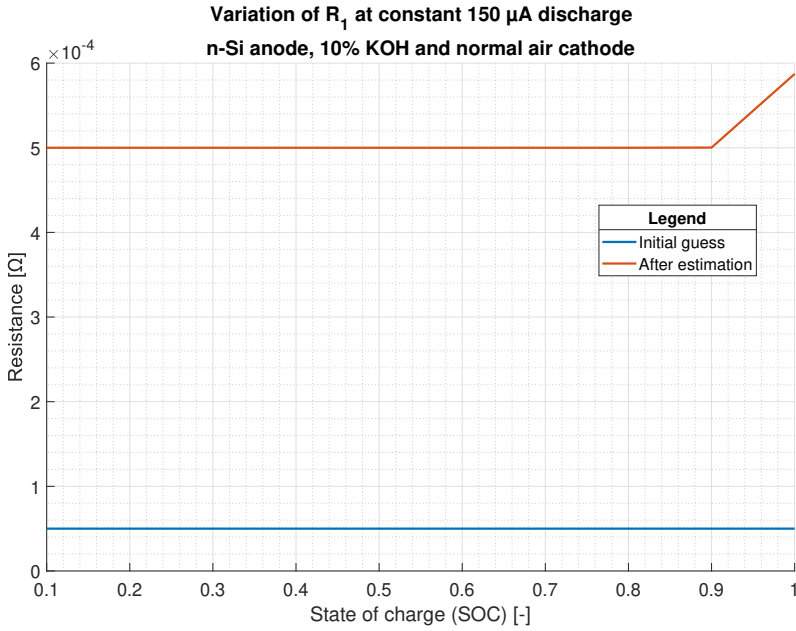


Figure B.4: R_1 variation

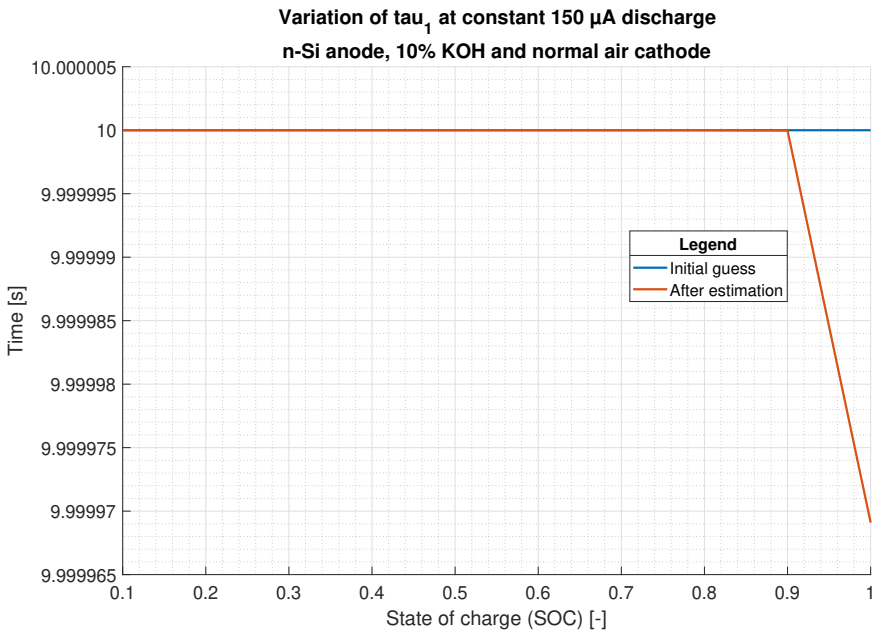


Figure B.5: τ_{a1} variation

B

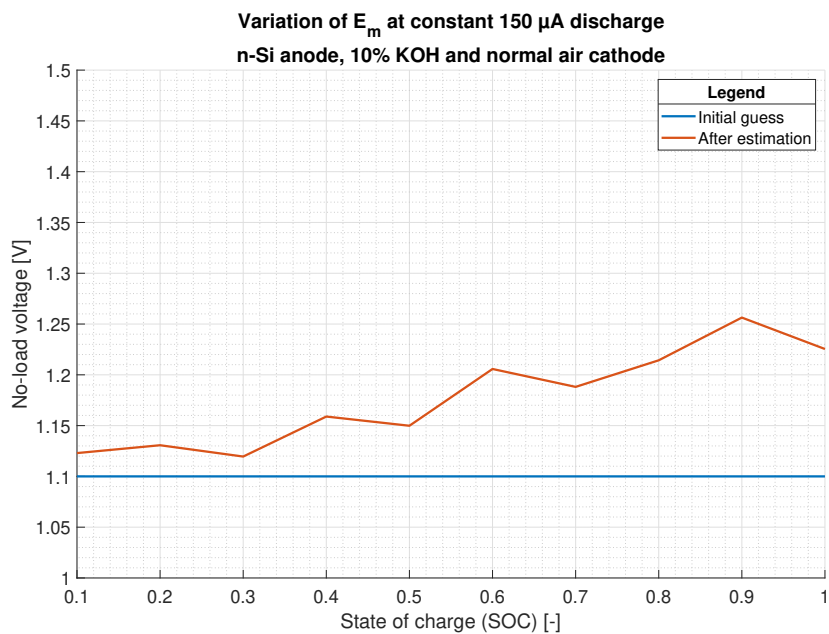
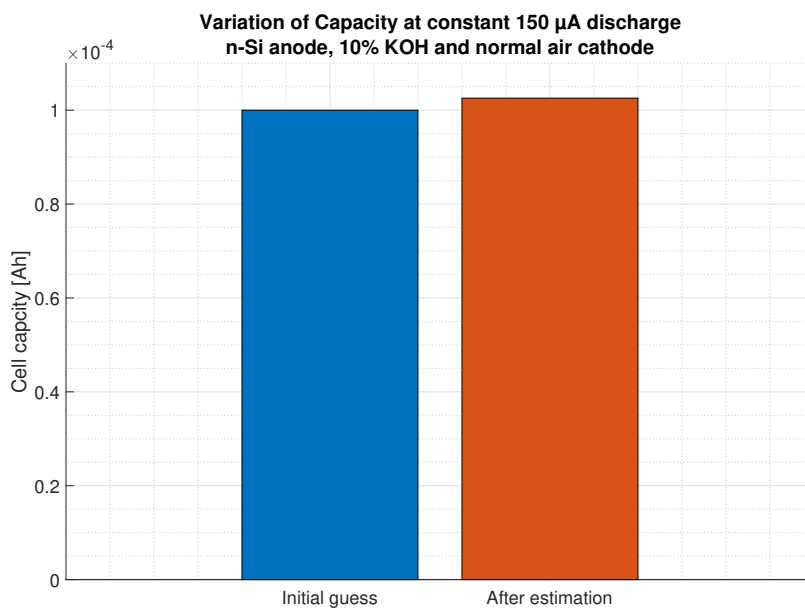
Figure B.6: E_m variation

Figure B.7: Cell capacity variation

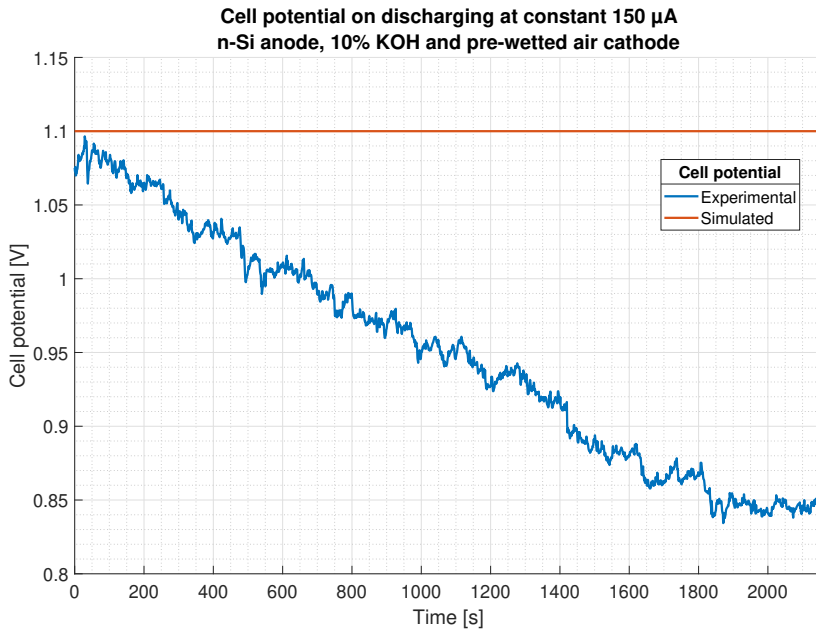


Figure B.8: Before parameter estimation

B

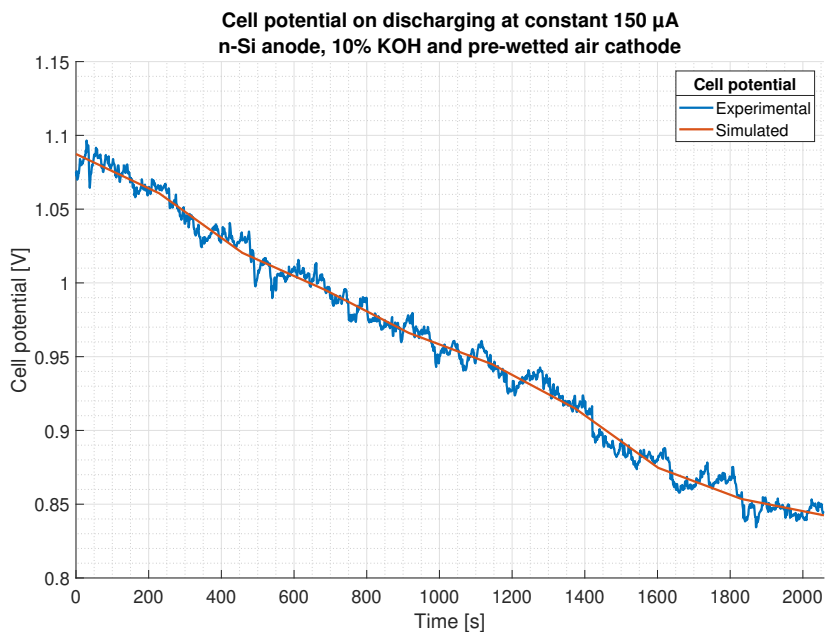
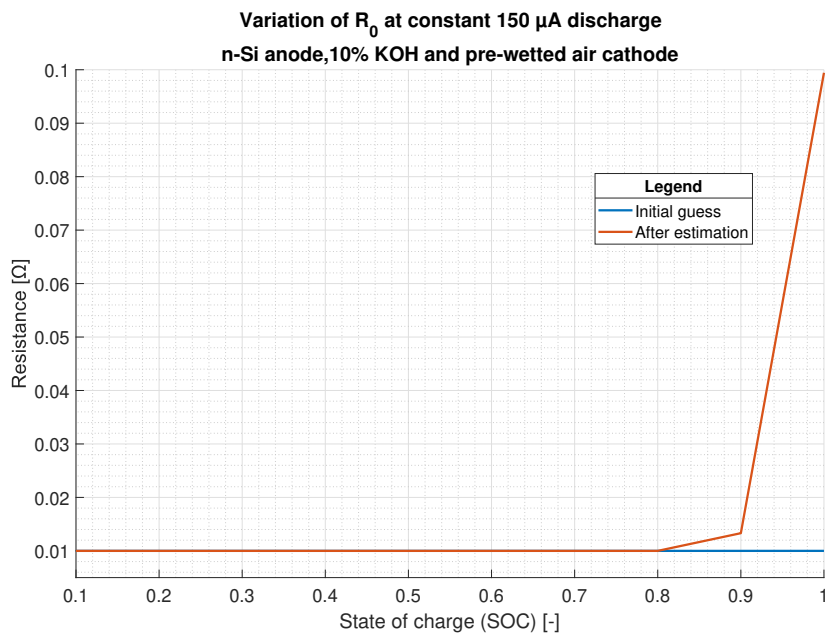


Figure B.9: After parameter estimation

Figure B.10: R_0 variation

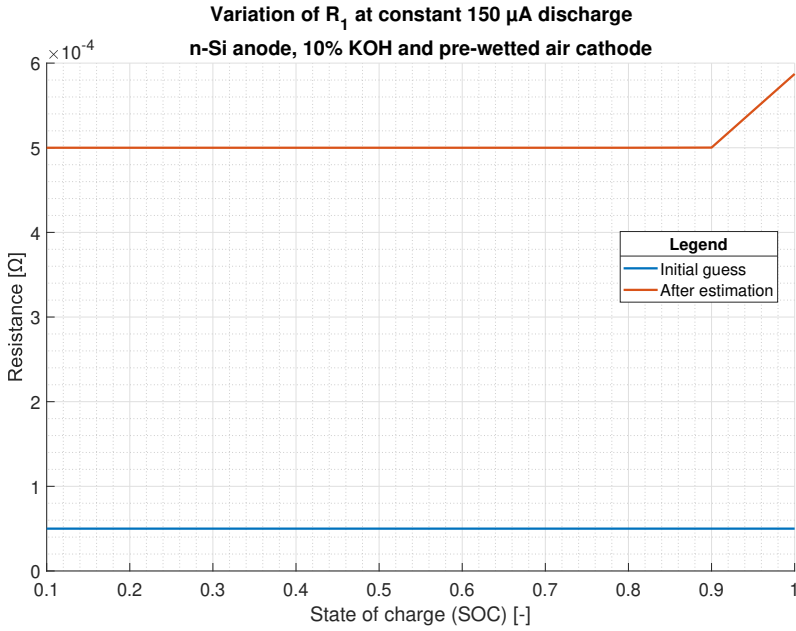


Figure B.11: R_1 variation

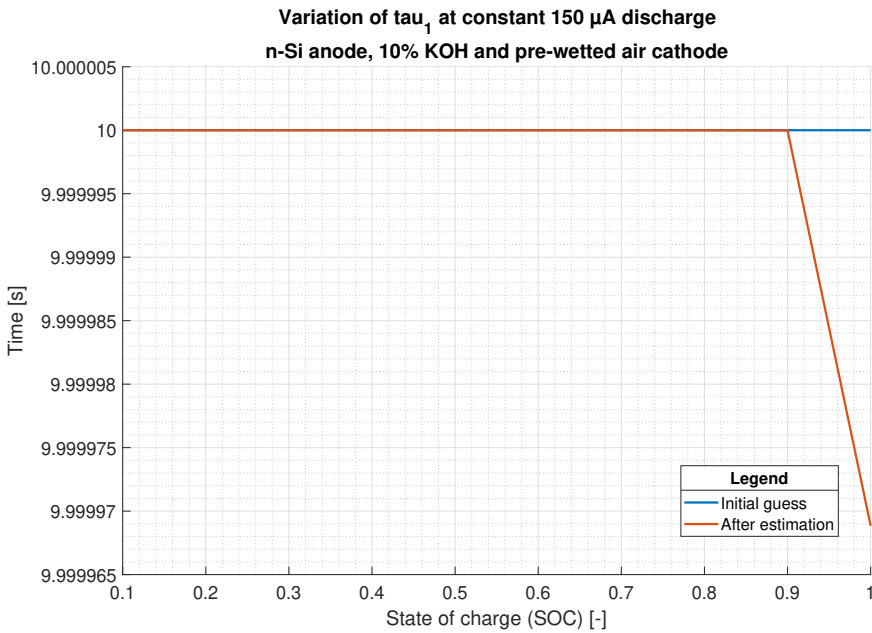


Figure B.12: τ_{a1} variation

B

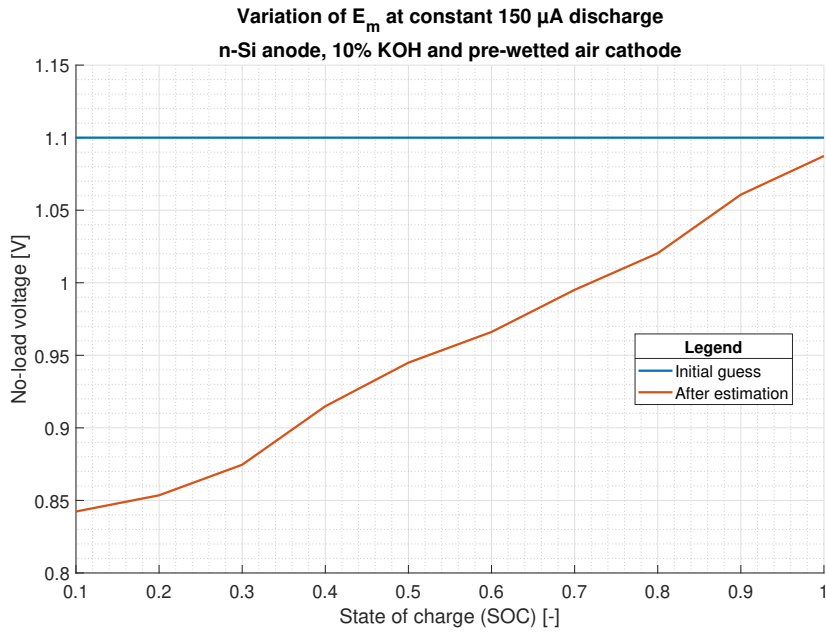
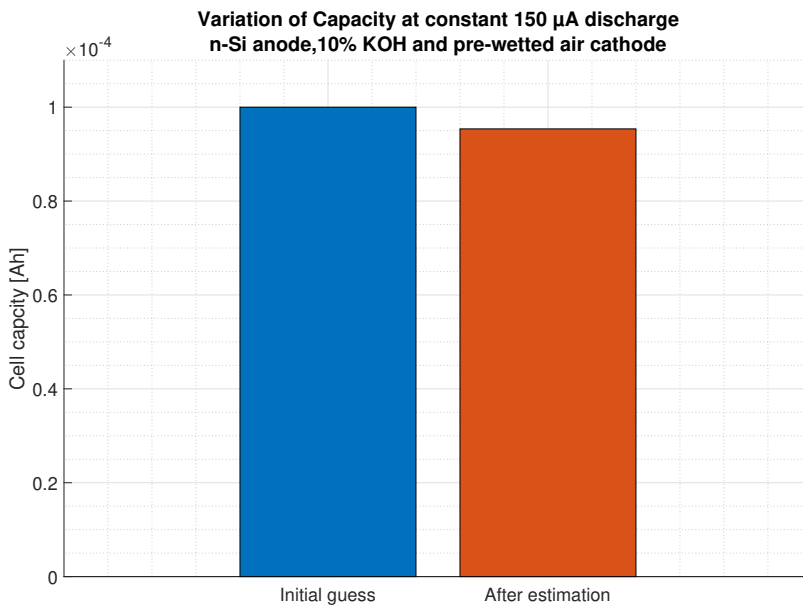
Figure B.13: E_m variation

Figure B.14: Cell capacity variation

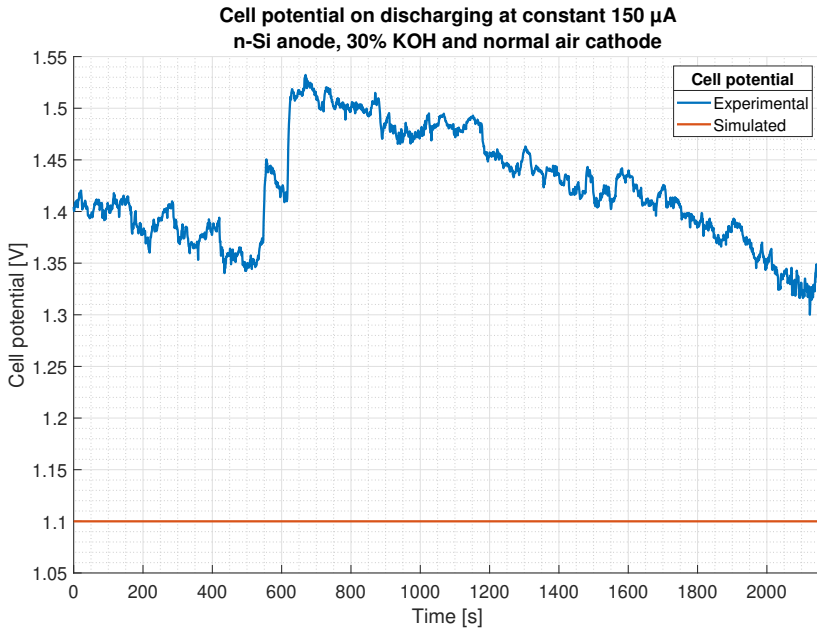


Figure B.15: Before parameter estimation

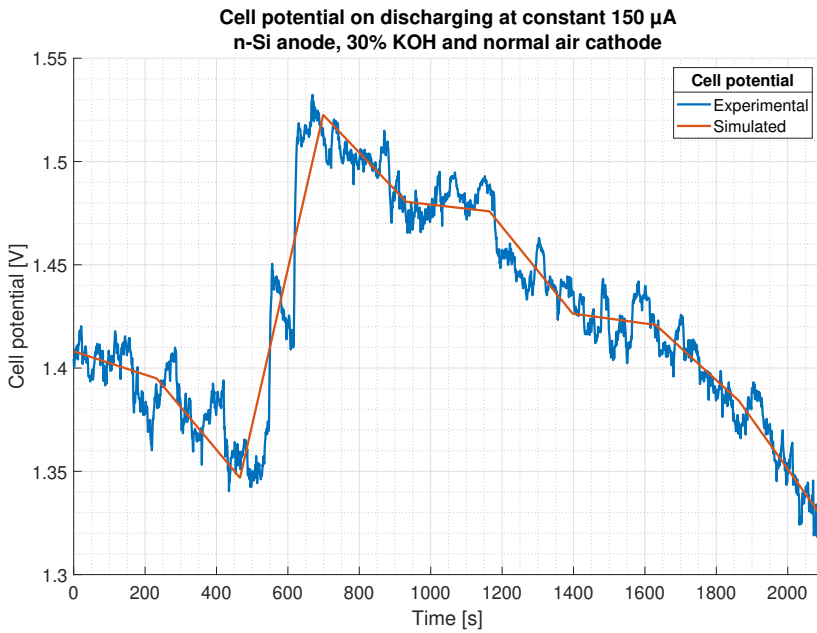
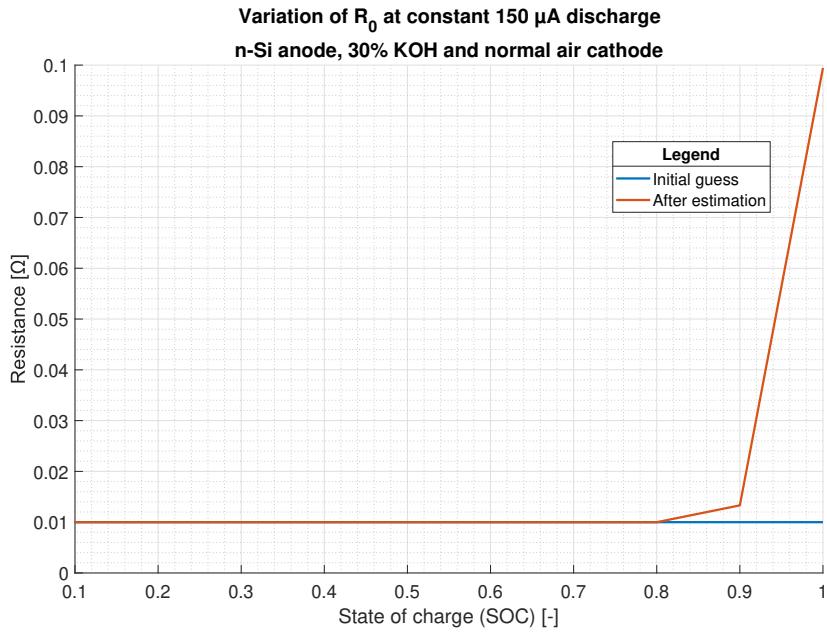
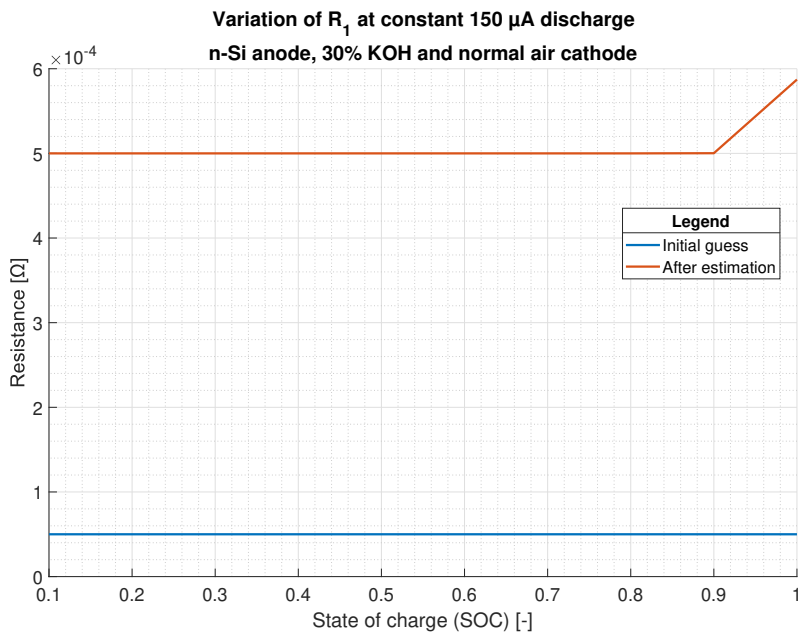


Figure B.16: After parameter estimation

B

Figure B.17: R_0 variationFigure B.18: R_1 variation

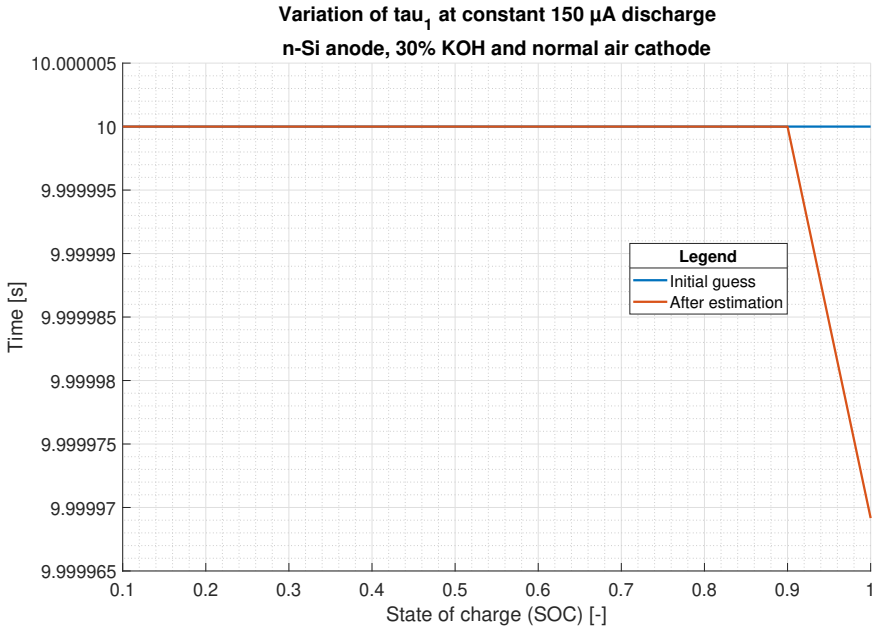


Figure B.19: τ_1 variation

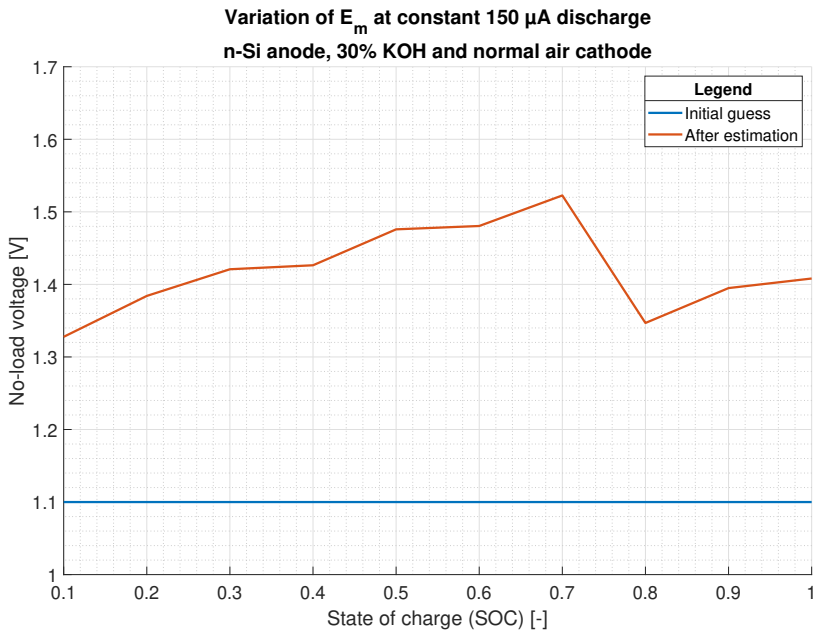


Figure B.20: E_m variation

B

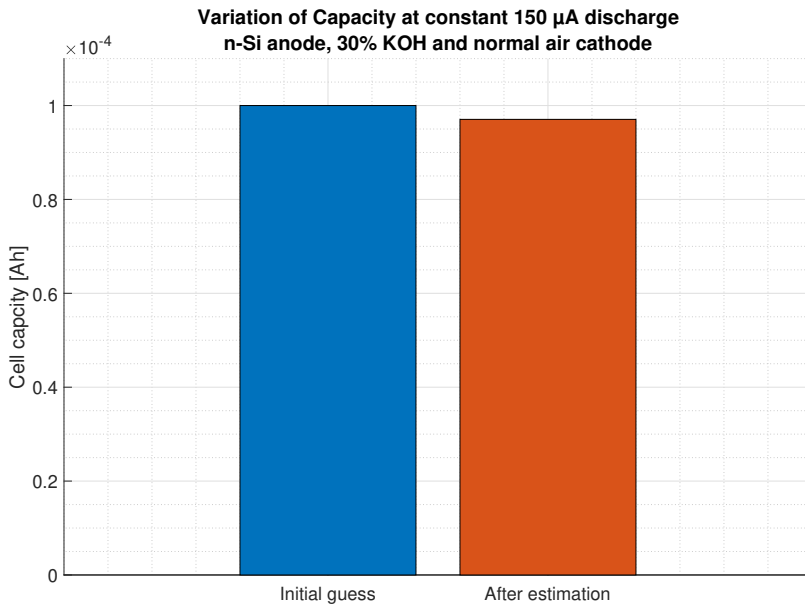


Figure B.21: Cell capacity variation

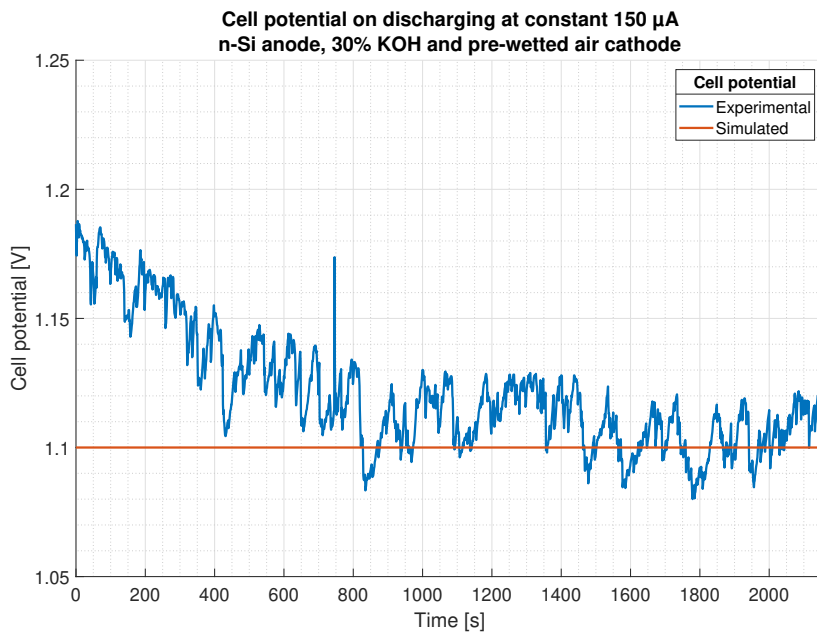


Figure B.22: Before parameter estimation

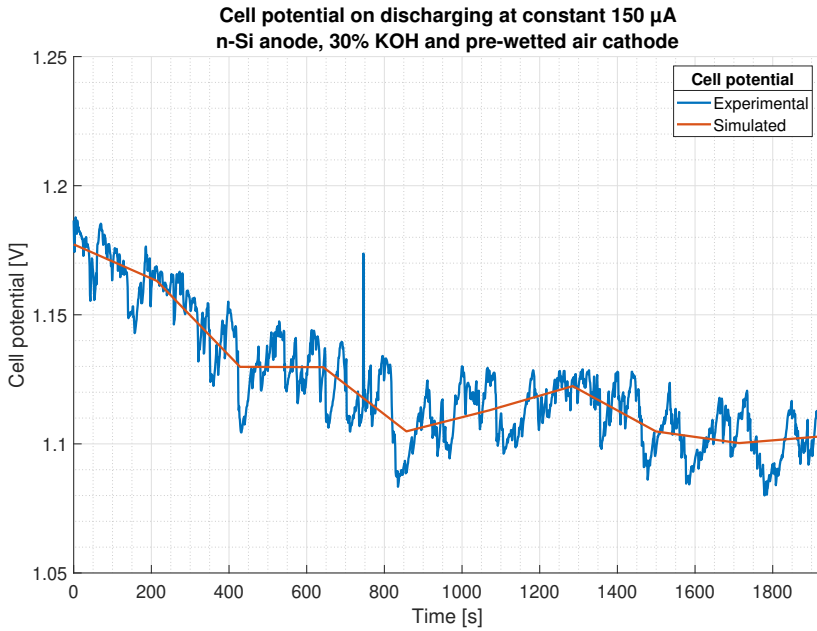


Figure B.23: After parameter estimation

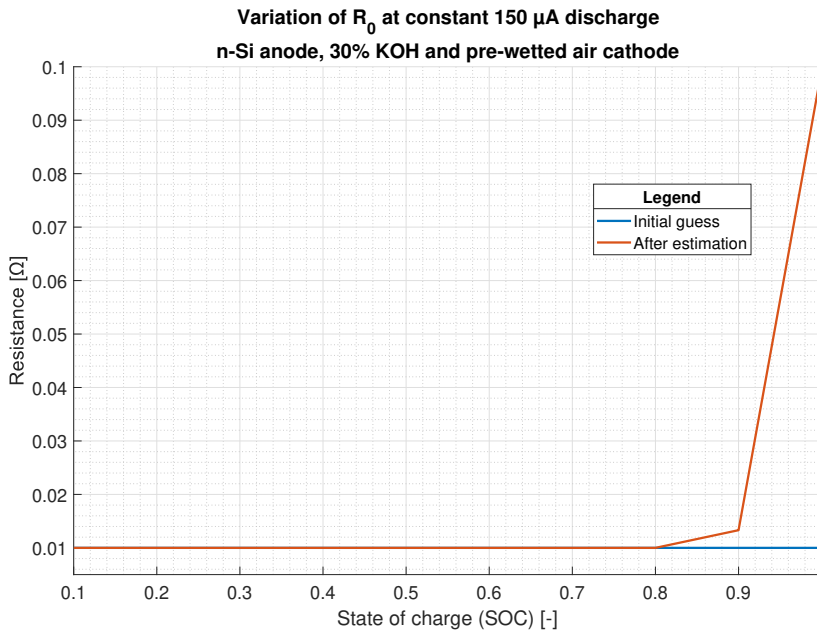
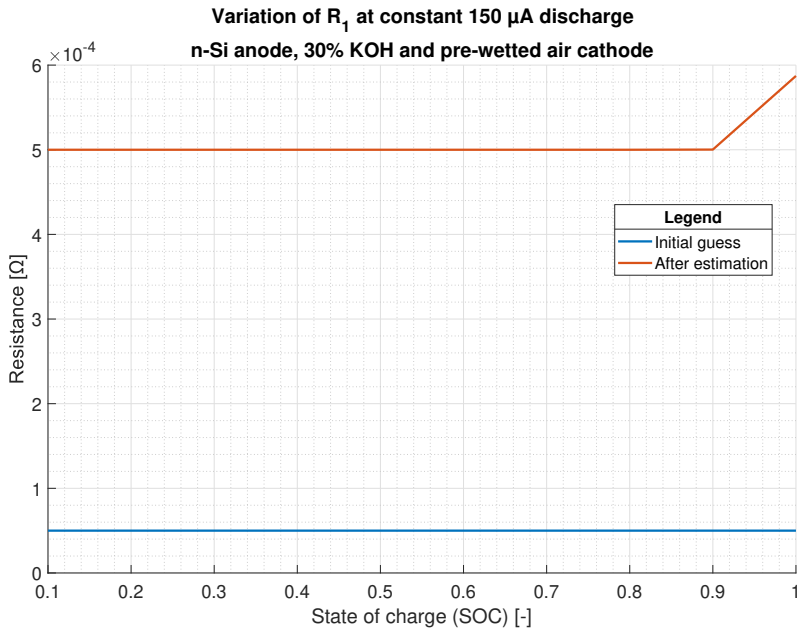
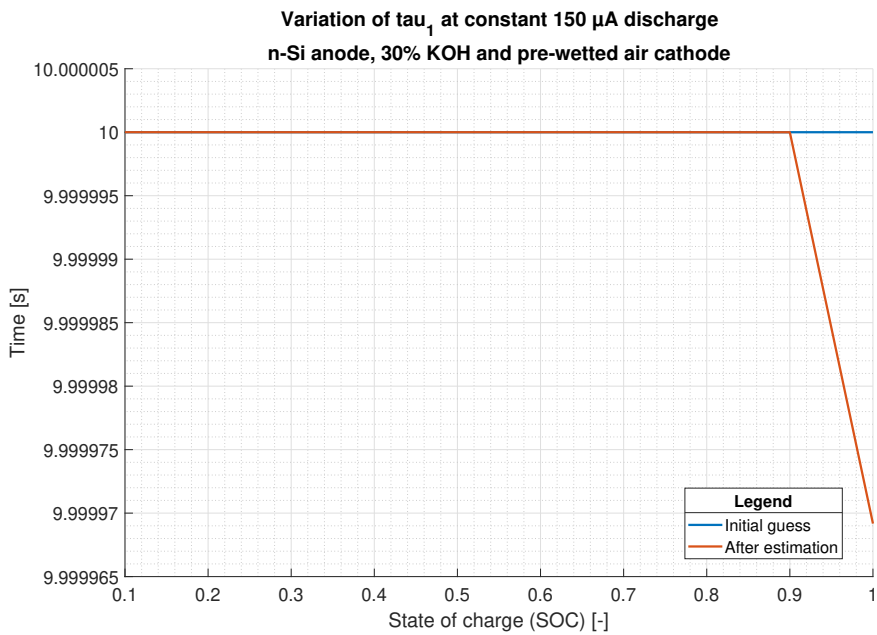


Figure B.24: R_0 variation

B

Figure B.25: R_1 variationFigure B.26: τ_{a1} variation

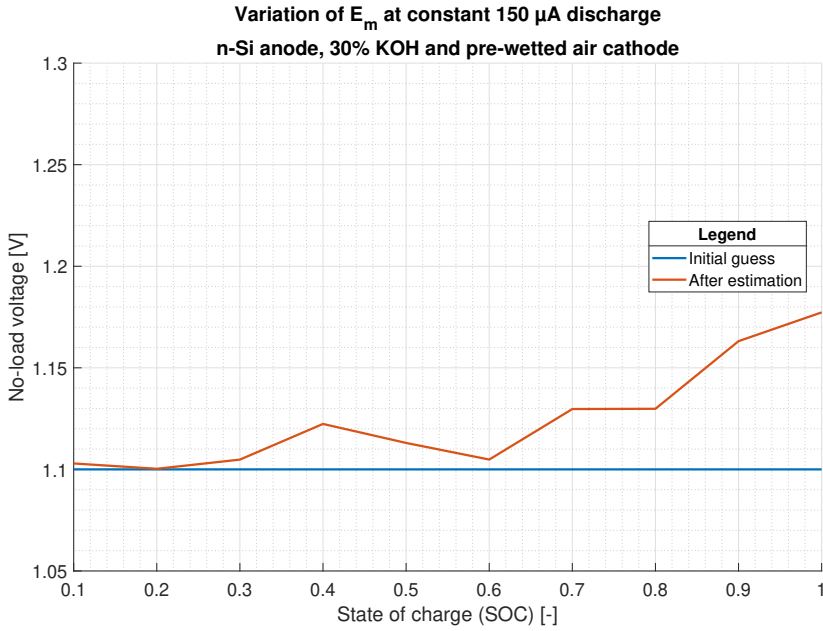


Figure B.27: E_m variation

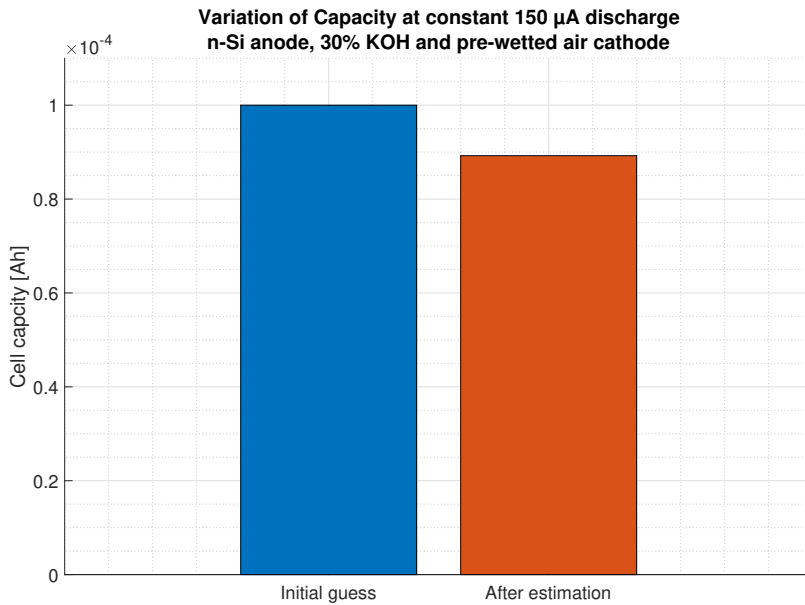


Figure B.28: Cell capacity variation

B

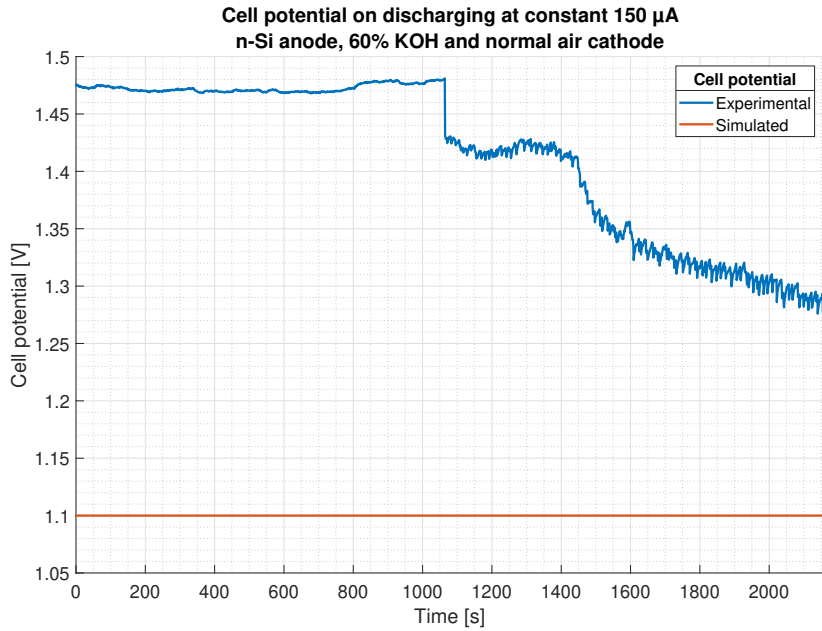


Figure B.29: Before parameter estimation

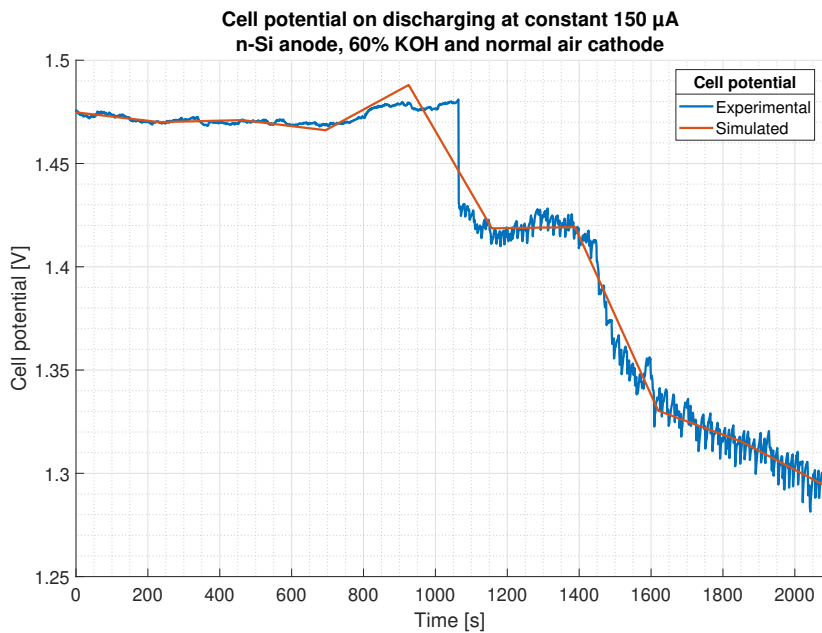


Figure B.30: After parameter estimation

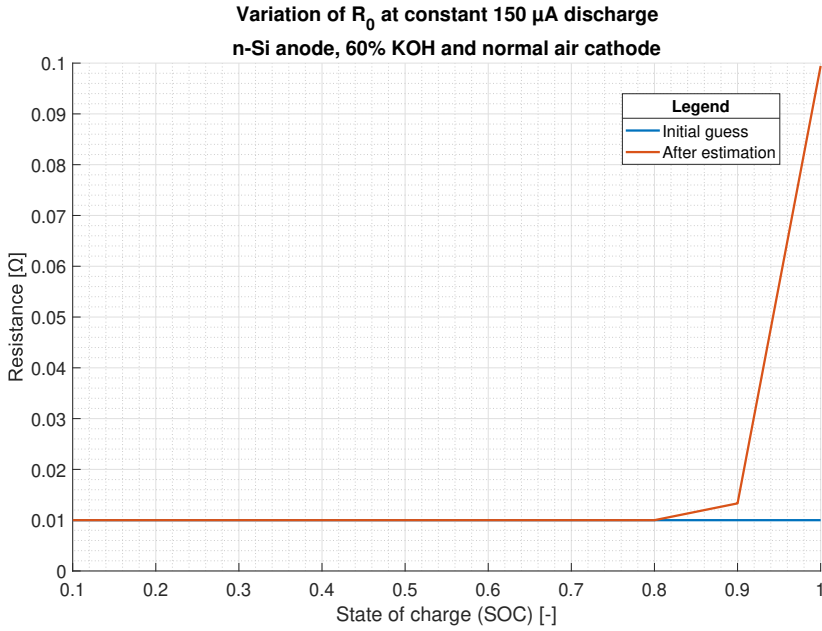


Figure B.31: R_0 variation

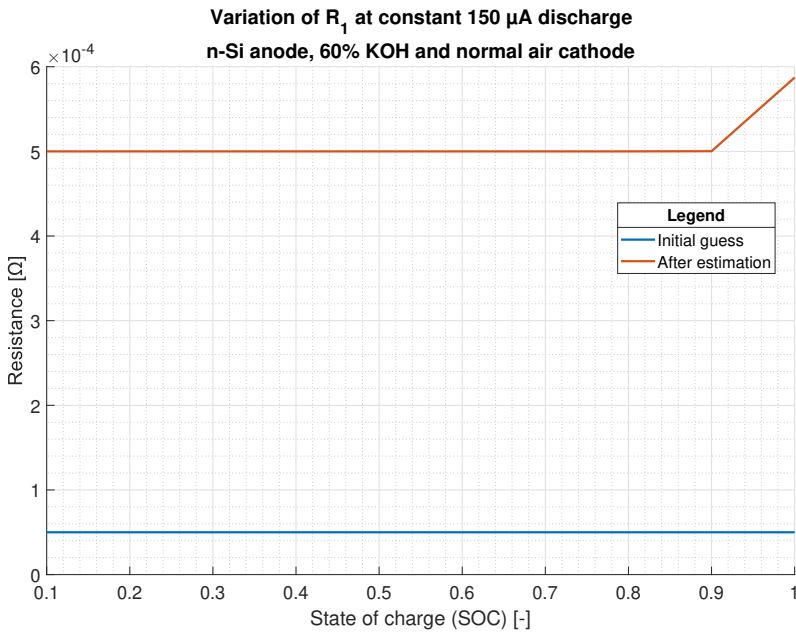


Figure B.32: R_1 variation

Variation of τ_1 at constant 150 μA discharge
n-Si anode, 60% KOH and normal air cathode

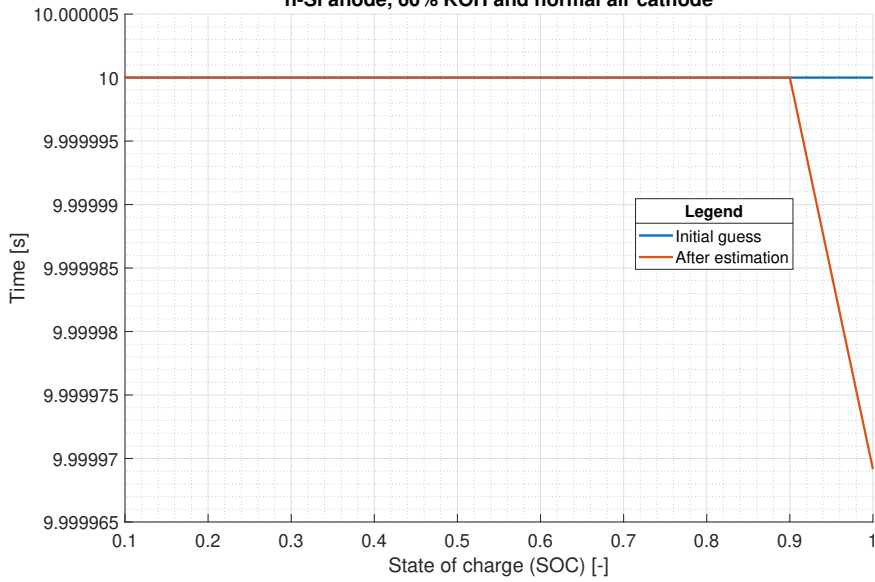


Figure B.33: τ_1 variation

Variation of E_m at constant 150 μA discharge
n-Si anode, 60% KOH and normal air cathode

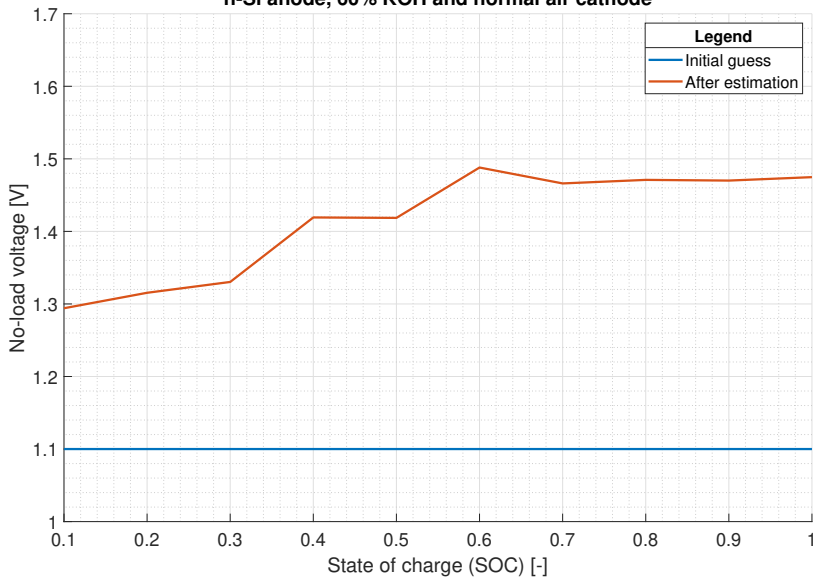


Figure B.34: E_m variation

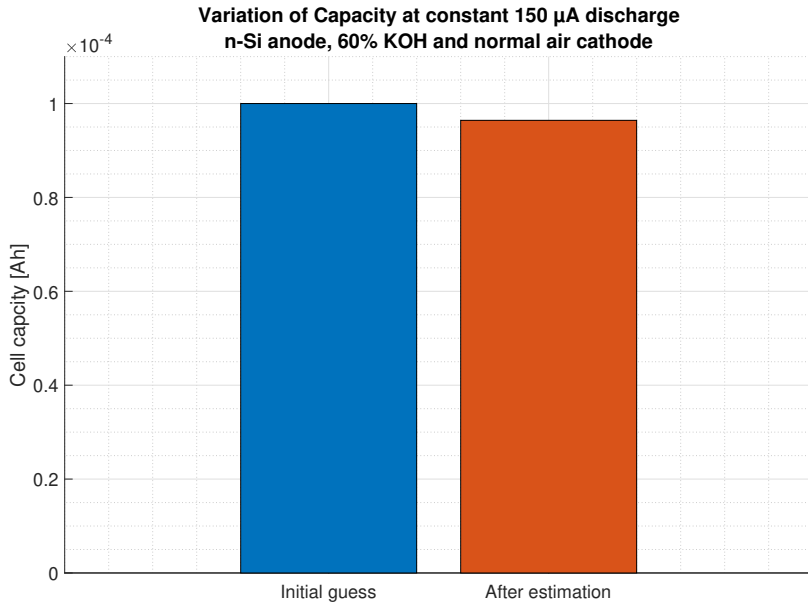


Figure B.35: Cell capacity variation

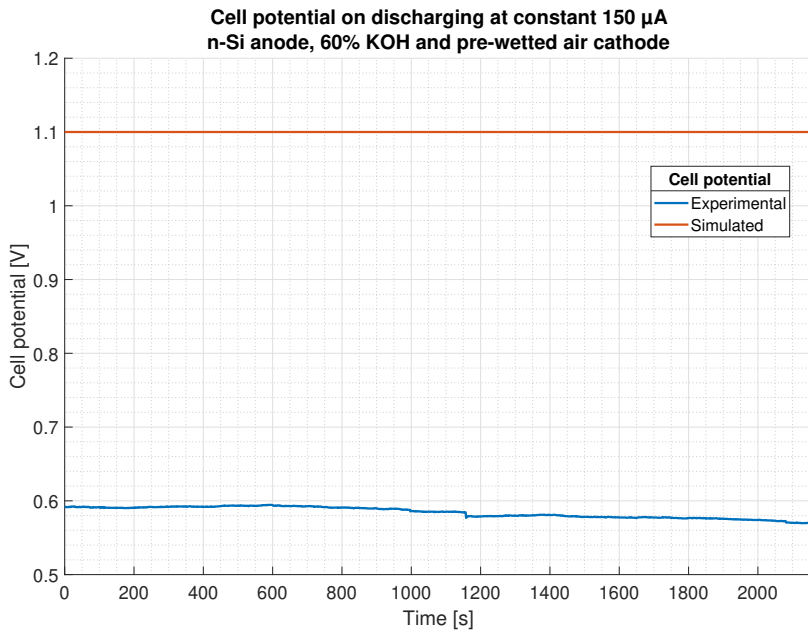


Figure B.36: Before parameter estimation

B

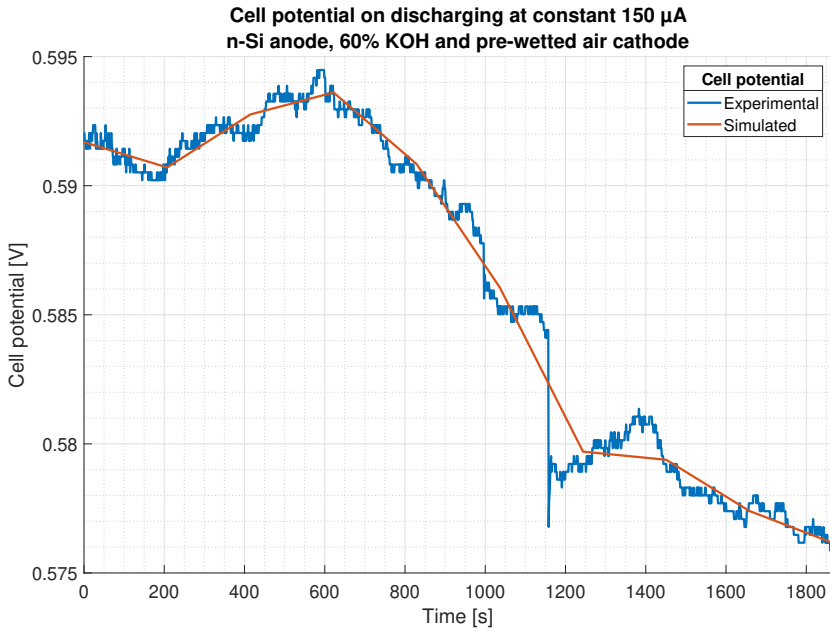
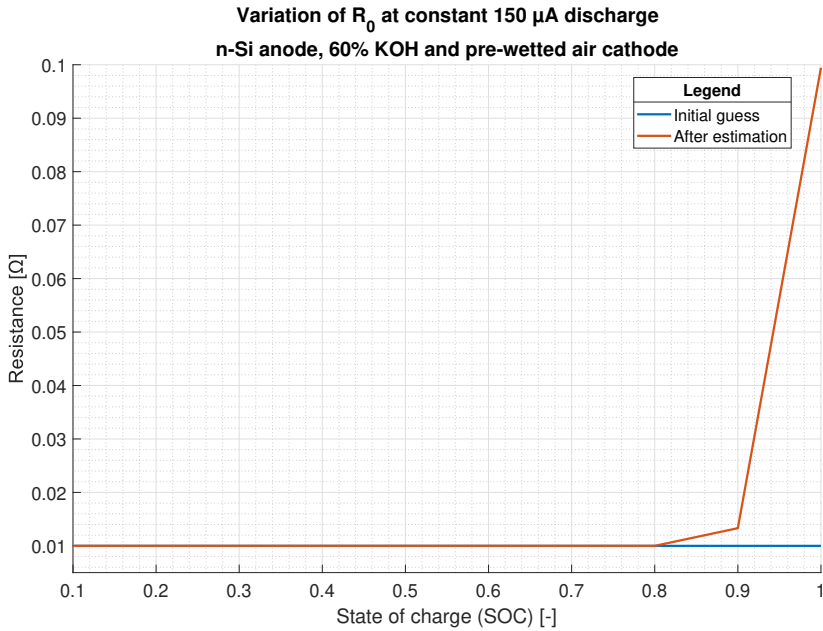


Figure B.37: After parameter estimation

Figure B.38: R_0 variation

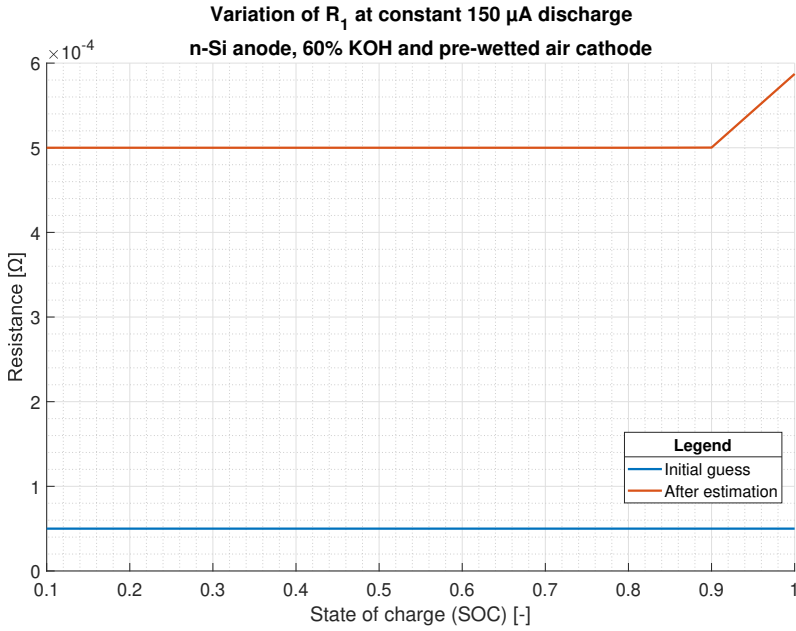


Figure B.39: R_1 variation

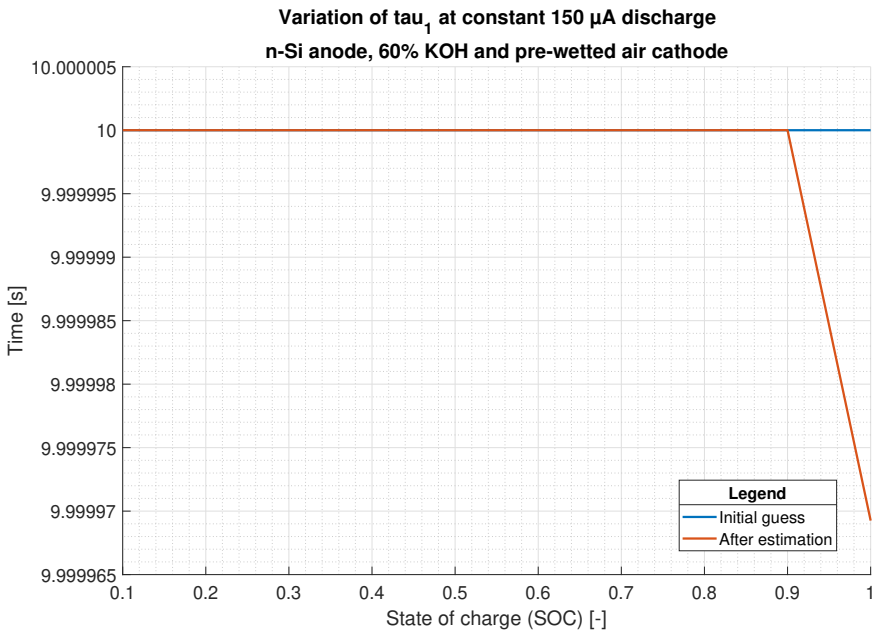


Figure B.40: τ_{a1} variation

B

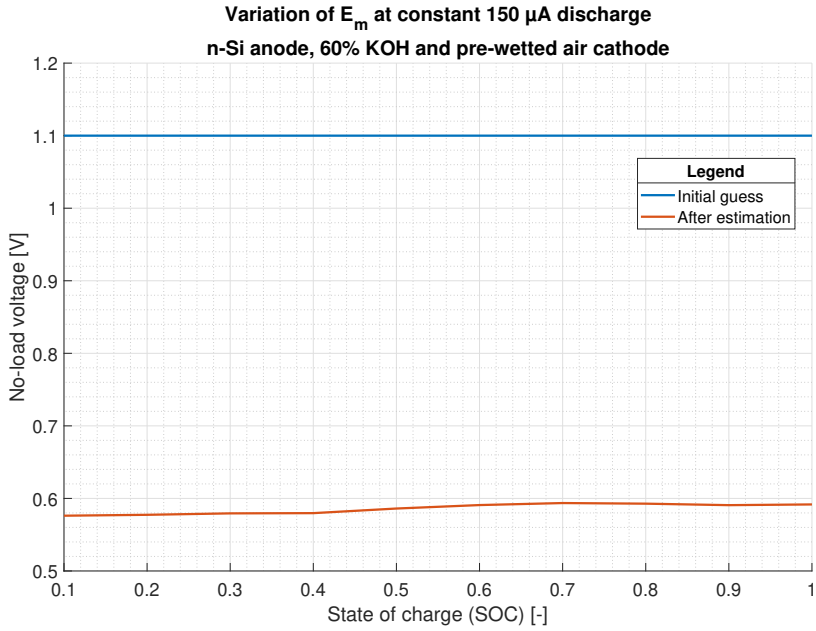
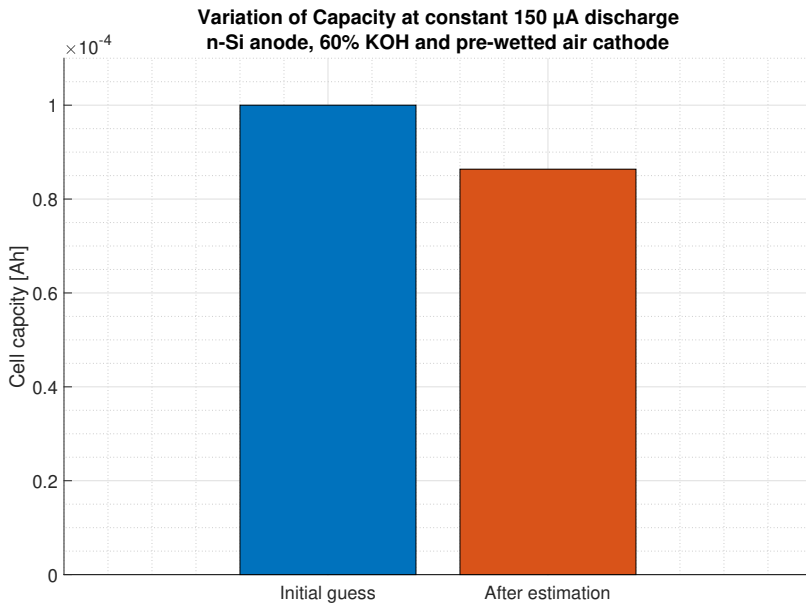
Figure B.41: E_m variation

Figure B.42: Cell capacity variation

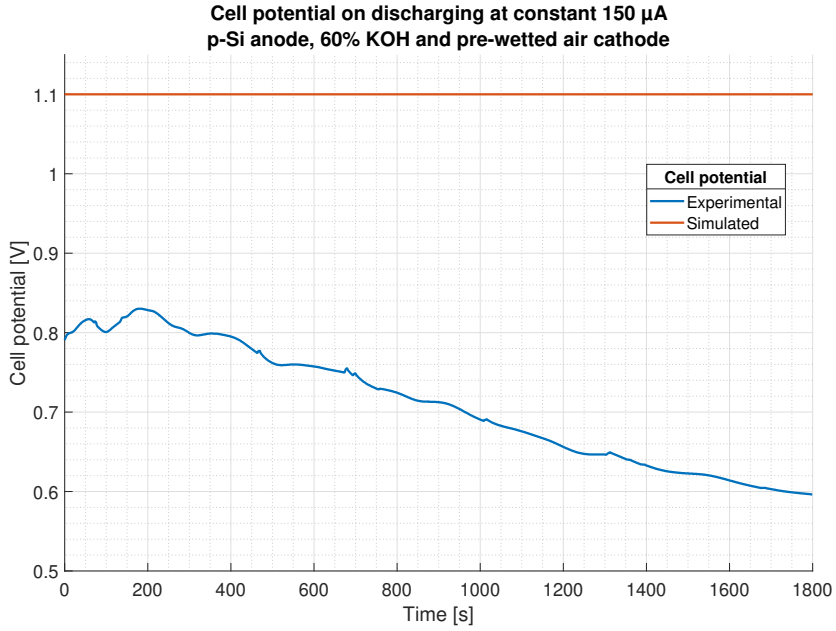


Figure B.43: Before parameter estimation

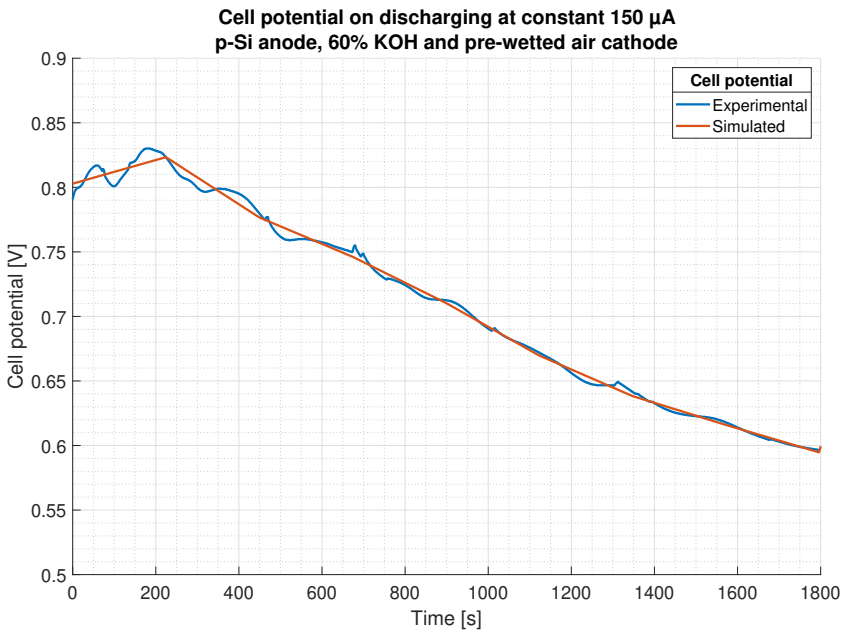
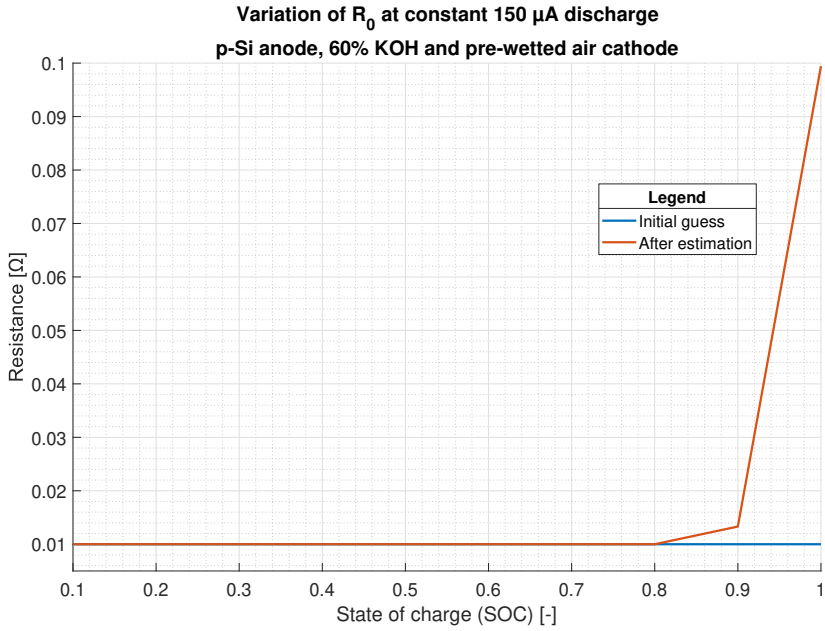
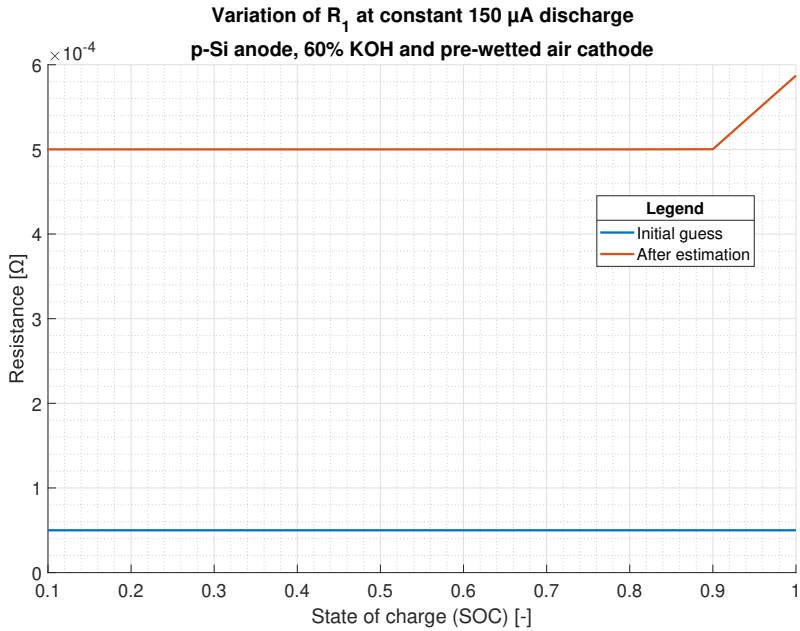


Figure B.44: After parameter estimation

B

Figure B.45: R_0 variationFigure B.46: R_1 variation

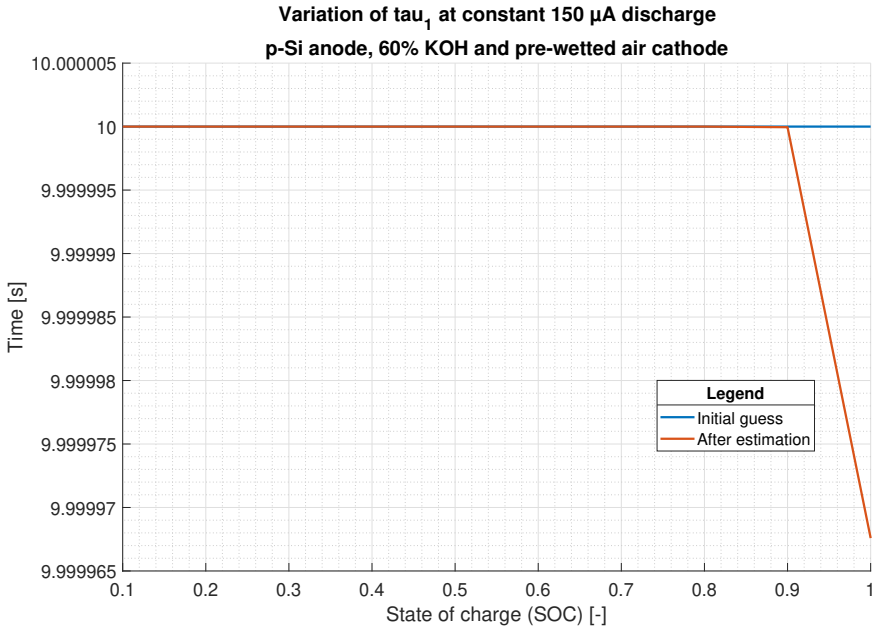


Figure B.47: τ_1 variation

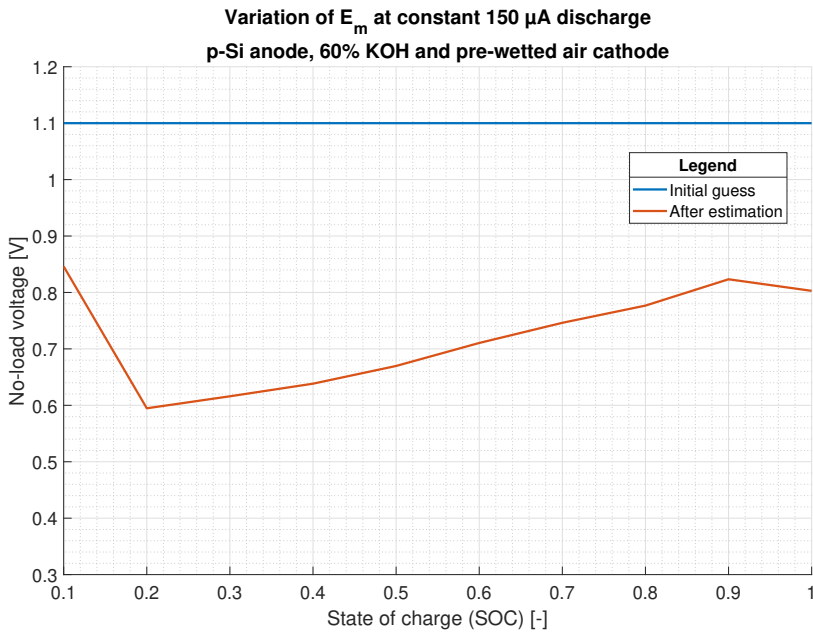


Figure B.48: E_m variation

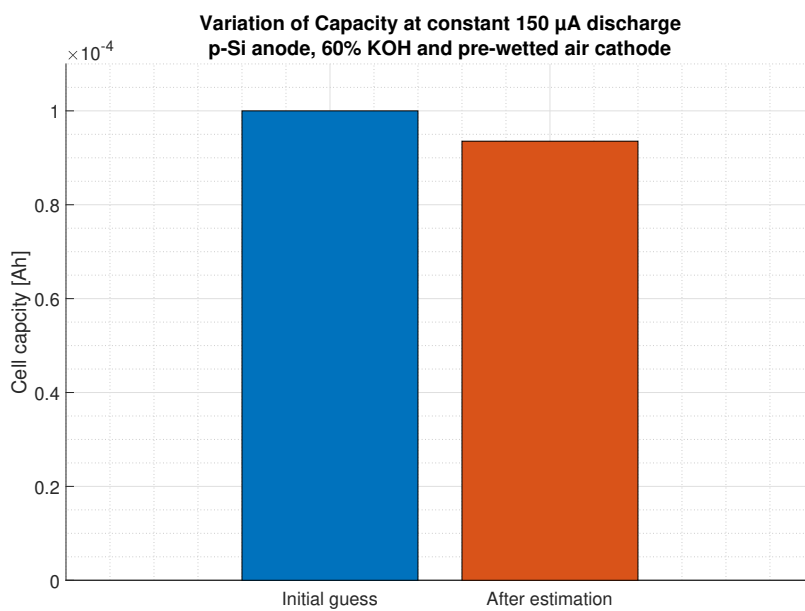


Figure B.49: Cell capacity variation

C

MATLAB SCRIPT

THIS section shows the MATLAB code that is used to run the model. The script contains section where the model is initialized and reads experimental data. Then, it opens the Simscape model where everything is done graphically next. The values are stored in the MATLAB workspace and then plotted using some plotting scripts that are present in this script as well.

```
clc;
load('first');
%save('first');
%%
%% Initializing from Li-ion model
%%
global R0 R1 tau1 R2 tau2 R3 tau3 Capacity Em;
SOC = (.1:.1:1)';

%initialize parameters with initial guesses
R0_in = [ones(1,10)*0.01]';
R1_in = [ones(1,10)*5E-5]';
tau1_in = [ones(1,10)*10]';
Em_in = [ones(1,10)*1.1]';
Capacity_in = 1E-4;

%initialize parameters with initial guesses
R0 = R0_in;
R1 = R1_in;
tau1 = tau1_in;
Em = Em_in;
Capacity = Capacity_in;
```

```
%% Reading n-Si --- KOH concentration data
%%
KOH_con = [10;30;60];

%inputting for specific variables - discharge
%this data will be used for input in the model
nSi_KOH_10 = ...
    xlsread('nSi_KOH_discharge.xlsx','B5:B3604');
nSi_KOH_10pw = ...
    xlsread('nSi_KOH_discharge.xlsx','C5:C3604');
nSi_KOH_30 = ...
    xlsread('nSi_KOH_discharge.xlsx','D5:D180404');
nSi_KOH_30_1 = ...
    xlsread('nSi_KOH_discharge.xlsx','E5:E3604');
nSi_KOH_30_2 = ...
    xlsread('nSi_KOH_discharge.xlsx','F5:F3604');
nSi_KOH_30pw = ...
    xlsread('nSi_KOH_discharge.xlsx','G5:G3604');
nSi_KOH_60 = ...
    xlsread('nSi_KOH_discharge.xlsx','H5:H3604');
nSi_KOH_60pw_1 = ...
    xlsread('nSi_KOH_discharge.xlsx','I5:I3604');
nSi_KOH_60pw_2 = ...
    xlsread('nSi_KOH_discharge.xlsx','J5:J7204');
nSi_KOH_60pw_3 = ...
    xlsread('nSi_KOH_discharge.xlsx','K5:K14404');
nSi_KOH_60pw_4 = ...
    xlsread('nSi_KOH_discharge.xlsx','L5:L3604');

%inputting for OCP data
%this data will NOT be used for input in the model
nSi_KOH_10_OCP = ...
    xlsread('nSi_KOH_discharge.xlsx','nSi_OCP','B5:B1804');
nSi_KOH_10pw_OCP = ...
    xlsread('nSi_KOH_discharge.xlsx','nSi_OCP','C5:C3604');
nSi_KOH_30_OCP = ...
    xlsread('nSi_KOH_discharge.xlsx','nSi_OCP','D5:D1804');
nSi_KOH_30_1_OCP = ...
    xlsread('nSi_KOH_discharge.xlsx','nSi_OCP','E5:E21604');
nSi_KOH_30_2_OCP = ...
    xlsread('nSi_KOH_discharge.xlsx','nSi_OCP','F5:F3604');
nSi_KOH_30pw_OCP = ...
    xlsread('nSi_KOH_discharge.xlsx','nSi_OCP','G5:G1804');
```

```

nSi_KOH_60_OCP = ...
    xlsread('nSi_KOH_discharge.xlsx', 'nSi_OCP', 'H5:H3604');
nSi_KOH_60pw_1_OCP = ...
    xlsread('nSi_KOH_discharge.xlsx', 'nSi_OCP', 'I5:I3604');
nSi_KOH_60pw_2_OCP = ...
    xlsread('nSi_KOH_discharge.xlsx', 'nSi_OCP', 'J5:J3604');
nSi_KOH_60pw_3_OCP = ...
    xlsread('nSi_KOH_discharge.xlsx', 'nSi_OCP', 'K5:K3604');
nSi_KOH_60pw_4_OCP = ...
    xlsread('nSi_KOH_discharge.xlsx', 'nSi_OCP', 'L5:L3604');

%% Reading pSi ---- KOH data
%%

%inputting for specific variables - discharge
%this data will be used for input in the model
pSi_KOH_60pw_1 = ...
    xlsread('nSi_KOH_discharge.xlsx', 'pSi_discharge', 'B5:B1804');
pSi_KOH_60pw_2 = ...
    xlsread('nSi_KOH_discharge.xlsx', 'pSi_discharge', 'C5:C1804');
pSi_KOH_60pw_3 = ...
    xlsread('nSi_KOH_discharge.xlsx', 'pSi_discharge', 'D5:D1804');
pSi_KOH_60pw_4 = ...
    xlsread('nSi_KOH_discharge.xlsx', 'pSi_discharge', 'E5:E1804');
pSi_KOH_60pw_5 = ...
    xlsread('nSi_KOH_discharge.xlsx', 'pSi_discharge', 'F5:F1804');
pSi_KOH_60pw_6 = ...
    xlsread('nSi_KOH_discharge.xlsx', 'pSi_discharge', 'G5:G1804');
pSi_KOH_60pw_7 = ...
    xlsread('nSi_KOH_discharge.xlsx', 'pSi_discharge', 'H5:H1804');

%inputting for OCP data
%this data will NOT be used for input in the model
pSi_time_OCP = ...
    xlsread('nSi_KOH_discharge.xlsx', 'pSi_OCP', 'B5:B45');
pSi_KOH_60pw_1_OCP = ...
    xlsread('nSi_KOH_discharge.xlsx', 'pSi_OCP', 'B5:B45');
pSi_KOH_60pw_2_OCP = ...
    xlsread('nSi_KOH_discharge.xlsx', 'pSi_OCP', 'C5:C45');
pSi_KOH_60pw_3_OCP = ...
    xlsread('nSi_KOH_discharge.xlsx', 'pSi_OCP', 'D5:D45');
pSi_KOH_60pw_4_OCP = ...
    xlsread('nSi_KOH_discharge.xlsx', 'pSi_OCP', 'E5:E45');

```

```

%% Initializing from experimental data
%%

%input data for simulink model here
test = pSi_KOH_60pw_6;
t = size(test) - 1;
t_exp = [0:1:t];
V_exp(:,1) = t_exp;
V_exp(:,2) = test;

%% Opening Si-air model
%%
sim('batteryParameterEstimation1.slx');

%% Getting parameter data
%%

%Print plots after parameter estimation

%% General plots
%%

%plotting for n-Si discharge with KOH variation
var5 = nSi_KOH_10;
var6 = nSi_KOH_30_2;
var7 = nSi_KOH_60;
f1 = figure;
f1.Units = 'centimeters';
f1.Position = [15 5 30 15];
title({'Discharge potential vs. Time and KOH ...
      concentration',
      ...'n-Si anode and normal air cathode'});
hold on;
grid on;
ax1 = gca;
ax1.FontSize = 16;
plot([0:1:size(var5)-1], var5, 'Linewidth', 2);
plot([0:1:size(var6)-1], var6, 'Linewidth', 2);
plot([0:1:size(var7)-1], var7, 'Linewidth', 2);
lgd1 = legend('10%', '30%', '60%');

```

```

lgd1.Title.String = 'KOH concentration';
xlim([0 3600]);
grid minor;
xlabel('Time [s]');
ylabel('Cell potential [V]');

%plotting for OCP for cells
var8 = nSi_KOH_10_OCP;
var9 = nSi_KOH_30_2_OCP;
var10 = nSi_KOH_60_OCP;
f11 = figure;
f11.Units = 'centimeters';
f11.Position = [15 5 30 15];
title({'Open circuit potential vs. Time and KOH ...
      concentration',
      ...'n-Si anode and normal air cathode'});
hold on;
grid on;
ax11 = gca;
ax11.FontSize = 16;
plot([0:1:size(var8)-1], var8, 'Linewidth',2);
plot([0:1:size(var9)-1], var9, 'Linewidth',2);
plot([0:1:size(var10)-1], var10, 'Linewidth',2);
lgd11 = legend('10%', '30%', '60%');
lgd11.Title.String = 'KOH concentration';
xlim([0 1800]);
grid minor;
xlabel('Time [s]');
ylabel('Cell potential [V]');

%plotting for n-Si discharge with PW variation
var1 = nSi_KOH_60;
var2 = nSi_KOH_60pw_3;
f9 = figure;
f9.Units = 'centimeters';
f9.Position = [15 5 30 15];
title({'Discharge potential of a normal vs. ...
      pre-wetted (PW) air cathode cell',
      ...'n-Si anode at 60% KOH'});
hold on;
grid on;
ax9 = gca;

```

```

ax9.FontSize = 16;
plot([0:1:size(var1)-1], var1, 'Linewidth',2);
plot([0:1:size(var2)-1], var2, 'Linewidth',2);
lgd9 = legend('Normal', 'Pre-wetted');
lgd9.Title.String = 'Air cathode condition';
xlim([0 3600]);
grid minor;
xlabel('Time [s]');
ylabel('Cell potential [V]');

%plotting for n-Si OCP with PW variation
var20 = nSi_KOH_60_OCP;
var21 = nSi_KOH_60pw_3_OCP;
f20 = figure;
f20.Units = 'centimeters';
f20.Position = [15 5 30 15];
title({'Open circuit potential of a normal vs. ...
      pre-wetted (PW) air cathode cell',
      ...'n-Si anode at 60% KOH'});
hold on;
grid on;
ax20 = gca;
ax20.FontSize = 16;
plot([0:1:size(var20)-1], var20, 'Linewidth',2);
plot([0:1:size(var21)-1], var21, 'Linewidth',2);
lgd20 = legend('Normal', 'Pre-wetted');
lgd20.Title.String = 'Air cathode condition';
xlim([0 1800]);
grid minor;
xlabel('Time [s]');
ylabel('Cell potential [V]');

%plotting for n-Si discharge with Si anode variation
var3 = nSi_KOH_60pw_3;
var4 = pSi_KOH_60pw_2;
f10 = figure;
f10.Units = 'centimeters';
f10.Position = [15 5 30 15];
title({'Discharge potential of a n type vs. p type ...
      Si anode cell',
      ...'in 60% KOH and pre-wetted air cathode'});
hold on;
grid on;
ax10 = gca;

```

```

ax10.FontSize = 16;
plot([0:1:size(var3)-1], var3, 'Linewidth',2);
plot([0:1:size(var4)-1], var4, 'Linewidth',2);
lgd10 = legend('n type','p type');
lgd10.Title.String = 'Si anode';
xlim([0 1800]);
grid minor;
xlabel('Time [s]');
ylabel('Cell potential [V]');

%plotting for n-Si OCP with Si anode variation
var33 = nSi_KOH_60pw_3_OCP;
var44 = pSi_KOH_60pw_2_OCP;
f30 = figure;
f30.Units = 'centimeters';
f30.Position = [15 5 30 15];
title({'Open circuit potential of a n type vs. p ...
      type Si anode cell',
      ...'in 60% KOH and pre-wetted air cathode'});
hold on;
grid on;
ax30 = gca;
ax30.FontSize = 16;
plot([0:1:size(var33)-1], var33, 'Linewidth',2);
plot([0:1:size(var44)-1], var44, 'Linewidth',2);
lgd30 = legend('n type','p type');
lgd30.Title.String = 'Si anode';
xlim([0 10]);
ylim([0.70 0.79]);
grid minor;
xlabel('Time [s]');
ylabel('Cell potential [V]');

%% one for all graph
%%

%plotting OCP and discharge
%for discharge
v1 = nSi_KOH_10;
v2 = nSi_KOH_10pw;
v3 = nSi_KOH_30_2;
v4 = nSi_KOH_30pw;
v5 = nSi_KOH_60;

```

```

v6 = nSi_KOH_60pw_3;
v7 = pSi_KOH_60pw_5;
%for OCP
% v1 = nSi_KOH_10_OCP;
% v2 = nSi_KOH_10pw_OCP;
% v3 = nSi_KOH_30_2_OCP;
% v4 = nSi_KOH_30pw_OCP;
% v5 = nSi_KOH_60_OCP;
% v6 = nSi_KOH_60pw_3_OCP;
% v7 = pSi_KOH_60pw_2_OCP;

a1 = mean(nSi_KOH_10_OCP);
a2 = mean(nSi_KOH_10pw_OCP);
a3 = mean(nSi_KOH_30_2_OCP);
a4 = mean(nSi_KOH_30pw_OCP);
a5 = mean(nSi_KOH_60_OCP);
a6 = mean(nSi_KOH_60pw_3_OCP);
a7 = mean(pSi_KOH_60pw_2_OCP);

b = pSi_KOH_60pw_5;
s = polyfit([0:1:size(b)-1],b,1)

%plotting OCP and discharge
var13 = pSi_KOH_60pw_2_OCP;
var14 = pSi_KOH_60pw_5;
temp_t1 = (size(var13)+size(var14));
temp_t = temp_t1(1,1);
f10 = figure;
f10.Units = 'centimeters';
f10.Position = [15 5 30 15];
title({'Cell potential vs. Time',
      ...'p-Si anode, 60% KOH and pre-wetted air ...
      cathode'});

hold on;
grid on;
ax10 = gca;
ax10.FontSize = 16;
plot([0:1:size(var13)-1], var13,'Linewidth',2);
plot([size(var13):1:(temp_t-1)], var14,'Linewidth',2);
lgd10 = legend('OCP','DP');
lgd10.Title.String = 'Potential type';
xlim([0 temp_t]);
grid minor;
xlabel('Time [s]');

```

```

ylabel('Cell potential [V]');

f50 = figure;
f50.Units = 'centimeters';
f50.Position = [15 5 30 15];
title({'Discharge potential vs. Time', 'Comparing ...
      discharge potentials'});
hold on;
grid on;
ax50 = gca;
ax50.FontSize = 16;
plot([0:1:size(v1)-1], v1, 'Linewidth', 2);
plot([0:1:size(v2)-1], v2, 'Linewidth', 2);
plot([0:1:size(v3)-1], v3, 'Linewidth', 2);
plot([0:1:size(v4)-1], v4, 'Linewidth', 2);
plot([0:1:size(v5)-1], v5, 'Linewidth', 2);
plot([0:1:size(v6)-1], v6, 'Linewidth', 2);
plot([0:1:size(v7)-1], v7, 'Linewidth', 2);
lgd50 = legend('n-Si 10%', 'n-Si 10% PW', 'n-Si ...
              30%', 'n-Si 30% PW', 'n-Si 60%',
              ... 'n-Si 60% PW', 'p-Si 60% PW');
lgd50.Title.String = 'Cell condition';
lgd50.Location = 'bestoutside';
xlim([0 1800]);
grid minor;
xlabel('Time [s]');
ylabel('Cell potential [V]');

%% Specific plots
%%

%plotting for n-Si discharge with KOH variation
f2 = figure;
f2.Units = 'centimeters';
f2.Position = [15 5 30 20];
title({'Cell potential on discharging at constant ...
      150  $\mu$ A',

```

```

        ....'p-Si anode, 60% KOH and pre-wetted air ...
            cathode - 2'});
hold on;
grid on;
ax2 = gca;
ax2.FontSize = 16;
plot(t_exp, V_exp(:,2), 'Linewidth',2);
plot(t_sim,V_sim, 'Linewidth',2);
lgd2 = legend('Experimental', 'Simulated');
lgd2.Title.String = 'Cell potential';
xlim([0 1800]);
%ylim([0.2 1.15]);
grid minor;
xlabel('Time [s]');
ylabel('Cell potential [V]');

%plotting cell parameters
%R0
f3 = figure;
f3.Units = 'centimeters';
f3.Position = [15 5 30 20];
title({'Variation of R_0 at constant 150  $\mu$ A discharge',
        ....'p-Si anode, 60% KOH and pre-wetted air ...
            cathode - 2'});
hold on;
grid on;
ax3 = gca;
ax3.FontSize = 16;
plot(SOC, R0_in, 'Linewidth',2);
plot(SOC, R0, 'Linewidth',2);
lgd3 = legend('Initial guess', 'After estimation');
lgd3.Title.String = 'Legend';
xlim([0.1 1]);
ylim([0.005 0.1]);
grid minor;
xlabel('State of charge (SOC) [-]');
ylabel('Resistance [ ]');

%R1
f4 = figure;
f4.Units = 'centimeters';
f4.Position = [15 5 30 20];
title({'Variation of R_1 at constant 150  $\mu$ A discharge',

```

```

        ....'p-Si anode, 60% KOH and pre-wetted air ...
            cathode - 2'});
hold on;
grid on;
ax4 = gca;
ax4.FontSize = 16;
plot(SOC, R1_in, 'Linewidth',2);
plot(SOC, R1, 'Linewidth',2);
lgd4 = legend('Initial guess', 'After estimation');
lgd4.Title.String = 'Legend';
xlim([0.1 1]);
grid minor;
xlabel('State of charge (SOC) [-]');
ylabel('Resistance [Ω]');

%tau1
f5 = figure;
f5.Units = 'centimeters';
f5.Position = [15 5 30 20];
title({'Variation of tau_1 at constant 150 μA ...
        discharge',
        ....'p-Si anode, 60% KOH and pre-wetted air ...
            cathode - 2'});
hold on;
grid on;
ax5 = gca;
ax5.FontSize = 16;
plot(SOC, tau1_in, 'Linewidth',2);
plot(SOC, tau1, 'Linewidth',2);
lgd5 = legend('Initial guess', 'After estimation');
lgd5.Title.String = 'Legend';
xlim([0.1 1]);
grid minor;
xlabel('State of charge (SOC) [-]');
ylabel('Time [s]');

%Em
f6 = figure;
f6.Units = 'centimeters';
f6.Position = [15 5 30 20];
title({'Variation of E_m at constant 150 μA discharge',
        ...'p-Si anode, 60% KOH and pre-wetted air ...
            cathode - 2'});

```

```

hold on;
grid on;
ax6 = gca;
ax6.FontSize = 16;
plot(SOC, Em_in, 'Linewidth',2);
plot(SOC, Em, 'Linewidth',2);
lgd6 = legend('Initial guess', 'After estimation');
lgd6.Title.String = 'Legend';
xlim([0.1 1]);
ylim([0.3 1.2]);
grid minor;
xlabel('State of charge (SOC) [-]');
ylabel('No-load voltage [V]');

%Capacity
f7 = figure;
f7.Units = 'centimeters';
f7.Position = [15 5 30 20];
title({'Variation of Capacity at constant 150  $\mu$ A ...
      discharge',
      ...'p-Si anode, 60% KOH and pre-wetted air ...
      cathode - 2'});
hold on;
grid on;
ax7 = gca;
ax7.FontSize = 16;
bar(1, Capacity_in);
bar(2, Capacity);
ylim([0 1.1E-4]);
xticks([1 2]);
xticklabels({'Initial guess', 'After estimation'});
grid minor;
ylabel('Cell capacity [Ah]');

%% Sensitivity analysis
%%

[sens_val, sens_var] = ...
    xlsread('nSi_KOH_discharge.xlsx', 'Sens', 'A1:B41');

%plotting sensitivity analysis results
f8 = figure;

```

```
f8.Units = 'centimeters';
f8.Position = [15 5 30 20];
title('Sensitivity analysis of all the parameters in ...
      the model');
hold on;
grid on;
ax8 = gca;
ax8.FontSize = 14;
bar(sens_val, 'Linewidth',2);
grid minor;
xlabel('Cell parameters');
xticks([1:1:41]);
xticklabels(sens_var);
xtickangle(90);
ylabel('Parameter value [-]');

%% The end
%%
```


D

SI-AIR CELL RECHARGEABILITY USING ELECTRODEPOSITON

IN order to manufacture Si at cheaper and nominal temperature condition, electrodeposition of Si was a viable option. In recent years, it is possible to electrodeposit Si using RTILs at room temperature. It is further discussed in this section where we see the need for electrodeposition and further elaborate on how to electrodeposit Si.

D.1. PRIMARY NON-AQUEOUS SI-AIR CELL

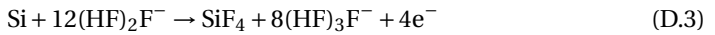
A Si-air cell is fabricated a surface area of 0.5 cm². The air cathode consists of PTFE (PolyTetraFluroEthylene) powder and activated carbon black structured catalyzed with MnO₂, pressed onto a Ni 200 mesh. The Si anode can be n-type Si (for high cell voltage) and p-type Si (lower corrosion current indicating larger shelf life) [27]. Since alkaline electrolytes cause high corrosion rate in Si, the electrolyte used in the cell is EMI - 2.3HEF which is made from the reaction of 1 - ethyl-3-methylimidazolium chloride and hydrogen fluoride. The postulated reduction of O₂ with the room temperature ionic liquid (RTIL) occurs in 2 reactions as shown [27]:



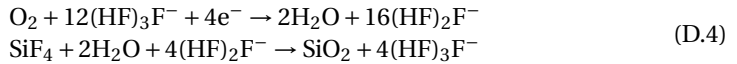
The cell potential difference was about 1.25 - 1.5 V. The n-doped (1 0 0) Si was the only anode that showed no anodic passivity [8]. Cohn et al. [8] advises to use heavily doped p-type Si anode at high current densities. It was observed that the cell voltage decreases with time and this is attributed to the build up of reaction products in the electrolyte and progressive deactivation of the air electrode. This is supported by data from the discharge profile and Scanning electron microscopy (SEM) micrographs that showed Si being sedimentation and covering the active carbon. By x-ray spectroscopy (XPS) analysis, it was found that SiO₂ is being produced as a battery discharge product. The cell

delivered a total capacity of 21 mAh over a discharge period of 350 h. It was concluded that a novel air battery with Si wafer anodes can have an average working potential of 1 - 1.2 V and support high current densities of about 0.3 mA/cm².

The fabrication of a Si-air battery with non-aqueous electrolyte is described by Cohn and Ein-Eli [8]. The electrolyte used in this system is hydrophilic 1-ethyl-3-methyl imidazolium oligofluorohydrogenate [EMI·(HF)_{2.3}F]. The anode used in this study is a single-crystal heavily doped n-type silicon wafer anode. The air cathode used here is composed of polytetrafluoroethylene (PTFE) powder and carbon black. On cell operation, it was found that the working potential was around 1.1 - 0.8 V. Voltage fluctuations during galvanostatic discharge can be attributed to due to the formation of gaseous SiF₄ as a byproduct of the reaction between Si and the RTIL. The anodic electrochemical dissolution reaction is as follows:



The complete cell discharge reaction at the cathode side can be given as:



The overall cell reaction during discharging is written as:



SiO₂ is a non-soluble product that gets trapped in the air cathode electrode, similar to the Li-air battery cell and it has a significant effect of the cell capacity. As seen in Figure D.1, it should be noted that during high current discharges, bulky deposits are produced and during lower current densities, finer deposits are produced.

From the results, we see that high current densities are preferred over lower current densities. This is mainly because oxygen diffusion is still available in the micro-pores of the air electrode while the deposition of SiO₂ takes place in the meso- and macro-pore sites of the air electrode. XPS studies were carried out in-order to study the structural changes of the electrodes during cell discharge. On further testing of the cathode using X-ray photoelectron spectroscopy (XPS) and EPR spectroscopy, it was found that along with the SiO₂ deposits there were also MnF₂ deposits on the MnO₂ catalyst surface. Not only do they increase the particulate size of the MnO₂ particulate which blocks the pores of the air electrode. It also reduces the catalyst area thereby causing the cell to discharge faster and reducing oxygen uptake. This formation also changes the oxidation state of the Mn ion from +4 in MnO₂ to +2 in MnF₂ [9].

A simple illustration of the Si-air cell can be seen in the Figure D.2 above. In order to reduce the formation of MnF₂ as shown in Figure D.3. Similar to what was suggested to reduce the formation of SiO₂ deposits in [38]. Water can shift the equilibrium reaction to the left side thereby reducing the formation of MnF₂ as well [9].

Although initially it was assumed that the cell performance was limited due to the SiO₂ clogging the air cathode [27] similar to the way metal oxide products clog the air cathode

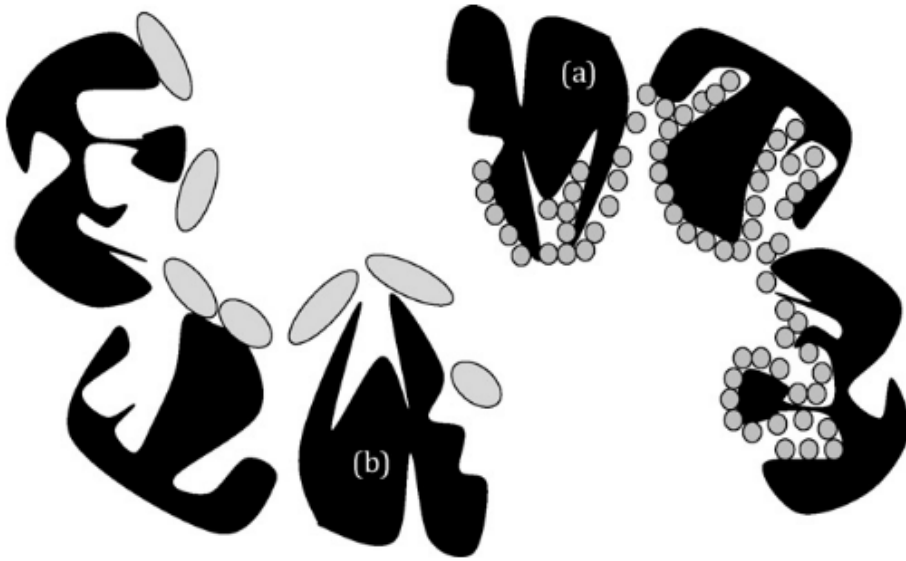


Figure D.1: SiO_2 deposition in the air electrode a.) during high discharge current density b.) during low discharge current density [8]

in metal-air batteries [2]. This was later contradicted by Cohn et al. using electrochemical impedance spectroscopy (EIS), in which they showed that Si anode potential is what varies during the discharge period and the air cathode is stable throughout the discharge period. This was further confirmed by mechanically replacing the Si anode and air cathode when they are completely discharged [10].

In Figure D.4 above we see that the OCP of the cell is varying only due to the variation in the OCP of the anode and it is very interesting to note that the OCP of the air cathode is stable across the whole discharge period. It can also be seen in Figure D.5 that the impedance of the electrode-electrolyte interface Si anode is very high compared to that of the air cathode. Hence, unlike previous findings, the cell failure would be due to Si anode inactivation rather than the clogging of air cathode [10]. From this, it is concluded that the battery can be recharged only by replenishing the Si anode as Si is the dominant electrode [10]. A mathematical model of the operation of this cell was developed by Yasin Durmus as part of his thesis. However, it is to be noted that this model is very computational intensive since it takes into account the different mechanisms taking place in the Si-air cell [47].

D.2. ELECTRODEPOSITION OF SI IN ROOM TEMPERATURE

The need for electrodeposition of Si and the role it plays in the rechargeable Si - Air battery. I shall also make an experimental setup based on the literature that I have referred. We shall also study the relevance of room temperature ionic liquids (RTILs) (1-butyl-1-methylpyrrolidiniumbis (trifluoromethanesulfonyl) imide and 1-butyl-3-methylimidazoliumbis

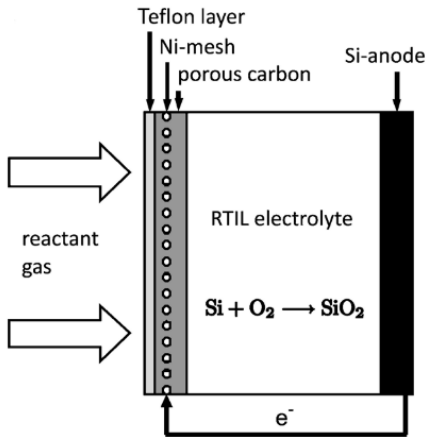
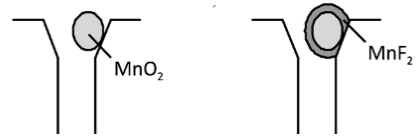


Figure D.2: Si-air cell illustration [9]

Figure D.3: MnF_2 formation on MnO_2 particulates in air electrode [9]

(trifluoromethylsulfonyl) imide) have in the Si - Air batteries and the possible influence it can have during discharge and charge in the Si - Air cell.

the Si-air cell converts the heavily doped Si anode to SiF_4 which is further reacted to form SiO_2 which is deposited in the air cathode as seen in Equation [8]. In order to make the Si - Air cell, we need to replenish the Si from the Si products that are formed during the discharge cycle in the charging cycle. The answer can be found using electrodeposition of Si which deposits Si at a working electrode when a significant amount of voltage is applied. Some other advantages that we can see other than making the cell a secondary cell are :

1. Increasing the lifetime of the cell - By making the cell a secondary cell, we can use the product more than once which is the case in a primary cell thereby reducing wastage and increasing the product's lifetime.
2. Battery of the future - As seen in Section , the power generation sources in the future have large variations daily and seasonal as well. Therefore, the role for a secondary cell in future power systems is a vital one.
3. Reducing Li dependency - At present, Li batteries can be found in application anywhere and everywhere. Due its high energy density and power density, it is the perfect candidate for energy storage in an electric vehicle (EV). However, it is known that Li is a rare earth metal and is not as abundant as Si.

There are various ways in which electrodeposition of Si is carried out from papers and what method is most suited for our application. The various methods in which the authors studied their deposits which will give an idea how we should analyze our deposits as well. Si electrodeposition can be compared to electroplating or even the electrochemistry in batteries. Due to the potential across one electrode to another, the Si ions move

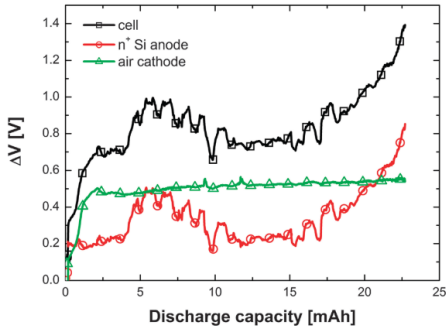
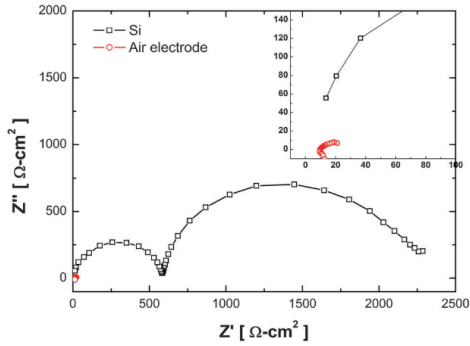
Figure D.4: ΔV cell, anode and cathode [10]

Figure D.5: Impedences of the Si anode and the air cathode [10]

D

towards the negative electrode as it has the positive oxidation state. There are various papers that shows how various ways electrodeposition of Si is carried out. The general electrodeposition set up consists of :

1. Si precursor - the raw material form of Si.
2. Electrolyte - the material the connects the two electrodes that allows the propagation of Si ions through.
3. Working electrode - the electrode that Si moves away from
4. Counter electrode/ Substrate - the electrode that Si gets deposited on or moves towards
5. Reference electrode - the electrode that has the cell potential zero. It is always a Pt wire or ring.

In the above Table D.1, we see the different types of methods of electrodeposition of Si performed nowadays. On closer examination of the above Table. We can see that 3 papers use room temperature ionic liquids (RTILs) as their electrolyte. This was an interesting observation as the main Si - Air cell prepared by Cohn et al. uses also an RTIL as the electrolyte for the discharge cycle [8]. It also critical to note the temperatures at which the electrodepositions are occurring as well. In Rao et al. and Islam et al. use molten salts as their Si precursor and require temperatures above 700 °C [48] [54]. On thinking about real world applications, charging a battery at 700 °C is not at all realistically possible. However, we see that on using RTILs, electrodeposition of Si can be done in room temperature itself thus making it an ideal candidates for our system [56] [52] [51]. **Note:** All the electrodeposition systems that use SiCl_4 as the Si precursor are done under Argon atmosphere with no trace of water. This is because the SiCl_4 reacts with water instantly to form hydrochloric acid. [3]

Table D.1: Different methods of electrodeposition of Si

Paper	Si Precursor	Solvent	Substrate	Counter electrode	Temp.
					°C
[48]	$K \sim SiF_6$	LiK – KF molten salt	Graphite	Pt or Ag	745 ± 5
[49]	$SiHCl_3$	Propylene carbonate with tertabutyl ammonium chloride	Pt, Ti, Ti-6 Al-4V alloy, n-Si, and indium-tin oxide coated fused silica were used for the substrate.	Pt	35 - 145
[50]	$SiCl_4$	acetonitril (CH_3CN) and tetraethylammonium chloride supporting electrolyte dichloromethane (CH_2Cl_2) and tetraethylammonium chloride supporting electrolyte	TCO with Au or Tin	Pt	RT
[51]	$SiCl_4$	RTIL - BMimTf2N - 1-bulyl-3methylimidazolium-bis(trifluoromethyl-sulfonyl)imide ([BMIm]Tf2N)	Au [111] sealed to a cell with teflon coated O ring	Pt ring	RT
[52]	$SiCl_4$	RTIL - Py1,4[TFSI] - 1-butyl-1-methylpyrrolidinium-bis(trifluoromethane-sulfonyl) imide	(Au) coated silicon (100) substrate was used as the working electrode for the deposition.	Pt wire	50
[53]	Na_2SiF_6	electrolytic bath consisted of the NaF – KF(40–60 mol%) eutectic mixture	Graphite substrate showed best results compared to Ni, Ag, $C_{graphite}$ and $C_{vitreous}$	N/A	820 - 950
[54]	$SiO_2 - NP$	calcium chloride ($CaCl_2$)	Ag	Graphite	855
[55]	$SiCl_4$	Propylene carbonate	Copper foil	Pt	N/A
[56]	$SiCl_4$	RTIL - P1,4 - 1-Butyl-1-methylpyrrolidinium-bis(trifluoromethane-sulfonyl) imide	HOPG (Highly oriented pyrolytic graphite)	Pt	RT

D.3. ROOM TEMPERATURE IONIC LIQUIDS (RTILS)

There is 2 RTILs that are used in electrodeposition of Si are 1-butyl-1- methylpyrrolidinium bis(trifluoromethanesulfo-nyl)imide (RTIL1) whose chemical structure can be seen in Figure D.7 and 1-butyl-3methylimidazolium- bis (trifluoromethylsulfonyl)imide (RTIL2) whose chemical structure can be seen in Figure D.6. These RTILs have fluoroine groups which is similar to the RTIL used by Cohn et al. which is 1-ethyl-3-methylimidazoliumoligofluorohydrogenate which is given in Figure D.8 [8].

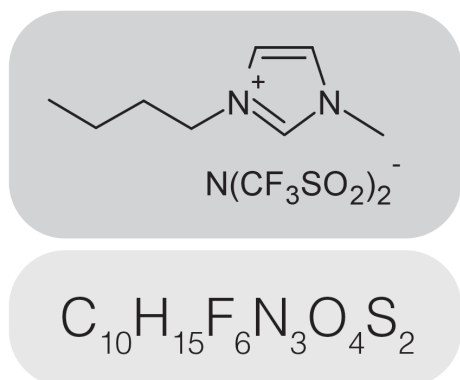


Figure D.6: RTIL2 Chemical structure [11]

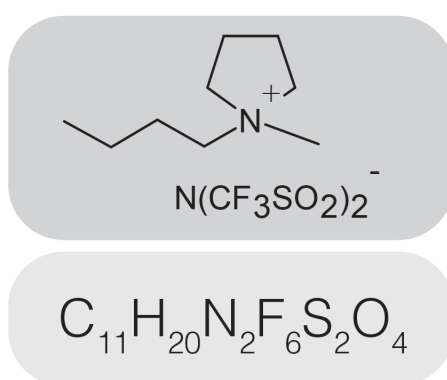
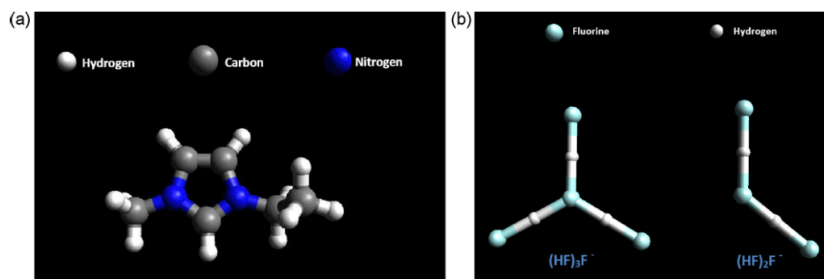


Figure D.7: RTIL1 Chemical structure [11]

Figure D.8: Chemical structure of EMI-(HF)₂.3F RTIL (a) EMI cation, (b) H₃F₄ (30%) and H₂F₃ (70%) anions [8]

Although there is no conclusive study that supports this. It is something that needs to be validated experimentally. If this is possible that means using the same organic solvent, electrodeposition is also possible thereby getting the Si - Air secondary cell closer. On comparing the chemical structures of the 3 RTILs, we see that RTIL2 is having a similar cation structure when you compare Figure D.6 and Figure D.8 in the previous Section. However, due to the lack of literature. The same cannot be said for anion structures. There isn't much literature on the electrochemical properties of the RTIL as well. Hence, electrochemical parameters must be validated experimentally.

D.4. VOLTAGE MEASUREMENT FROM AUTO LAB

Similar to the voltage measurement done for the fabricated Si-air cell with KOH in order to study the effect of discharge with changing KOH concentration in Voltage measurements studies were done on the fabricated Si-air cell in order to evaluate the formation of SiF_6 during the discharge cycle. This could potentially be used as a precursor for electrodeposition of Si on to the Si anode using methods similar to those described in [56] [52] and [51]. The only difference being that it would require excess energy as the precursors used above is SiCl_4 and not SiF_4 .

D.5. CONCLUSION

Further analysis of the discharge products formed couldn't be conducted due to the closure of EKL labs as per COVID regulations. Studies on the Si-air cell using 1-butyl-1-methylpyrrolidinium bis(trifluoromethanesulfonyl) imide were not conducted due to the closure of the EKL labs as well.

D.5.1. PREVIOUS THESIS PLAN

In order to evaluate the feasibility of using electrodeposition of Si as a means of recharging the Si-air battery cell. The following parameters must be studied in order to evaluate the feasibility of it. This was planned in the following phases.

INHIBITING THE SiO_2 FORMATION

In order to inhibit the SiO_2 crystallization reaction. We must study the reaction characteristics of SiO_2 formation. We must know what all are the parameters that affect the rate of formation of the SiO_2 deposits and the reaction mechanism of SiF_4 with water and the RTIL. This can only be done by seeing what are the physical constraints that affect the reaction such as:

1. Pressure
2. Temperature
3. Concentration

We won't be able to change the volume of the system as in the battery cell, the volume of the cell is constant throughout the process. By reducing the concentration of SiO_2 , it means that SiF_4 shall remain in the RTIL which can be used during charging for electrodeposition of Si on the Si anode.

ELECTRODEPOSITION OF SI USING SiF_4

In Section D.3, we see that SiCl_4 is mainly used as the Si precursor mostly when we use RTIL. This is mainly due to the low bond energy of Si - Cl bond. From literature this is confirmed with the bond energies of the following bonds. Once we are able to retain the SiF_4 that is formed in the RTIL due to the cathodic reaction. We can try to electrodeposit Si from it. However, we can approximate the extra amount of energy we might need for it. We can also estimate the heat of formation of these compounds using these bond energies:

Table D.2: Bond energies between different elements [17]

Bond	Bond Energy	Units
Si - F	565	kJ/mol
Si - Cl	381	kJ/mol
Cl - Cl	239	kJ/mol
F - F	154	kJ/mol

From the Table D.2, we see that the bond energy between Si - F is about 1.5 times larger than the bond energy of Si - Cl. Hence, we can approximate that the heat of formation of a compound is the difference between the energy of the bonds of reactants broken and the energy of the bonds of products formed. However, it is good to know that heat of formation is given as kJ/mol and the molecular weights of the two compounds are different. We find that the heat of formation of the compounds SiCl_4 and SiF_4 as :

Table D.3: Comparing heat of formations

Compound	Molecular Weight	Heat of formation	Heat of formation
	g	kJ/mol	kJ/kg
SiCl_4	169.9	-1046	-6156.56
SiF_4	104.09	-1952	-18754.96

From the Table D.3, we see that the amount of energy required for the formation or breaking of SiF_4 is approximately 3 times more than that of SiCl_4 for 1 kg of the compound. Hence, we would require 3 times the potential to electrodeposit Si from SiF_4 than SiCl_4 . This would definitely be an issue during charging and studies and experiments must be carried out to combat this issue.

EFFECT OF USING THE NEW RTIL vs. EMI·(HF)2.3F

Since, experiments have been already been done using EMI·(HF)2.3F RTIL. Similar experiments must be done using a Si - Air cell using RTIL2 and RTIL1 and the results can be compared.

D.5.2. ELECTRODEPOSITED SI BE USED AS ANODE FOR 2nd DISCHARGE?

As we see from literature, on electrodeposition we get only amorphous Si. However, in the primary Si - Air cell, we use heavily doped Si electrode as the anode. It must be experimentally validated and studied if it is possible to make the Si - Air cell with electrodeposited Si and study what happens to the dopants during discharge and charging characteristics. This shows that we can use the cell once again after we discharge initially and charge it.

On answering these questions, we can say for sure if it is possible to make Si - Air cell a secondary cell.

OPEN-CIRCUIT POTENTIAL

In order to evaluate the functionality of the battery cell. We need to obtain an open-circuit potential (OCP) from the two electrodes of the battery cell.

1. Using new electrodeposited Si anode: It should be verified if it is possible to obtain an open-circuit potential when we use electrodeposited Si anode. This shows that the Si obtained after electrodeposition can be used as an anode during the discharge after charging. However, it should be noted that this should be done in a fresh batch of RTIL so that we know the reason the cell doesn't work is because of the Si anode and not the electrolyte.
2. Using RTIL after electrodepositon: It should be verified whether after electrodeposition takes place. The RTIL still can be used for discharging as well. This should be done with a RTIL that was used for electrodeposition and taking a cell with fresh Si anode. Hence, we know that the electrolyte still has functionality after charging.

It would be interesting to experimentally evaluate these theories and study the behaviours of the 2 RTILs more in depth and their action with the Si-air battery to give better understanding of the working of the Si-air battery.

E

EQUIPMENT USED

E.1. MECO CU PLATING EQUIPMENT



Figure E.1: MECO Cu plating equipment

In Figure E.1, we see the equipment used in interaction with the AUTOLAB cell where the electrochemical analysis can be conducted. The equipment is primarily used for Cu plating but for our use, various electrochemical analysis can be done such as Chronopotentiometry, Chrono-amperometry, Linear sweep voltage, etc. can be conducted on this equipment. The computer on the right contains the NOVA software that works in tandem with the AUTOLAB cell. The settings can be input using this software and the results of the analysis is output in this software as well. The equipment gives readings of the resolution of 1 mV.

E.2. FUMEHOOD

In order for safe working practise. The cell is assembled and KOH is poured in fume-hoods in order to avoid any chemical spills which is seen in Figure E.2. The user is enforced to work with PPE like safety goggles, lab coat and nitrile gloves.



Figure E.2: Fumehood used in MEMS lab

E.3. WEIGHING MACHINE



Figure E.3: Weighing machine in MEMS lab

The mass of KOH pellets used in the KOH electrolyte must be of a fixed concentration. The weighing balance in Figure E.3 is from All Scales EU and can take a maximum mass of 220 g. The mass readings have resolution of 1 mg and has a deviation of about ± 0.1 mg.

E.4. TRIKON SIGMA 204 DEALER



Figure E.4: Metal sputtering equipment in EKL lab

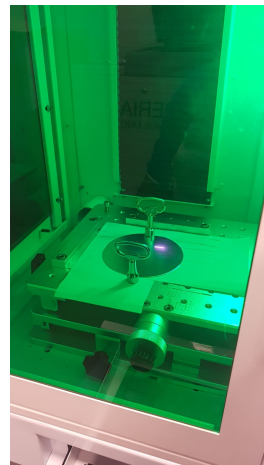
In order to create a Al:Si layer as the back contact of the Si-anode for better electron collection to the connecting wires. The Si wafers are sputtered with Al:Si on the back layer using the Trikon Sigma 204 dealer as shown in Figure E.4. The equipment can also sputter other materials such as As, Au/Cr, Cu and many more. It mostly used as a form of material layer deposition.

E

E.5. LASER CUTTER



(a) Laser cutter set up



(b) Laser cutter in operation

Figure E.5: Laser cutter in PV mini module manufacturing room

The laser cutter is available in the PV mini module manufacturing room which is part of the PVMD room. It is mainly used to cut solar cells. In this thesis, we use it to scribe Si

wafers and cut 2 cm x 2 cm samples which will be later used as in the Si anode. In Figure [E.5](#), it seen how the laser cutter set up is and how it is in operation.

BIBLIOGRAPHY

- [1] M. Fleischer, *Recent estimates of the abundances of the elements in this earth's crust*, Tech. Rep. (Washington DC, 1953).
- [2] Y. Li and J. Lu, *Metal-Air Batteries: Will They Be the Future Electrochemical Energy Storage Device of Choice?* (2017).
- [3] A. Inoishi, T. Sakai, Y. W. Ju, S. Ida, and T. Ishihara, *A rechargeable Si-air solid state oxygen shuttle battery incorporating an oxide ion conductor*, *Journal of Materials Chemistry A* **1**, 15212 (2013).
- [4] Y. E. Durmus, Ö. Aslanbas, S. Kayser, H. Tempel, F. Hausen, L. G. de Haart, J. Granwehr, Y. Ein-Eli, R. A. Eichel, and H. Kungl, *Long run discharge, performance and efficiency of primary Silicon-air cells with alkaline electrolyte*, *Electrochimica Acta* **225**, 215 (2017).
- [5] Electric Fuel, *Air Electrode*, (2018).
- [6] M. A. B.V., *Nova Software User manual*, **1** (2007), [arXiv:arXiv:1011.1669v3](https://arxiv.org/abs/1011.1669v3).
- [7] R. Jackey, *Battery Model Parameter Estimation Using a Layered Technique*, SAE Technical Paper, 1 (2013).
- [8] G. Cohn and Y. Ein-Eli, *Study and development of non-aqueous silicon-air battery*, *Journal of Power Sources* **195**, 4963 (2010).
- [9] P. Jakes, G. Cohn, Y. Ein-Eli, F. Scheiba, H. Ehrenberg, and R. A. Eichel, *Limitation of discharge capacity and mechanisms of air-electrode deactivation in silicon-air batteries*, *ChemSusChem* **5**, 2278 (2012).
- [10] G. Cohn, R. A. Eichel, and Y. Ein-Eli, *New insight into the discharge mechanism of silicon-air batteries using electrochemical impedance spectroscopy*, *Physical Chemistry Chemical Physics* **15**, 3256 (2013).
- [11] Solvionic, *Ionic Liquids / Catalogue 2016-2017*, (2017).
- [12] K. C. Divya and J. Østergaard, *Battery energy storage technology for power systems-An overview*, *Electric Power Systems Research* **79**, 511 (2009).
- [13] X. Luo, J. Wang, M. Dooner, and J. Clarke, *Overview of current development in electrical energy storage technologies and the application potential in power system operation*, *Applied Energy* **137**, 511 (2015).
- [14] Q. Li, Y. Liu, S. Guo, and H. Zhou, *Solar energy storage in the rechargeable batteries*, *Nano Today* **16**, 46 (2017).
- [15] H. Weinrich, Y. E. Durmus, H. Tempel, H. Kungl, and R. A. Eichel, *Silicon and iron as resource-efficient anode materials for ambient-temperature metal-air batteries: A review*, *Materials* **12** (2019), [10.3390/ma121321341-55](https://doi.org/10.3390/ma121321341).

- [16] R. Ahmed, J. Gazzarri, S. Onori, S. Habibi, R. Jackey, K. Rzemien, J. Tjong, and J. Lesage, *Model-Based Parameter Identification of Healthy and Aged Li-ion Batteries for Electric Vehicle Applications*, *SAE International Journal of Alternative Powertrains* **4**, 233 (2015).
- [17] T. L. Cottrell, *The Strengths of Chemical Bonds, 2nd Ed. Properties of atoms, radicals, and bond* (1966), [10.1002/ange.19600721618](https://doi.org/10.1002/ange.19600721618).
- [18] J. Pieters, *Hottest July 25th ever in NL; 10th heat record this year _ NL Times*, (2019).
- [19] M. R. Allen, D. J. Frame, C. Huntingford, C. D. Jones, J. A. Lowe, M. Meinshausen, and N. Meinshausen, *Warming caused by cumulative carbon emissions towards the trillionth tonne*, *Nature* **458**, 1163 (2009).
- [20] A. Fallis, *Global Warming of 1.5°C An IPCC Special Report on the impacts of global warming of 1.5°C above pre-industrial levels and related global greenhouse gas emission pathways, in the context of strengthening the global response to the threat of climate change*, *Journal of Chemical Information and Modeling* **53**, 3 (2018), [arXiv:arXiv:1011.1669v3](https://arxiv.org/abs/1011.1669v3).
- [21] D. Gielen, F. Boshell, D. Saygin, M. D. Bazilian, N. Wagner, and R. Gorini, *The role of renewable energy in the global energy transformation*, *Energy Strategy Reviews* **24**, 38 (2019).
- [22] G. P. Beretta, *World energy consumption and resources: An outlook for the rest of the century*, *International Journal of Environmental Technology and Management* **7**, 99 (2007).
- [23] N. Imanishi and O. Yamamoto, *Rechargeable lithium-air batteries: Characteristics and prospects*, *Materials Today* **17**, 24 (2014).
- [24] H. Blanco and A. Faaij, *A review at the role of storage in energy systems with a focus on Power to Gas and long-term storage*, *Renewable and Sustainable Energy Reviews* **81**, 1049 (2018).
- [25] J. James and Y. C. van Delft, *Power to ammonia process options: input to power to ammonia value chains and business cases*, (2017).
- [26] Y. Bennani, Y. Bennani, A. Perl, A. Patil, C. E. J. van Someren, L. J. M. Heijne, M. van Steenis, A. Patil, C. E. J. van Someren, L. J. M. Heijne, and M. van Steenis, *Power-to-Ammonia: Rethinking the role of ammonia – from a value product to a flexible energy carrier*, , 1 (2016).
- [27] G. Cohn, D. Starosvetsky, R. Hagiwara, D. D. Macdonald, and Y. Ein-Eli, *Silicon-air batteries*, *Electrochemistry Communications* **11**, 1916 (2009).
- [28] D. Gelman, B. Shvartsev, and Y. Ein-Eli, *Challenges and Prospect of Non-aqueous Non-alkali (NANA) Metal-Air Batteries*, *Topics in Current Chemistry* **374** (2016), [10.1007/s41061-016-0080-9](https://doi.org/10.1007/s41061-016-0080-9).

- [29] Y. E. Durmus, S. S. Montiel Guerrero, Ö. Aslanbas, H. Tempel, F. Hausen, L. G. de Haart, Y. Ein-Eli, R. A. Eichel, and H. Kungl, *Investigation of the corrosion behavior of highly As-doped crystalline Si in alkaline Si-air batteries*, [Electrochimica Acta](#) **265**, 292 (2018).
- [30] J. Prins, *Alkaline Pre-treatment of the Air Electrode in a Silicon-air Battery*, [Master](#), TU Delft (2020).
- [31] V. A. Shaposhnik, *Walter Nernst and analytical chemistry*, [Journal of Analytical Chemistry](#) **63**, 199 (2008).
- [32] M. Michalczyk, B. Ufnalski, L. M. Grzesiak, and P. Rumniak, *Przekształtnikowy emulator baterii elektrochemicznych*, [Przegląd Elektrotechniczny](#) **90**, 18 (2014).
- [33] R. Santbergen, C. C. Rindt, H. A. Zondag, and R. J. van Zolingen, *Detailed analysis of the energy yield of systems with covered sheet-and-tube PVT collectors*, [Solar Energy](#) **84**, 867 (2010).
- [34] MathWorks, *Simscape - MATLAB & Simulink*, (2020).
- [35] E. Krawczak and S. Gułkowski, *Electrical properties of aluminum contacts deposited by DC sputtering method for photovoltaic applications*, [E3S Web of Conferences](#) **19** (2017), 10.1051/e3sconf/20171903011.
- [36] V. Popovich, M. Maris, M. Janssen, I. Bennett, and I. Richardson, *Understanding the Properties of Silicon Solar Cells Aluminium Contact Layers and Its Effect on Mechanical Stability*, [Materials Sciences and Applications](#) **04**, 118 (2013).
- [37] J.-C. Stang, J. Haschke, M. Mews, A. Merkle, R. Peibst, B. Rech, and L. Korte, *Aluminium metallisation for interdigitated back-contact silicon heterojunction solar cells*, [Japanese Journal of Applied Physics](#) **56**, 08MB22 (2017).
- [38] G. Cohn, D. D. MacDonald, and Y. Ein-Eli, *Remarkable impact of water on the discharge performance of a silicon-air battery*, [ChemSusChem](#) **4**, 1124 (2011).
- [39] X. Zhong, H. Zhang, Y. Liu, J. Bai, L. Liao, Y. Huang, and X. Duan, *High-capacity silicon-air battery in alkaline solution*, [ChemSusChem](#) **5**, 177 (2012).
- [40] Y. Gao, Z. Zhang, R. Bondokov, S. Soloviev, and T. Sudarshan, *The Effect of Doping Concentration and Conductivity Type on Preferential Etching of 4H-SiC by Molten KOH*, [MRS Proceedings](#) **815** (2011), 10.1557/PROC-815-J5.20.
- [41] J. Johnson, *The effect of Temperature and Concentration on Galvanic Cells*, [Eei](#) **3.3**, 12 (2016).
- [42] S. S. Madani, E. Schaltz, and S. K. Kær, *An electrical equivalent circuit model of a lithium titanate oxide battery*, [Batteries](#) **5** (2019), 10.3390/batteries5010031.

- [43] A. K. Shrestha, N. Basnet, C. Bohora, and P. Khadka, *Variation of Electrical Conductivity of the Different Sources of Water with Temperature and Concentration of Electrolyte Solution NaCl*, International Journal of Recent Research and Review **10**, 24 (2017).
- [44] J. Gazzarri, *Battery Modeling*, (2020).
- [45] J. Gazzarri, N. Shrivastava, R. Jackey, and C. Borghesani, *Battery Pack Modeling, Simulation, and Deployment on a Multicore Real Time Target*, SAE International Journal of Aerospace **7** (2014), 10.4271/2014-01-2217.
- [46] MathWorks, *Developing Battery Management Systems with Simulink and Model-Based Design*, (2018).
- [47] Y. E. Durmus, *MODELING OF SILICON-AIR BATTERIES*, Masters, Ulm University (2016).
- [48] G. M. Rao, D. Elwell, and R. S. Feigelson, *Electrodeposition of Silicon onto Graphite*, ELECTROCHEMICAL SCIENCE AND TECHNOLOGY **128**, 1708 (1981).
- [49] A. Agrawal and A. Austin, *Electrodeposition of Silicon from Solutions of Silicon Halides in Aprotic Solvents*, ELECTROCHEMICAL SCIENCE AND TECHNOLOGY **128**, 2292 (1981).
- [50] M. Bechelany, J. Elias, P. Brodard, J. Michler, and L. Philippe, *Electrodeposition of amorphous silicon in non-oxygenated organic solvent*, Thin Solid Films **520**, 1895 (2012).
- [51] N. Shah and I. Mukhopadhyay, *Electrodeposition of Silicon (Si) from ionic liquid at room temperature (for EWT solar cell)*, Materials Today: Proceedings **4**, 12716 (2017).
- [52] S. Thomas, D. Kowalski, M. Molinari, and J. Mallet, *Role of electrochemical process parameters on the electrodeposition of silicon from 1-butyl-1-methylpyrrolidinium bis(trifluoromethanesulfonyl)imide ionic liquid*, Electrochimica Acta **265**, 166 (2018).
- [53] A. L. Bieber, L. Massot, M. Gibilaro, L. Cassayre, P. Taxil, and P. Chamelot, *Silicon electrodeposition in molten fluorides*, Electrochimica Acta **62**, 282 (2012).
- [54] M. M. Islam, I. Abdellaoui, C. Moslah, T. Sakurai, M. Ksibi, S. Hamzaoui, and K. Akimoto, *Electrodeposition and characterization of silicon films obtained through electrochemical reduction of SiO₂ nanoparticles*, Thin Solid Films **654**, 1 (2018).
- [55] R. Epur, M. Ramanathan, F. R. Beck, A. Manivannan, and P. N. Kumta, *Electrodeposition of amorphous silicon anode for lithium ion batteries*, Materials Science and Engineering B: Solid-State Materials for Advanced Technology **177**, 1157 (2012).
- [56] J. Mallet, M. Molinari, F. Martineau, F. Delavoie, P. Fricoteaux, and M. Troyon, *Growth of silicon nanowires of controlled diameters by electrodeposition in ionic liquid at room temperature*, Nano Letters **8**, 3468 (2008).

